PULLOUT RESISTANCE OF BEARING REINFORCEMENT AND FINITE ELEMENT ANALYSIS OF BEARING REINFORCEMENT EARTH WALL

Cherdsak Suksiripattanapong

A Thesis Submitted in Partial Fulfillment of the Requirements for the

Degree of Doctor of Philosophy in Civil Engineering

Suranaree University of Technology

Academic Year 2012

กำลังต้านทานแรงฉุดของเหล็กเสริมแบกทานและการวิเคราะห์ไฟไนท์อิลลิเมนต์
ของกำแพงกันดินเหล็กเสริมแบกทาน

นายเชิดศักดิ์ สุขศิริพัฒนพงศ์

PULLOUT RESISTANCE OF BEARING REINFORCEMENT
AND FINITE ELEMENT ANALYSIS OF BEARING
REINFORCEMENT EARTH WALL

Suranaree University of Technology has approved this thesis submitted in partial fulfillment of the requirements for the Degree of Doctor of Philosophy.

Thesis Examining Committee

_____

(Prof. Dr. Dennes T. Bergado)
Chairperson

_____

(Prof. Dr. Suksun Horpibulsuk)
Member (Thesis Advisor)

_____

(Prof. Dr. Jin Chun Chai)
Member

_____

(Dr. Martin D. Liu)
Member

_____

(Assoc. Prof. Dr. Panich Voottipruex)
Member

_____

(Assoc. Prof. Dr. Avirut Chinkulkijniwat)
Member

_____   _____

(Prof. Dr. Sukit Limpijumnong)   (Assoc. Prof. Flt. Lt. Dr. Kontorn Chamniprasart)
Vice Rector for Academic Affairs   Dean of Institute of Engineering

เชิดศักดิ์ สุขศิริพัฒนพงศ์ : กำลังต้านทานแรงฉุดของเหล็กเสริมแบกทานและการวิเคราะห์
ไฟไนท์อิลลิเมนต์ของกำแพงกันดินเหล็กเสริมแบกทาน (PULLOUT RESISTANCE OF
BEARING REINFORCEMENT AND FINITE ELEMENT ANALYSIS OF BEARING
REINFORCEMENT EARTH WALL) อาจารย์ที่ปรึกษา : ศาสตราจารย์ ดร.สุขสันติ์
หอพิบูลสุข, 189 หน้า

วิทยานิพนธ์นี้ประกอบด้วยหกบทซึ่งมีสามส่วนหลัก ส่วนแรกศึกษาอิทธิพลของคุณสมบัติ
ของดิน ขนาดของเหล็กตามขวาง และระยะห่างของเหล็กตามขวางต่อกลไกแรงฉุด (pullout
mechanism) ของเหล็กเสริมแบกทานกลไกการวิบัติแบกทานของเหล็กตามขวางหนึ่งตัวสามารถ
แบ่งออกเป็นสองโซน ซึ่งขึ้นอยู่กับค่า B/D_{50} โดยที่ B คือความยาวของขาเหล็กฉาก และ D_{50} คือ
ค่าเฉลี่ยของเม็ดดิน โซนที่ 1 $(B/D_{50} < 12)$ คือกลไกการวิบัติที่เกิดจากการขัดตัวของเม็ดดิน และ
โซนที่ 2 $(B/D_{50} \geq 12)$ คือกลไกการวิบัติแบบเฉือนทะลุปรับปรุง อิทธิพลการรบกวนของเหล็กตาม
ขวางสามารถแบ่งออกเป็นสามโซน ซึ่งขึ้นอยู่กับอัตราส่วนระยะห่างของเหล็กตามขวางต่อความยาว
ของขาเหล็กฉาก(S/B) โซนที่ 1 คือกลไกการวิบัติแบบบล็อก เมื่อ (S/B) มีค่าน้อยกว่า 3.75 โซน
2 คือกลไกการวิบัติแบบรบกวนกัน เมื่อ (S/B) มีค่าระหว่าง 3.75 และ 25 และโซน 3 คือกลไกการ
วิบัติแบบอิสระ เมื่อ (S/B) มีค่าเกินกว่า 25

งานวิจัยในส่วนที่สอง คือการวิเคราะห์ไฟไนท์อิลลิเมนต์ของกำแพงกันดินเหล็กเสริมแบก
ทานโดยโปรแกรม PLAXIS 2D วิธีการอย่างง่ายสำหรับการจำลองเหล็กเสริมแบกทานถูกนำเสนอ
โดยการดัดแปลงกำลังต้านทานแรงเสียดทานและแบกทานไปเป็นกำลังต้านทานแรงเสียดทาน
เทียบเท่า เหล็กเสริมแบกทานถูกจำลองในรูปของแผ่นใยสังเคราะห์ กำลังต้านทานแรงเสียดทาน
เทียบเท่าแทนได้ด้วยพารามิเตอร์ผิวสัมผัสของดินกับวัสดุเสริม(R) ซึ่งได้จากการคำนวณกลับของ
ผลทดสอบแรงฉุดของเหล็กเสริมแบกทาน ค่าพารามิเตอร์ผิวสัมผัสของดินกับวัสดุเสริม (R) เท่ากับ
0.55, 0.65, 0.75 และ 0.85 สำหรับเหล็กเสริมแบกทานที่มีเหล็กตามขวาง 1, 2, 3 และ 4 ตัว
ตามลำดับ การจำลองผลการทดสอบให้ค่าใกล้เคียงกับผลการตรวจวัดในสนาม

งานวิจัยในส่วนสุดท้าย คือการวิเคราะห์ความไวตัวของกำแพงกันดินเหล็กเสริมแบกทาน
ด้วยโปรแกรม PLAXIS 2D การวิเคราะห์ความไวตัวของกำแพงกันดินเหล็กเสริมแบกทานกระทำ
โดยการเปลี่ยนแปลงเงื่อนไขของฐานราก (ความหนา และค่าโมดูลัสของยัง ของชั้นดินผุกร่อน)
และคุณสมบัติของกำแพงกันดินเหล็กเสริมแบกทาน (จำนวนของเหล็กตามขวาง ความยาวของ
เหล็กเสริมแบกทาน ความสูงของกำแพง และระยะห่างในแนวดิ่งของเหล็กเสริมแบกทาน) การ
ทรุดตัวของกำแพงกันดินเหล็กเสริมแบกทานขึ้นอยู่กับความหนาของชั้นดินผุกร่อน ค่าโมดูลัสของ
ยังของชั้นดินผุกร่อน และความสูงของกำแพง การทรุดตัวของกำแพงกันดินเหล็กเสริมแบกทาน

ค่อนข้างที่จะสม่ำเสมอเนื่องจากอิทธิพลของสติฟเนสที่สูงของดินฐานราก ดังนั้น ความเค้นในดินใต้
ฐานรากมีรูปร่างเกือบจะสม่ำเสมอสำหรับเงื่อนไขของฐานรากและคุณสมบัติของกำแพงกันดิน
เหล็กเสริมแบกทานที่ต่างกัน การเคลื่อนตัวด้านข้างสูงสุดเกิดที่บริเวณกึ่งกลางของความสูงกำแพง
สำหรับชั้นดินผุกร่อนที่แข็งปานกลาง และที่ด้านบนของความสูงกำแพงสำหรับชั้นดินผุกร่อนที่
อ่อน กำแพงกันดินเหล็กเสริมแบกทานมีแนวโน้มที่จะพลิกคว่ำบริเวณ Toe สำหรับดินผุกร่อนที่
อ่อนสำหรับชั้นดินผุกร่อนที่แข็งปานกลางถึงแข็ง การเปลี่ยนแปลงการเคลื่อนตัวด้านข้างที่ฐาน
กำแพงไม่มีนัยสำคัญกับการเปลี่ยนแปลงจำนวนของเหล็กตามขวาง เนื่องจากแรงกดทับในแนวดิ่งที่
สูงมาก แรงดึงสูงสุดเกิดขึ้นของกำแพงกันดิน สำหรับเหล็กเสริมแบกทานที่ระดับบน ตำแหน่งที่
เกิดแรงดึงสูงสุดแปรผันตามลักษณะการทรุดตัว สำหรับเหล็กเสริมแบกทานที่ระดับล่าง

สาขาวิชา<u>วิศวกรรมโยธา</u>   ลายมือชื่อนักศึกษา _____

ปีการศึกษา 2555   ลายมือชื่ออาจารย์ที่ปรึกษา _____

CHERDSAK SUKSIRIPATTANAPONG : PULLOUT RESISTANCE OF

BEARING REINFORCEMENT AND FINITE ELEMENT ANALYSIS OF

BEARING REINFORCEMENT EARTH WALL. THESIS ADVISOR :

PROF. SUKSUN HORPIBULSUK, Ph.D., P.E., 189 PP.

BEARING REINFORCEMET/COARSE-GRAINED SOILS/PULLOUT

RESISTANCE/FINITE ELEMENT ANALYSIS

This thesis consists of six chapters with three main parts. First part presents an influence of the soil properties and dimension and spacing of the transverse members on the pullout mechanism of the bearing reinforcement. The bearing failure mechanism of a single transverse member is classified into two zones, which is dependent upon the B/D_{50} value, where B is the leg length of the transverse member and D_{50} is the average grain size of the soil. Zone 1 $(B/D_{50} < 12)$ is defined as the interlocking induced failure and Zone 2 $(B/D_{50} \geq 12)$ is the modified punching shear failure. The transverse member interference is classified into three zones depending on the ratio of spacing of transverse member to leg length of the transverse member (S/B). Zone 1 $(S/B \leq 3.75)$ is block failure where all transverse members act like a rough block. Zone 2 $(3.75 < S/B < 25)$ is member interference failure. Zone 3 $(S/B > 25)$ is individual failure.

Second part presents a finite element analysis simulation of the bearing reinforcement earth wall by PLAXIS 2D. The simplified method for modeling the bearing reinforcement, which converts the contribution of friction and bearing resistance to the equivalent friction resistance, is introduced. The bearing

reinforcement is modeled as the geotextile and the equivalent friction resistance is represented by the soil/reinforcement interface parameter, *R*, which was obtained from a back analysis of the laboratory pullout test results. The *R* values are 055, 0.65, 075 and 0.85 for the bearing reinforcement with 1, 2, 3 and 4 transverse members, respectively. Overall, the simulated test results are in good agreement with the measured ones.

Last part presents a parametric study on the performance of the bearing reinforcement earth wall using PLAXIS 2D. The parametric study of BRE wall was performed by varying the foundation conditions and the BRE wall properties. The simulated settlement of the BRE wall is dependent on the weathered crust thickness, the modulus of elasticity of the weathered crust and wall height. The settlement is relatively uniform due to the contribution from the high stiffness of foundation. Consequently, the bearing stress distribution is almost uniform for different foundation conditions and BRE wall properties. The maximum lateral movement occurs at about the mid of the wall height for medium weathered crust and at the top of the wall height for weak weathered crust. The BRE wall tends to overturn around the toe for the weak weathered crust. For medium to hard weathered crust, the change in the lateral movement at the wall base is insignificant even with the change in number of transverse members due to very high overburden pressure. The maximum tension forces locate at the wall front for the top reinforcement layers. The location of the maximum tension forces for the bottom reinforcement layers is dependent upon the settlement pattern.

School of <u>Civil Engineering</u>   Student's Signature _____

Academic Year 2012   Advisor's Signature _____

ACKNOWLEDGEMENTS

equipment and financial support. I also would like to acknowledge Thailand Research Fund (TRF) for financial support.

Finally, I would like to appreciate my family and my wife for their love, support, understanding, and providing me the opportunity to pursue my graduate studies.

Cherdsak Suksiripattanapong

TABLE OF CONTENTS

<div align="right">**Page**</div>

TABLE OF CONTENTS (Continued)

TABLE OF CONTENTS (Continued)

TABLE OF CONTENTS (Continued)

TABLE OF CONTENTS (Continued)

TABLE OF CONTENTS (Continued)

LIST OF TABLES

LIST OF FIGURES

Figure   **Page**

LIST OF FIGURES (continued)

LIST OF FIGURES (continued)

LIST OF FIGURES (continued)

LIST OF FIGURES (continued)

LIST OF FIGURES (continued)

LIST OF FIGURES (continued)

LIST OF FIGURES (continued)

LIST OF FIGURES (continued)

SYMBOLS AND ABBREVIATIONS

$\dagger_{b\max}$ = maximum bearing stress

D_{50} = average grain sizes

R_{inter} = interface factor

$\dagger_{n}$ = normal stress

A_{t} = total surface area of soil sliding

f_{ds} = coefficient of direct shear resistance

w_{ds} = friction angle of soil obtained from a direct shear test

u = angle of skin friction

r_{ds} = fraction of grid surface area

E_{c} = efficiency of grid reinforcement on cohesion

E_{w} = efficiency of grid reinforcement on friction

c_{a} = cohesion between soil and grid reinforcement

c, c' = cohesion between soil and soil

A_{s} = frictional area between soil and grid reinforcement

$\overline{\dagger_{s}}$ = average normal stress

$\overline{\dagger_{b}}$ = maximum bearing stress against a single transverse members

n = number of transverse members

d = diameter or width of a single transverse member

SYMBOLS AND ABBREVIATIONS (Continued)

N_c, N_q = bearing capacity factors

ς = angle of rotational failure zone

k = horizontal earth pressure coefficient

R = transverse member interference

a, b, nr = constants

P_f = Maximum pullout friction resistance

L = length of the longitudinal member

D = diameter of the longitudinal member

P_{bn} = maximum pullout bearing force

$\dagger_h$ = lateral earth pressure

S_v = Vertical spacing

S_h = Horizontal spacing

T = axial tension in reinforcing wire

E = modulus of elasticity of steel

A = cross-sectional area of the reinforcing wire

$\vee$ = axial strain in the reinforcing wires

f = yield function

g = plastic potential function

SYMBOLS AND ABBREVIATIONS (Continued)

D^e	=	elastic constitutive matrix
G_{ref}	=	reference shear modulus
G	=	shear modulus of soil
G_i	=	shear of interface element
$\wedge$	=	reinforcement stiffness factor
J	=	reinforcement stiffness
K_a	=	Rankine's active earth pressure coefficient
χ	=	unit weight of the soil
H	=	wall height
B	=	leg length of the transverse member
F	=	interference factor
a,b,c,d,e,f	=	constants
$\in$	=	elastic constitutive matrix
G_{ref}	=	reference shear modulus
G	=	shear modulus of soil

CHAPTER I

INTRODUCTION

1.1 Statement of problem

The inextensible reinforcements such as strips and grids have been developed in the past two decades so as to increase their functional abilities for reinforced structures. They can be laid continuously along the width of the reinforced soil system (grid type) or laid at intervals (strip type). Both grid and strip reinforcements are widely used around the world, including Thailand. The construction cost of the mechanically stabilized earth (MSE) wall is mainly dependent upon the transportation of backfill from a suitable borrow pit and the reinforcement type. The backfill is generally granular materials, according to a specification of the Department of Highways, Thailand. The transportation of the backfill is thus a fixed cost for a particular construction site. Consequently, the reinforcement becomes the key factor. For the inextensible reinforcement, the lower the steel volume used and the faster the installation, the lower the construction cost. In Thailand, a widely used strip reinforcement is the ribbed steel reinforcing strip. It is 50 mm in width and 4.2 mm in thickness with yield strength of 520 MPa. This reinforcement is conveniently transported to a factory for galvanization and to a construction site as well as simple and fast to install due to its strip shape. Because it is not produced in Thailand and is imported from Africa, the construction cost is relatively high due to the high import charges. The steel grid reinforcement can be locally manufactured. This reinforcement

has been extensively studied at the Asian Institute of Technology by Prof. D.T. Bergado and his co-workers (Bergado et al., 1988, 1996; Shivashankar, 1991; Chai, 1992; Tin et al., 2011). The advantage of the grid reinforcement is that the pullout bearing resistance in the resistant zone is high. However, the total volume (weight) of steel grid required is still high because of wasted transverse (bearing) bars in the active (unstable) zone. The transportation and installation of the grid reinforcement are less convenient than those of the strip reinforcement.

Horpibulsuk and Neramitkornburee (2010) have introduced a cost-effective earth reinforcement designated as "Bearing reinforcement". It is simply installed, conveniently transported, and possesses high pullout and rupture resistances with less steel volume. Figure 1 shows the typical configuration of the bearing reinforcement, which is composed of a longitudinal member and transverse (bearing) members. The longitudinal member is a steel deformed bar and the transverse members are a set of steel equal angles. The welding strength is designed to sustain a load not less than the tensile strength of the longitudinal member, according to the American Institute of Steel Construction (AISC).

The reinforcement is connected to the wall facing (1.5 x1.5 m) at the tie point (2 U-shaped steel) by a locking bar (a deformed bar) (*vide* Figure 2). The vertical spacing between tie points is usually 0.75 m and the horizontal spacing is 0.75 and 0.375 m, depending upon the loading level. The mechanically stabilized earth (MSE) wall by bearing reinforcements is designated as "Bearing Reinforcement Earth (BRE) wall" (Horpibulsuk et al., 2011).
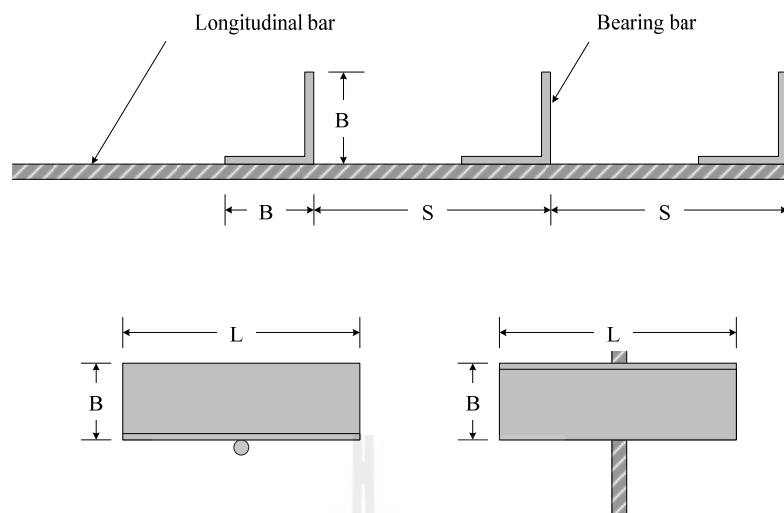
Figure 1.1 Configuration of the bearing reinforcement of the test wall (Horpibulsuk and Neramitkornburee, 2010)
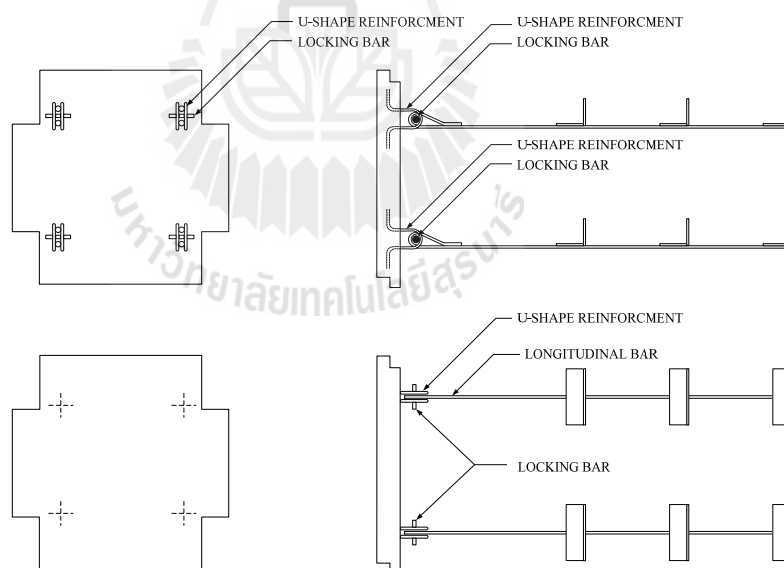
Figure 1.2 Connection of the bearing reinforcement to wall facing (Horpibulsuk and Neramitkornburee, 2010)

For a MSE wall design, an examination of external and internal stability is a routine design procedure. The examination of external stability is generally performed using the conventional method (limit equilibrium analysis) assuming that the composite backfill-reinforcement mass behaves as a rigid body (McGown et al., 1998). The internal stability of the BRE wall deals with the rupture and pullout resistances of the reinforcement. The pullout resistance is the sum of the pullout friction and bearing resistance. For the BRE wall, Horpibulsuk and Neramitkornburee (2009) proposed equations for estimating pullout resistance of the bearing reinforcement embedded in a poorly graded sand with different transverse members. The equations were useful for internal stability analysis of the BRE wall. Based on the equations, Horpibulsuk et al. (2011) designed and constructed a full scale BRE wall in the campus of Suranaree University of Technology to understand the performance of the wall during and after construction. The performance of the BRE wall was measured and reported. The small lateral movement and settlement were observed.

Even though there is available research on the pullout resistance of the bearing reinforcement and the performance of the full-scale BRE wall, the research is for a poorly-graded sand. Horpibulsuk and Niramitkornburee (2010) depicted that the maximum bearing stress, $\sigma_{b\max}$, of a single transverse member for the bearing reinforcement embedded in a poorly graded sand is predicted satisfactorily based on the modified punching shear mechanism. The proposed equation was applicable to a particular compacted sand with small particles. The applicability of the proposed equation for different coarse-grained soils, which are commonly used as backfill materials, is thus needed to be examined. Also, the finite element analysis and The

parametric studies on the bearing reinforcement earth (BRE) wall are needed to be performed to obtain an useful information for further analysis and design of the other BRE walls with different BRE wall properties and ground conditions. Therefore, the objectives of the study are as follows.

- To understand the pullout resistance mechanism of bearing reinforcement embedded in different coarse-grained soils and to suggest a practical approach for approximating the pullout resistance.

- To model the behavior of the bearing reinforcement earth (BRE) wall by 2D finite element analysis using Horpibulsuk et al. (2011) data.

- To perform the parametric studies on the bearing reinforcement earth (BRE) wall by 2D finite element analysis.

1.2   Structure of presentation

This thesis consists of six chapters and outlines of each chapter are presented as follows:

Chapter II presents the review of previous research on the interaction between reinforcements and soils, the behavior of the reinforced walls and the numerical analysis of the reinforced walls.

Chapter III presents the pullout resistance of bearing reinforcement embedded in different coarse-grained soils with different dimensions of transverse member, gradations, average grain sizes, D_{50} and friction angles. The soils used in this investigation consist of 4 soil types classified by the Unified Soil Classification

System (USCS), which were collected from different locations in Nakhon Ratchasima, Thailand. They are well-graded gravel (GW), well-graded sand (SW), poorly-graded sand (SP) and crushed rock (GP). The mode of failure and the transverse member interference of the bearing reinforcement are presented. Finally, the equations of predicting pullout resistance of the bearing reinforcement in different coarse-grained soils are proposed and verified.

Chapter IV presents the finite element simulation of the bearing reinforcement earth wall by PLAXIS 2D. The equivalent friction method is proposed to simulate the pullout mechanism of the reinforcement. A comparison between the simulated and the measured bearing stress, settlement, lateral movement and tension in the reinforcements during and after the construction is presented. The interface factor, R of 0.65 and 0.75 were used to represent 2 and 3 transverse members, respectively. Overall, the simulated and measured performance of the BRE wall is in very agreement. This implies that the proposed method can be used to design and predict the performance of the BRE wall in practice.

Chapter V presents the parametric studies on the bearing reinforcement earth (BRE) wall by PLAXIS 2D. The effects of the foundation conditions (thickness and modulus of elasticity of the weathered crust) and the BRE wall properties (number of transverse members, reinforcement length, wall height and reinforcement vertical spacing) on the performance of BRE wall are presented.

Chapter VI concludes the present work and suggests the topics for further study.

1.3 References

AASHTO (2002), *Standard Specifications for Highway and Bridge*, 7th edition. Washington D.C., **American Association of State Highway and Transportation Officials**.

Alfaro, M.C., Hayashi, S., Miura, N., and Watanabe, K. (1995). "Pullout interaction mechanism of geogrid strip reinforcement", **Geosynthetics International**, Vol.2, No.4, pp.679-698.

Bergado, D.T., Chai, J.C., and Miura, N. (1996), "Prediction of pullout resistance and pullout force-displacement relationship for inextensible grid reinforcements", **Soils and Foundations**, Vol.36, No.4, pp.11-22.

Chai, J. C. (1992), "Interaction between grid reinforcement and cohesive-frictional soil and performance of reinforced wall/embankment on soft ground", **D.Eng. Dissertation**, Asian Institute of Technology, Bangkok, Thailand.

Chen, R.H., and Chiu, Y.M. (2008), "Model tests of geocell retaining structures", **Geotextiles and Geomembranes**, Vol.25, No.1, pp.56-70.

Horpibulsuk, S., and Niramitkornburee, A. (2010), "Pullout resistance of bearing reinforcement embedded in sand", **Soils and Foundations**, Vol.50, No.2, pp.215-226.

Horpibulsuk, S., Suksiripattanapong, C., and Niramitkornburee, A. (2010). "A method of examining internal stability of the bearing reinforcement earth (BRE) wall." **Suranaree Journal of Science and Technology**, Vol.17, No.1, pp.1-11.

Horpibulsuk, S., Suksiripattanapong, C., Niramitkornburee, A., Chinkulkijniwat, A., and Tangsuttinon, T. (2011), "Performance of earth wall stabilized with bearing reinforcements", **Geotextiles and Geomembranes**, Vol.29, pp.514-524.

Jewell, R.A., Milligan, G.W.E., Sarsby, R.W., and Dubois, D. (1984). "Interaction between soil and geogrids", **Proceedings of the Symposium on Polymer Grid Reinforcement in Civil Engineering**, Thomas Telford Limited, London, UK, pp.11-17.

McGown, A., Andrawes, K.Z., Pradhan, S., and Khan, A.J. (1998), "Limit state analysis of geosynthetics reinforced soil structures", Keynote lecture, **Proceedings of 6th International Conference on Geosynthetics**, March, 25-29, 1998, Atlanta, GA, USA, pp.143-179.

Peterson, L.M., and Anderson, L.R. (1980). "Pullout resistance of welded wire mats embedded in soil", **Research Report Submitted to Hilfiker Co, from the Civil and Environmental Engineering Department**, Utah State University, USA.

Shivashankar, R. (1991), "Behaviour of mechanically stabilized earth (MSE) embankment with poor quality backfills on soft clay deposits", including a Study of the pullout resistance, **D.Eng. Dissertation**, Asian Institute of Technology, Bangkok, Thailand.

Tin, N., Bergado, D.T., Anderson, L.R., Voottipruex, P. (2011), "Factors affecting kinked steel grid reinforcement in MSE structures", **Geotextiles and Geomembranes**, Vol.29, pp.172-180.

CHAPTER II

THEORETICAL BACKGROUND AND

LITERATURE REVIEW

2.1 General

Historical records indicate that the use of reinforcements to improve soil properties have been done long time ago. Thousands of years back, the Chinese used sticks and branches to reinforced dikes made of mud. The development of the earth reinforcement technique was pioneered by the French architect and inventor, Henri Vidal, who investigated the frictional effects of reinforcement in soil with the aim of improving the properties of soil in the direction in which the soil is subject to tensile strain. Since that time, reinforced earth has been extensively used for the construction of earth retaining walls and embankment slopes and in the stabilization of embankments placed on soft ground. Consequently, numerous reinforcement types of proprietary systems have been developed and, in comparison with conventional construction, they offer the advantages of simple construction, low cost and ability to tolerate large deformations without structural distress.

Mechanical stabilized earth (MSE) structure is a composite construction material in which the compressive strength of engineering fill is enhanced by the addition of tensile strength to the reinforcements. The mechanism of reinforced earth involves the generation of frictional and bearing resistances between the soil and the reinforcement. These forces are manifested in the soil in a form analogous to

increased confining pressure and/or anisotropic cohesion that enhances the strength of the composite material. Additionally the reinforcement has the ability to unify mass of soil that would otherwise part along a failure surface. Reinforced soil is potentially a very versatile material. However, the vast majority of applications to date involve walls in various forms. These structures embody two basic components, namely: engineering fill and reinforcement. MSE structures can be divided into three main parts:

- Facing elements, which act like an armor to protect and prevent erosion of the retained fill materials,

- Reinforcing elements, which add tensile strength in the retained fill materials,

- Engineered retained fill, consisting of soil materials making up the bulk of the structure.

The backfill materials are usually chosen based on the ability to develop good frictional interface with the reinforcing elements. Although a well-graded and good quality granular material is preferred, Bergado et al., (1991) have shown that weathered clay can be used as backfill for MSE construction. The selection of each or the combination of each of the components depends upon aesthetic, environmental, economic and functional considerations. MSE systems are differentiated primarily by the type of reinforcement utilized.

2.2 The basic principles and concept of reinforced earth

To understand the mechanisms of reinforced earth, several experimental and theoretical investigations have been done. The comprehensive triaxial tests using the aluminum disks reinforced sand sample was carried out. The results indicated that the reinforced samples have higher shear strength than unreinforced samples. The results were interpreted using two different assumptions: the anistropic cohesion assumption and the enhanced confining pressure assumption (Ingold, 1982a)

The anisotropic cohesion concept is based on the assumption that when the reinforced soil sample is at failure state and if the major principal stress is the same as the unreinforced soil sample, the minor principal stress is reduced. Therefore, the failure envelope of the reinforced soil sample will lie above that of the unreinforced sample (Schlosser and Long, 1973). Hausmann (1976) pointed out that at low normal stress levels, the reinforced sample fails by slippage, and there is no apparent anisotropic cohesion intercept but only the internal friction angle is increased. At high normal stress, however, the reinforced earth fails by breakage of reinforcements and has an anisotropic cohesion soil sample, as shown in Figure 2.la.

The enhanced confining pressure concept is based on the assumption that the horizontal and vertical planes are no longer the principal stress planes, due to the shear stresses induced between the soil and the reinforcement. The minor principal stress within the reinforced soil sample increases when the major principal stress is increased, resulting in the shifting of the Mohr's circle of stress. The additional strength of the reinforced soil can be attributed to the enhanced confining pressure effect. The failure envelope is the same for both reinforced and unreinforced samples

as shown in Figure 2.lb (Yang, 1972). In Figure 2.lb, the dashed line shows the anisotropic cohesion concept for comparison.
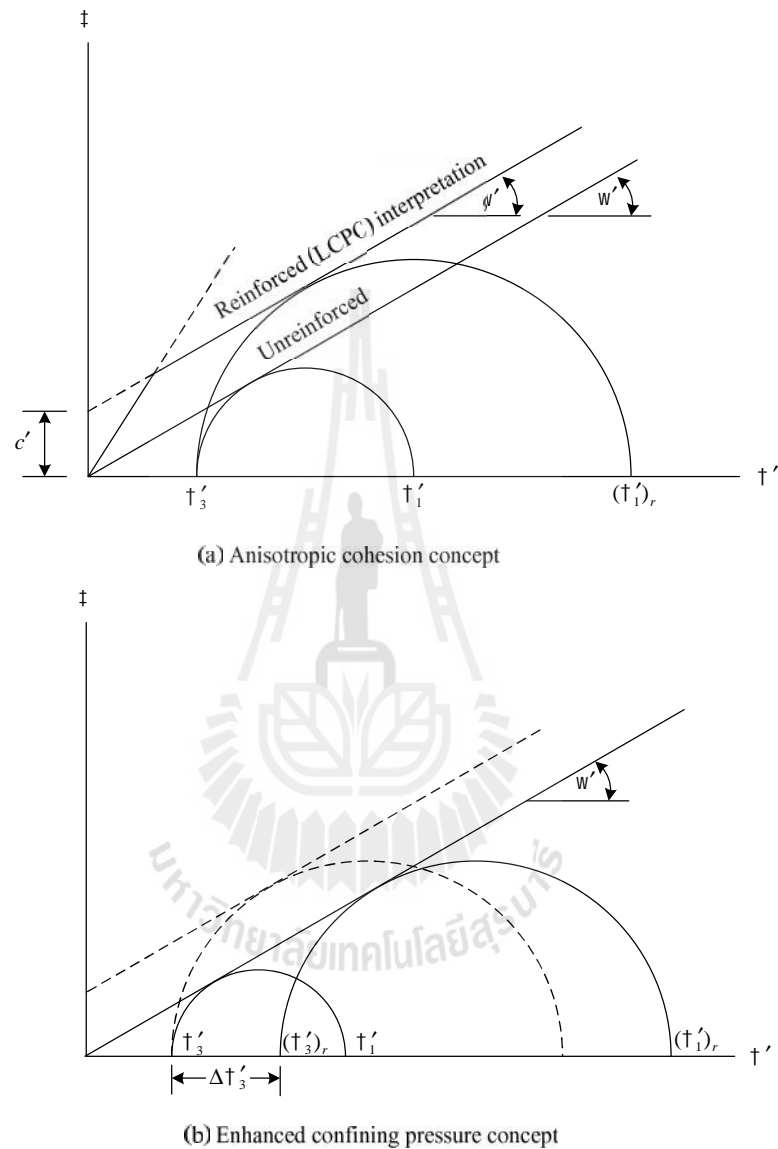
Figure 2.1 Basic concepts of reinforced earth

Under low confining stresses in a given reinforcement, the MSE system tends to fail by slippage or pullout of the reinforcement while under high confining pressures same systems fail by breakage of reinforced (Mitchell and Villet, 1987). As shown in

Figure 2.2, the zones of reinforcement breakage or slippage are indicated. Both anisotropic cohesion and enhanced confining pressure concepts explain the same phenomenon that due to interaction between soil and reinforcement, the reinforced soil has a higher strength than unreinforced soil. The interaction mechanism developed in a reinforced soil is characterized by the mobilization of shear stress along the soil/reinforcement interface. This process, consequently, results in the generation of tension forces in the reinforcement.
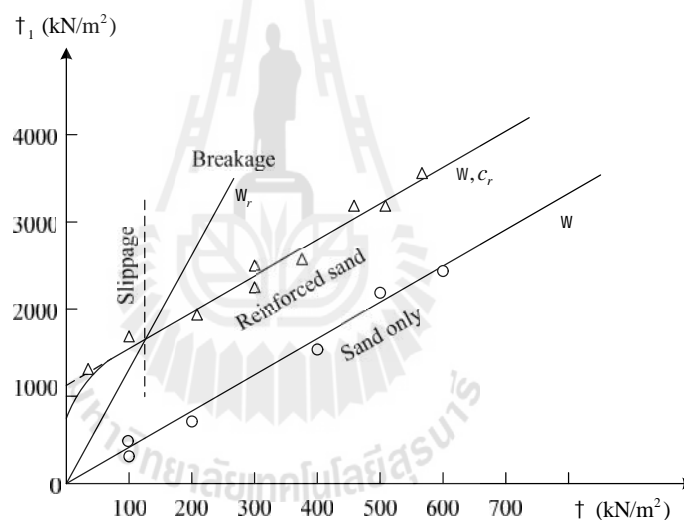
Figure 2.2   Strength envelopes for sand and reinforced sand

(Mitchell and Villet, 1987)

2.3 Failure Mode of Mechanically Stabilized Earth (MSE)

Design of mechanically stabilized earth (MSE) structures consists of determining its geometric shape and reinforcement requirements to prevent external

and internal failure. Internal stability requires that the reinforced soil structure is coherent and self-supporting under the action of its own weight and any externally applied forces. The reinforcement must be sized and spaced so that it does not fail in tension under the stresses that are applied, and does not pull out of the soil mass. For external stability, the MSE slope must satisfy the same external design criteria as a conventional retaining wall.

2.3.1 External failure

Similar to traditional reinforced concrete cantilever and gravity retaining walls, MSE structures also consider the following four potential external failure mechanisms:

1) Sliding of the reinforced soil block over the foundation soil.

2) Overturning of the reinforced soil block.

3) Bearing capacity failure of the foundation soil.

4) Deep sated stability failure (rotational slip-surface or slip along a plan of weakness).

These external failures of the MSE structures are shown in Figure 2.3. Due to their flexibility and satisfactory field performance, adopt factor of safety values for external failure are lower than those used for classical unreinforced retaining structures. For example, the factor of safety for overall bearing capacity is 2 lower than the conventional value of which is used for more rigid structures. The sliding requirement for external stability generally governs the dimension of the MSE structure.
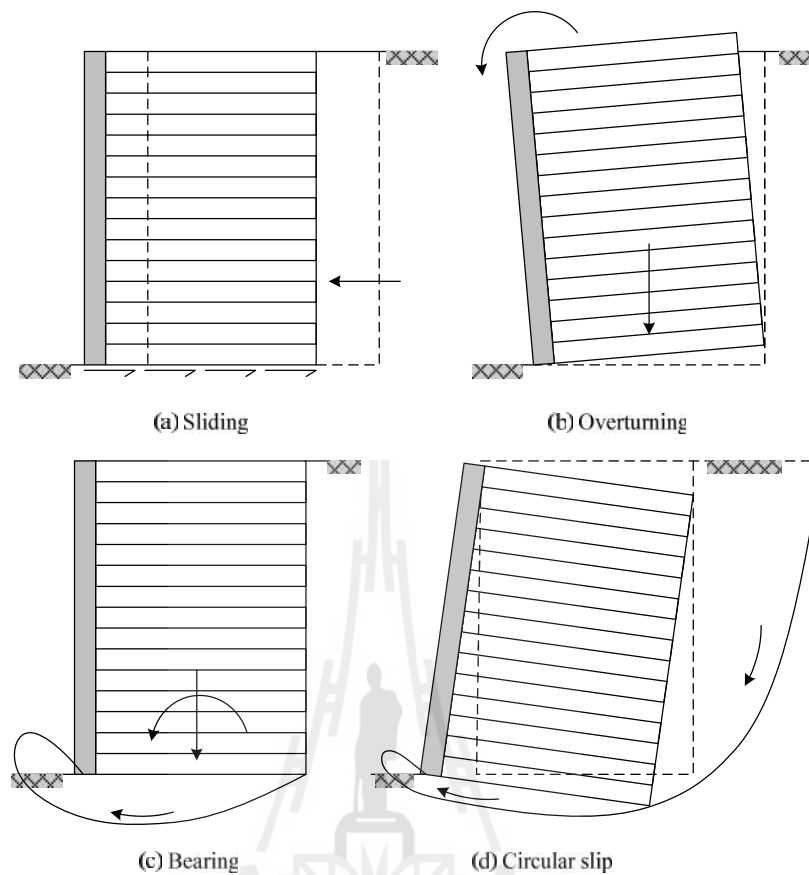
Figure 2.3   Potential external failure mechanisms of MSE structures

2.3.2   Internal failure

The reinforced soil structure will be internally stable if the reinforcement can to carry the tensile stress, bending stress and shear stress.

The internal failure mode can be categorized into two concepts (Figure 2.4):

1) Tensile failure is caused by rupture of reinforcement. Tension failure occurs when the tension developed in the reinforcement exceeds its tensile strength.

2) Slippage failure is caused by slippage between soil and reinforcement which may be called pullout, friction or bond failure of the reinforcement. Friction on failure will occur when tension is less than its tensile strength but greater than friction or bond resistance of the reinforcement.

Tension Failure   Pullout Failure
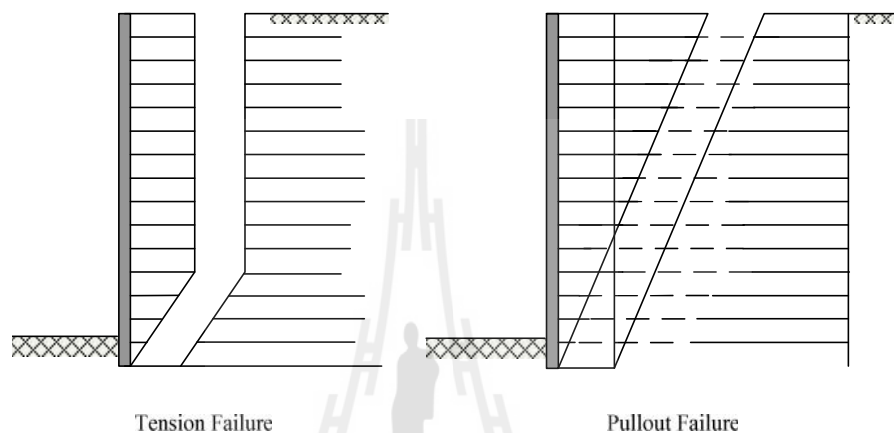
Figure 2.4   Internal failure mechanisms of MSE structures

2.4 Reinforcing Materials

More recently, several reinforcing materials have been used in the construction and design of foundations, retaining walls, embankment slopes, and other reinforced earth structures. The basic function of the reinforcing materials is adding tensile properties to soil, thereby improving the internal stability of structures. By considering their extensibility, these reinforcing materials can be classified into two typical types; inextensible and extensible reinforcements.

2.4.1 Inextensible reinforcement

This type of reinforcements is normally assumed to be rigid, and the deformation of inextensible reinforcements at failure is much less than the soil

deformability. In simple words, inextensible reinforcements can refer to metallic reinforcing materials e.g. metallic strips, metallic grids, hexagonal wire meshes, etc.

2.4.1.1 Metallic strips

In most reinforced earth structures, metallic strips e.g. stainless, galvanize or coated steel strips are used as reinforcements in backfills (see Figure 2.5). They are flexible linear elements normally having their breadth greater than their thickness. Their dimensions vary with application and structure, but breadth and thickness are usually within the range of 5 to 100 mm, and 3 to 5 mm, respectively. The form of metallic strips is either plain or has several protrusions, such as rib or gloves to increase the friction between the reinforcing material and backfill. However, there is an obvious shortcoming when using metallic strips as reinforcement in reinforced earth structures is that they are subjected to corrosion. The corrosion depends on several environmental factors.
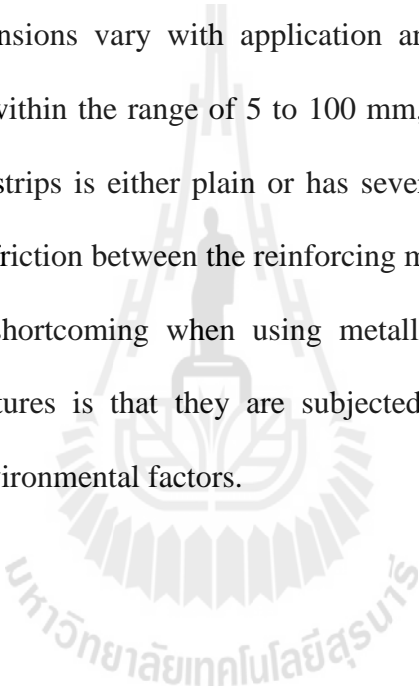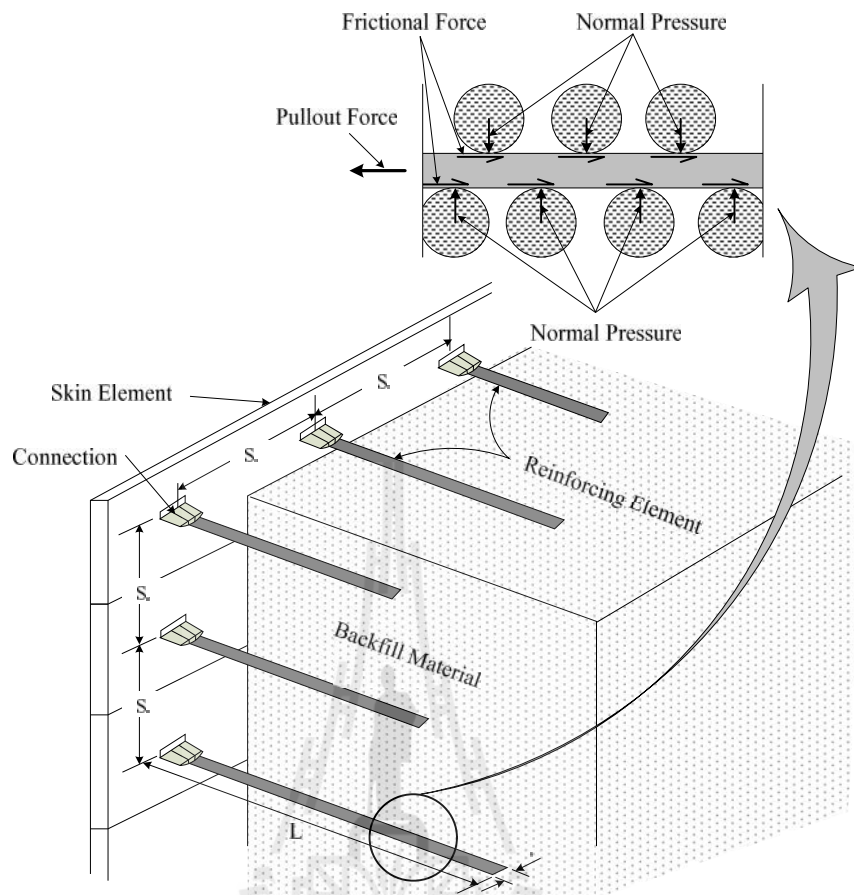
Figure 2.5 Metallic strips used in a concrete-faced structure

2.4.1.2 Metallic grids

Typically, metallic grids consist of two member component: transverse member and longitudinal member. In field application, transverse members will be arranged parallel to the face or free edge of structures and behave as abutment or anchor. The main purpose of the arrangement is to retain the transverse members in position. Transverse members are normally stiff relative to their length to be able to act as abutment or anchor. The longitudinal members are slightly flexible, having high modulus of elasticity but not susceptible to creep. Metallic grids can be formed from

(a)

Width

Length

(b)

Steel core
wire

Zinc
coating

PVC
coating

Steel core
wire

Zinc coating
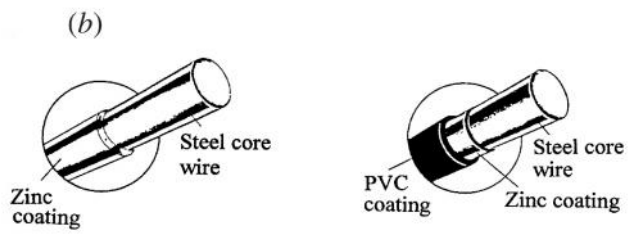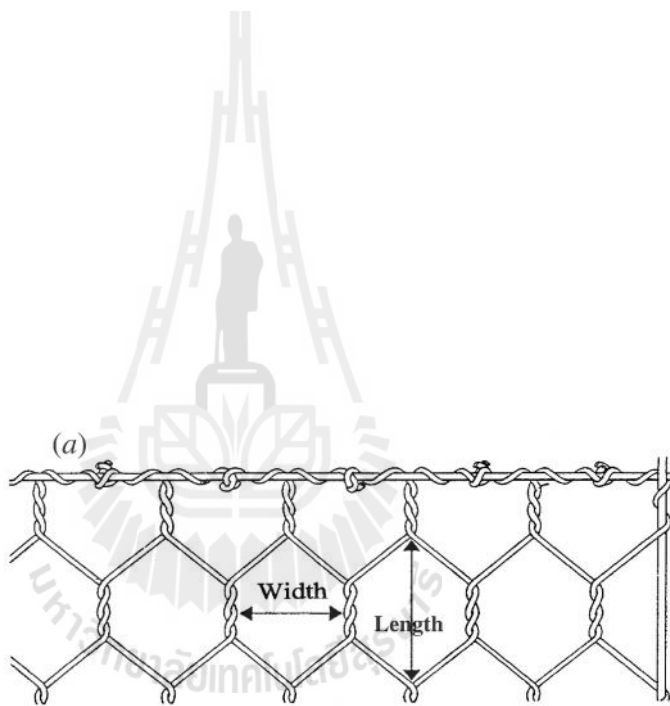
2.4.1.4   Bearing reinforcement

Figure 2.7 shows the typical configuration of the bearing reinforcement, which is composed of a longitudinal member and transverse (bearing) members. The longitudinal member is a steel deformed bar and the transverse members are a set of steel equal angles.
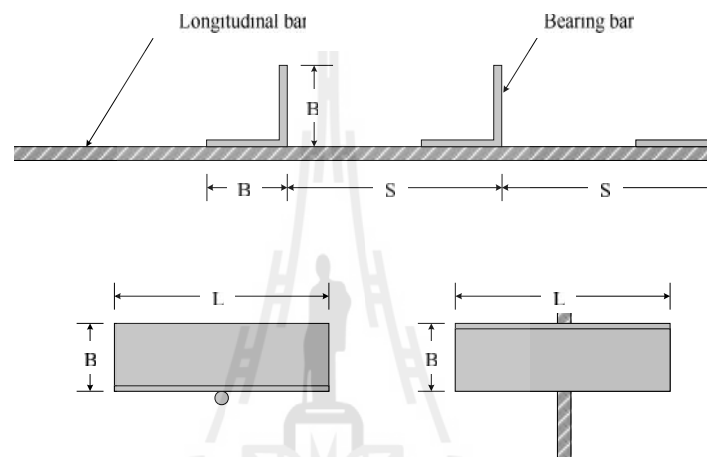
Figure 2.7   Configuration of the bearing reinforcement of the test wall

(Horpibulsuk and Niramitkornburee, 2010)

2.4.2   Extensible reinforcements

In general, the extensible reinforcement materials have lower strength and more extensible than the inextensible counterparts. The deformation of the extensible reinforcements at failure is comparable to or even greater than the soil deformability. So extensible reinforcements can refer to non-metallic reinforcing materials such as geosynthetics, which includes geotextiles, geogrids, and geocomposites (consisting of geotextile and geogrid) on the basis of their strength, stiffness, and relatively large strain characteristics.

One considerable advantage of the extensible reinforcements is that they do not suffer from corrosion. However, a less desirable property of polymers is the tendency to creep, which is a time-dependent phenomenon manifested by strain at constant load or in excess of that caused by initial loading. In temporary structures, creep would cause little problem, but in permanent structures, creep could have more serious effects.

For the term geosynthetics, "geo" refer to earth, and "synthetics" is given for human-made products. Most of the materials used for producing geosynthetics are from polymers; however, sometimes, some materials are used e.g. fiber glass, rubber, and natural material. Hence, they are almost exclusively made of one or a combination of the many polymers available with the strength and deformation properties of reinforcement.

2.4.2.1 Geotextiles

There are two main types of conventional geotextile: a) woven geotextile and b) non-woven geotextile. The former is composed of two perpendicular sets of parallel linear elements systematically interlaced to form a planar structures, while the latter is formed from filaments or fibers randomly arranged and bonded together to form a planer structure, which can be achieved by mechanical, thermal or chemical means. There are now four main applications for using geotextiles as soil reinforcement: a) vertical walls and abutments, b) steep slopes, c) slip prevention and remedial measure, and d) embankments on soft soil (Jewell, 1986) as illustrated in Figure 2.8.

(a) Abutments

(b) Steep slopes

(c) Slip prevention and remedial measure

(d) Embankments on soft soil
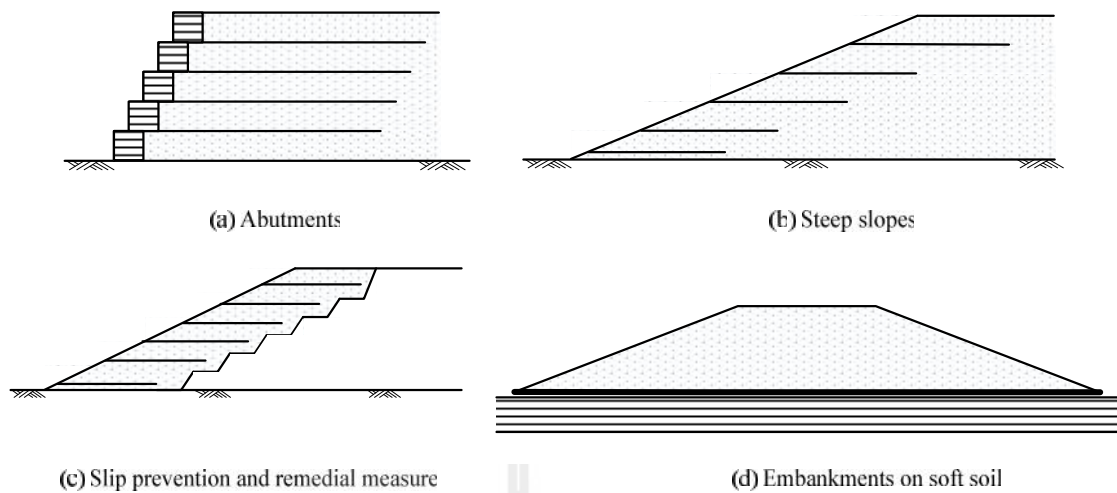
Figure 2.8   Examples of geotextile applications as soil reinforcement

2.4.2.2   Geogrids

Geogrids is normally composed of connected parallel sets of tensile ribs with apertures sufficient to allow strike-through of surrounding soil, stone, or other geotechnical materials. It is originated by adopting polymer materials (e.g. polypropylene and polyethylene), however, today most geogrids are made of polyesters by using textile weaving machinery. Such woven-type geogrids are generally coated with some chemical substances (e.g.PVC, latex, bitumen) for dimensional stability, providing protection for the ribs during installation, and preventing them from biochemical degradation.

Generally, geogrids made of polymers and can be classified into two types: a) uniaxial and b) biaxial. Figure 2.15(a) and 2.15(b) illustrate these two types of such geogrids. Uniaxial geogrids are normally stronger than biaxial geogrids. Geogrid reinforcement material can be used in all main reinforced soil applications although it is not strong as heavier woven geotextile products. A particular feature of
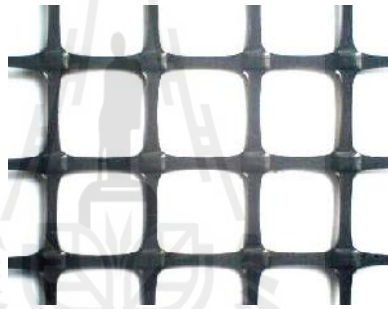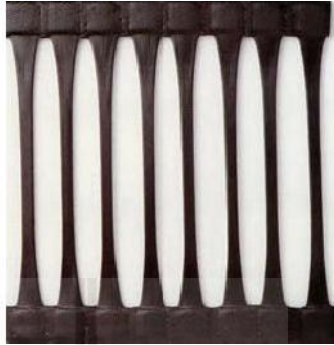
component is the resistance from soil bearing surfaces of grid reinforcement (Jewell et al., 1984). Since the last component is too difficult to assess, the influence of the reinforcement apertures on the direct shear resistance is usually treated as to increase the skin friction resistance between the soil and surface area of grid reinforcement.

Thus, the direct shear resistance between soil and grid reinforcement can normally be expressed in terms of only two shearing resistance contribution; one is the shearing resistance between soil and surface area of the grid reinforcement, and the other is the shearing resistance between soil and soil at the apertures of the grid reinforcement:

$$F_s = \sigma_n A_t f_{ds} \tan \varphi_{ds} \tag{2.1}$$

$$f_{ds} \tan \varphi_{ds} = \rho_{ds} \tan \delta + (1 - \rho_{ds}) \tan \varphi_{ds} \tag{2.2}$$

where σ_n is normal stress at the shear plane, A_t is total surface area of soil sliding, f_{ds} is coefficient of direct shear resistance, φ_{ds} is friction angle of soil obtained from a direct shear test, δ is angle of skin friction and ρ_{ds} is fraction of grid surface area providing the directs shear resistance.

If ρ_{ds} is equal to zero, it will be the case of soil shearing over soil and then f_{ds} will be equal to one; but if ρ_{ds} is equal to one, it will be the case of soil shearing over the surface area of grid reinforcement and the f_{ds} will be equal to $\tan \delta / \tan \varphi_{ds}$.

Being relatively simple to perform, direct shear tests are often conducted to determine shear parameters not only between soil and soil, but soil and reinforcement as well. If such parameters are obtained by performing separate tests, the efficiency values of grid reinforcement either on cohesion or on friction could be determined by using the following equations:

$$E_c = \left(\frac{c_a}{c}\right) \times 100 \tag{2.3}$$

$$E_w = \left(\frac{\tan u}{\tan w}\right) \times 100 \tag{2.4}$$

where E_c is efficiency of grid reinforcement on cohesion, E_w is efficiency of grid reinforcement on friction, c_a is cohesion between soil and grid reinforcement, c is cohesion between soil and soil, u is skin friction angle between soil and grid reinforcement and w is friction angle between soil and soil.

2.5.2 Pullout resistance

Pullout resistance of grid reinforcement embedded in backfill soils basically consists of two resistance contributions; the former is frictional resistance and the latter is passive or bearing resistance, which is stated herein in the following sections:

2.5.2.1 Frictional resistance

Bergado and Chai (1994) concluded that the mobilization process of frictional resistance from a pullout force is similar to the friction resistance of an axially loaded pile, which just needs a small relative displacement to be

$$P_f = A_s \overline{\dagger}_s \tan u$$

A_s $\overline{\dagger}_s$

$\dagger$

u

Frictional Resistance

Pullout Force

Passive Resistance
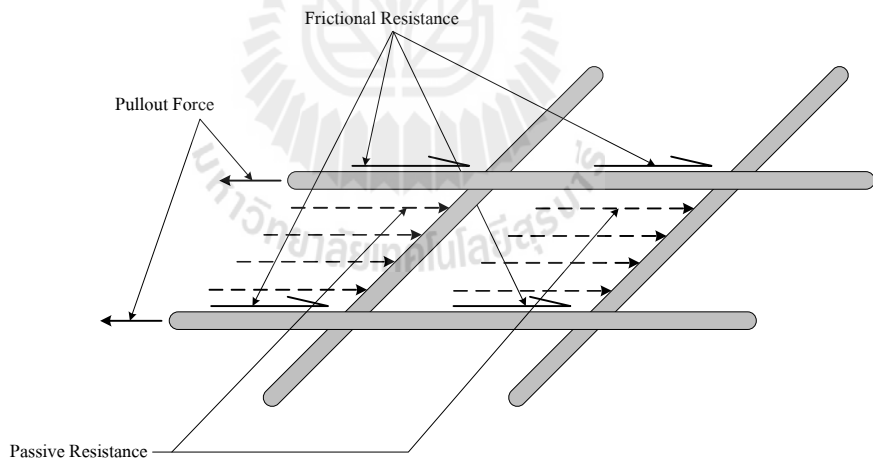
only the surface area of the longitudinal ribs, but also the surface area of the transverse ones as shown in Figure 2.10.

According to Abiera (1991) 's research on the pullout resistance of steel grid and geogrid samples, about 10 % of pullout resistance of the steel grid reinforcement was governed by the frictional resistance that mobilized at a small pullout displacement. In contrast, about 90 % of pullout resistance of the geogrid reinforcements (i.e. Tensar SR80) was governed by the frictional resistance, and the test results of two geogeid samples—one with transverse ribs and the other without and transverse ribs are shown in Figure 2.11a. This was implemented by cutting all transverse ribs of one geogrid sample and then conducting the pullout test on the remaining longitudinal ribs embedded in weathered Bangkok clay. The obtained results of pullout resistance were assumed to be equal to the frictional resistance mobilized along the surface area of the longitudinal ribs.

For highly extensible geogrid reinforcements, the contribution of longitudinal ribs to the pullout force is more significant than that of the transverse ribs during the deformation stage because large elongation occurring in the geogrids restricts the mobilization of the full effect of the transverse ribs as reported by Alagiyawanna et al. (2001). They performed pullout tests on highly extensible geogrid samples with different spacing arrangements of the longitudinal and transverse ribs. The friction resistance mobilized along the longitudinal rib surface governs the pullout resistance, F_p, not the bearing resistance against the front of the transverse ribs (see Figure 2.11b).
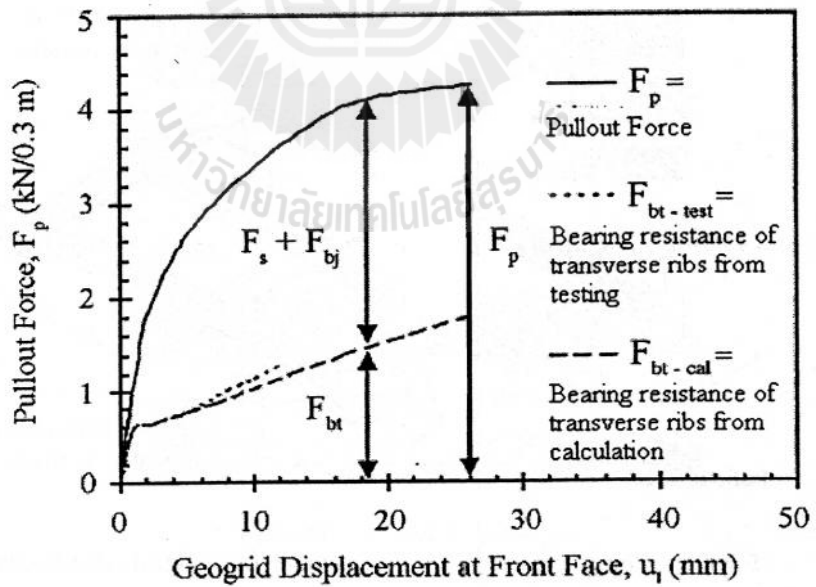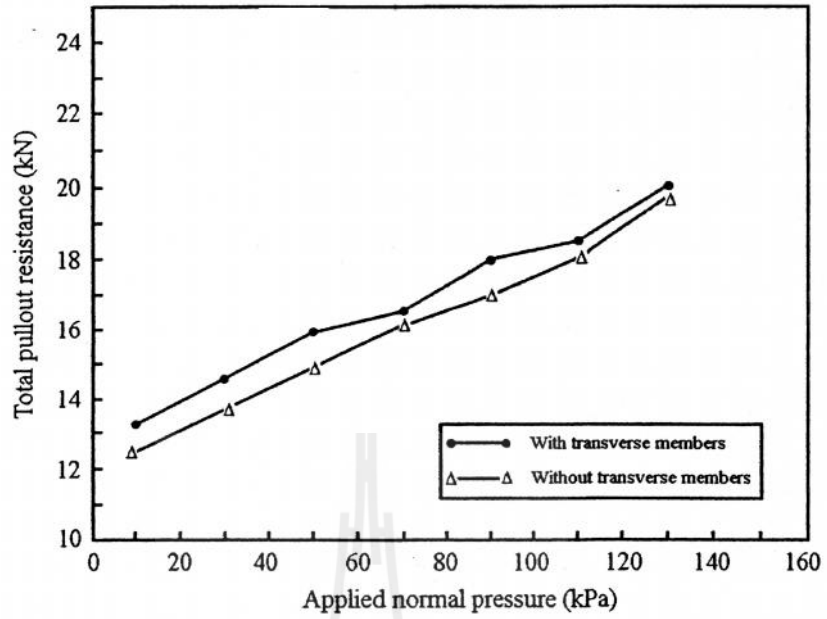
2.5.2.2 Bearing resistance

The bearing resistance is induced only on the area of grid transverse members perpendicular to the pullout force (see Figure 2.10 for inextensible grid reinforcement) and denoted as P_b. For grid reinforcements, bearing resistance can be expressed simply in the following equation:

$$P_b = \overline{\sigma}_b nd \tag{2.6}$$

where $\overline{\sigma}_b$ is maximum bearing stress against a single transverse members, n is number of transverse members and d is diameter or width of a single transverse member being normal to the maximum bearing stress.

The maximum bearing stress of a single transverse member can be estimated by applying three different failure mechanisms; the first is general shear failure mode or known as bearing capacity failure mode (Peterson and Anderson, 1980), the second is punching shear failure mode (Jewell et al., 1984), and the last is modified punching shear failure mode (Chai, 1992). The first failure mode tends to occur possibly for inextensible grid reinforcements, while the second and the last are likely to occur for extensible grid reinforcements. Such three failure mechanisms are illustrated in Figure 2.12a, 2.12b, and 2.12c.
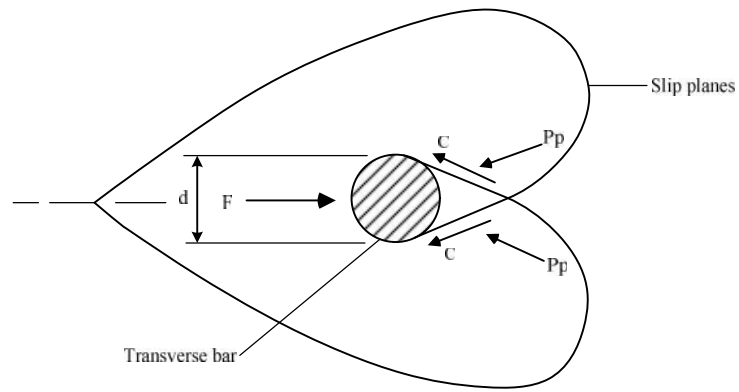
a) Bearing capacity failure mode
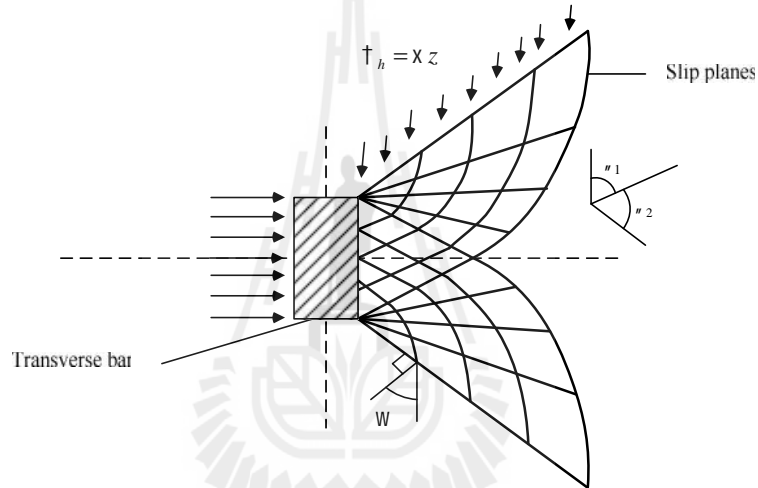
b) Punching shear failure mode
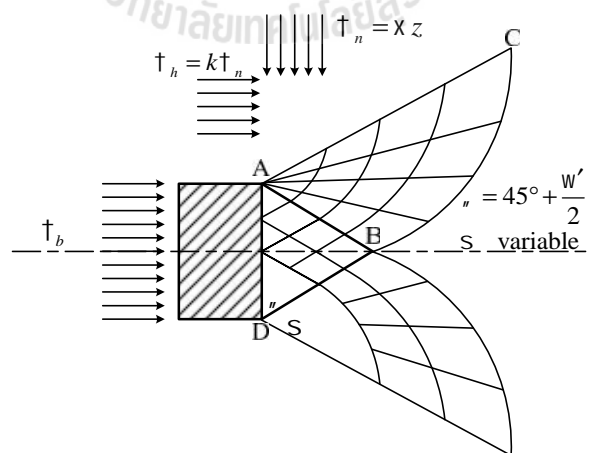
c) Modified punching shear failure mode

Figure 2.12   Modes of failure mechanism

a) **Bearing capacity failure mode**

Bearing capacity equation was proposed by Prandtl (1992). This equation is based on inextensible grid reinforcements, and Terzaghi's bearing capacity equation of a shallow foundation. The equation can thus be expressed as follows:

$$\overline{\dagger}_b = cN_c + \dagger_n N_q \tag{2.7}$$

$$N_c = \cot w (N_q - 1) \tag{2.8}$$

$$N_q = \exp(f \tan w) \tan^2 \left(\frac{f}{2} + \frac{w}{2} \right) \tag{2.9}$$

where $\dagger_b$ is maximum bearing stress of a single transverse member, c is cohesion based on effective stress, w is effective friction angle of backfill soil and N_c, N_q are bearing capacity factors.

b) **Punching shear failure mode**

This failure mode is based on extensible grid reinforcements and will occur if the ratio of foundation depth to width is more than 6.0. According to Jewell et al. (1984), the maximum bearing stress, $\overline{\dagger}_b$ can be calculated as follows:

$$\overline{\dagger}_b = \dagger_n N_q \tag{2.10}$$

$$N_q = \exp\left\{ \left(\frac{f}{2} + w \right) \tan w \right\} \left(\frac{f}{4} + \frac{w}{2} \right) \tag{2.11}$$

where $\dagger_n$ is applied normal stress, N_q is bearing capacity factor different from those in Eqs. 2.8 and 2.10.

If the soil behavior is perfectly plastic and the problem satisfies the above equation, the solution is the exact solution. From several test results, they revealed that the bearing capacity and punching shear failure modes provided the apparent upper and lower bounds for the actual pullout test results (Palmeira and Miligan, 1989; Jewell, 1990). In other words, neither of such failure modes might represent pullout failure mechanisms well.

c) Modified punching failure mode

This failure mode is based on extensible grid reinforcements as well. However, Chai (1992) proposed the modified N_c and N_q for Eq. 2.7 as follows:

$$N_c = \frac{1}{\sin w} \exp^{(2s\,\tan w)} \tan\left(\frac{f}{4} + \frac{w}{2}\right) - \cot w \tag{2.12}$$

$$N_q = \left[\frac{1+k}{2} + \frac{1-k}{2}\sin(2s - w)\right]\frac{1}{\cos w}\exp^{(2s\,\tan w)}\tan\left(\frac{f}{4} + \frac{w}{2}\right) \tag{2.13}$$

where s is angle of rotational failure zone and k is horizontal earth pressure coefficient.

2.5.3 Interference factor coefficients

The transverse member interference, R, of the bearing member has a strong influence on pullout resistance. Generally, the larger this ratio, the higher the pullout passive bearing resistance for an individual bearing member (Bergado and Chai, 1994). Introduced as a bearing resistance ratio, R is a function of S/D as follows:

$$R = a + b\left(S/D\right)^{nr} \tag{2.14}$$

where a, b and nr are constants.

Bergado et al. (1996) found that the bearing resistance ratio, R, corresponds to S/D ratios. The S/D ratios influence the bearing resistance of individual member in range of 1 to 45. If S/D is closed to one, the grid behaves like a rough sheet and for S/D beyond 45 the bearing resistance of individual transverse member is not affected by S/D ratios. Furthermore, some constant parameters have been defined and expressed in term of S/D ratio which is needed for prediction of pullout force/displacement relationship.

2.5.4 The factors affecting the interference resistance

There are a large number of factors that affect the pullout resistance of the grid reinforcement. The parameters pertaining to the type of soil are the shear strength characteristics, dilatancy properties, relative density, the overburden pressure and the fine grained portion of soil. The parameter pertaining to the reinforcement type is the geometry, apertures on the reinforcement, extensibility, creep and the orientation of the grid.

2.5.4.1 Grain size

Previous studies on influence of grain size particle have only been performed on geogrid and geotextiles. The influence of grain size on grid pullout resistance is expressed by the ratio between bearing member thickness, D and the diameter of soil particles at which 50% of the soil is finer, D_{50} (D/D_{50}). Under the condition of D_{50} less than the grid opening, the larger the grain size, smaller the $D/$
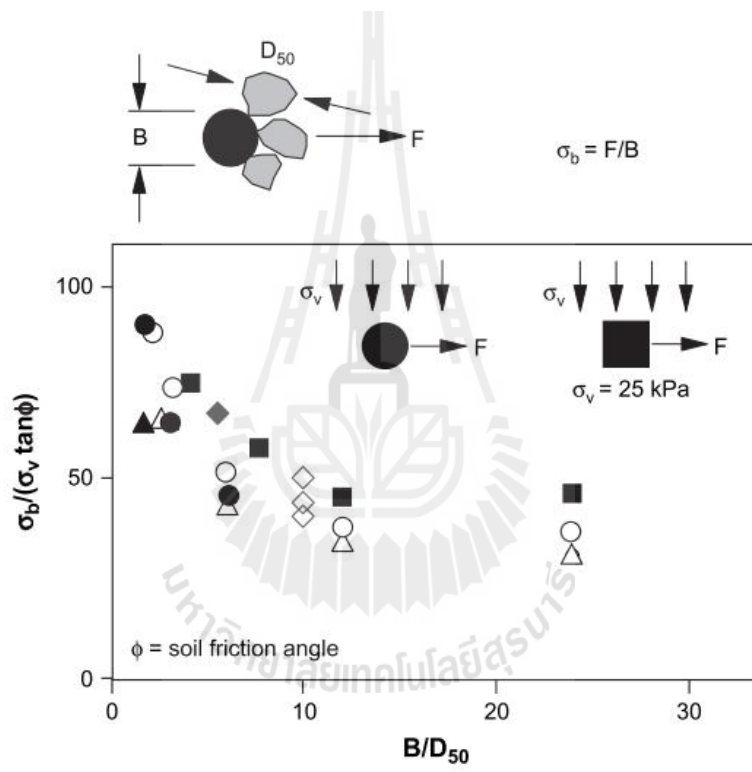
the sides of the soil block and increasing the average normal stress on the reinforcement. The degree of the influence is controlled largely by the friction characteristics of the front wall and the distance between the first bearing member and the front wall. The rougher the front wall, the higher the pullout resistance. The pullout resistance for perfect rougher case with glued sand on the front wall can be 2 times that of a smooth case where an arrangement of double layers of polythene, grease and oil were laid on the front wall (Palmeira and Milligan, 1989). The influence of the distance between the front wall and first bearing member on the pullout resistance has also been investigated by Palmeira and Milligan (1989). It has been found that for a single bearing member, when the distance is smaller than 15 times the bearing member thickness, the front wall begins to influence the pullout resistance significantly. For direct shear test near the boundary, the stress condition is very complex and the stress distribution over the shear plane is not uniform influencing the interpretation of the test result.

2.6 Pullout resistance of bearing reinforcement

2.6.1 Pullout Friction Resistance

Figure 2.14 shows a pullout test result of a longitudinal member with a diameter of 16 mm and length of 2.6 m. Maximum pullout friction resistance, P_f of the longitudinal member can be calculated from

$$P_f = f\, DL\, \sigma_n \tan u \tag{2.15}$$

where D and L are diameter and length of the longitudinal member, respectively, σ_n is normal stress and δ is the skin friction angle.

It is of interest to mention that δ is quite high with its value of 58.7 degrees. Consequently, δ/ϕ ratio is greater than unity and is about 1.47. The δ/ϕ ratio of 1.0 was recommended for design (Horpibulsuk and Niramitkornburee, 2010). This high ratio is due to the contribution of the skin roughness of the deformed bar.

Figure 2.15 shows comparison of maximum pullout bearing resistance of a single isolated transverse member. It is found that the maximum pullout bearing resistance can be determined from the plasticity solutions. The maximum bearing stress, $\sigma_{b\max}$, of a single transverse member in coarse-grained soil can be predicted by modified punching shear failure mechanism.

$$\sigma_{b\max} = N_q \sigma_n \tag{2.16}$$

$$N_q = \frac{1}{\cos\phi} \exp[\pi \tan\phi] \tan\left(\frac{\pi}{4} + \frac{\phi}{2}\right) \tag{2.17}$$

(a)

(b)
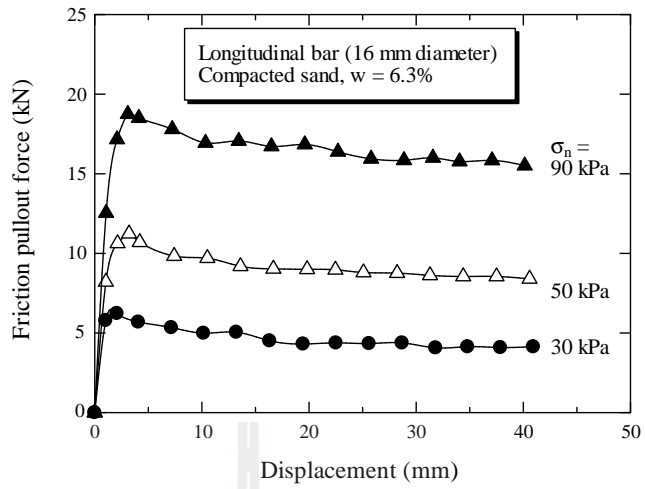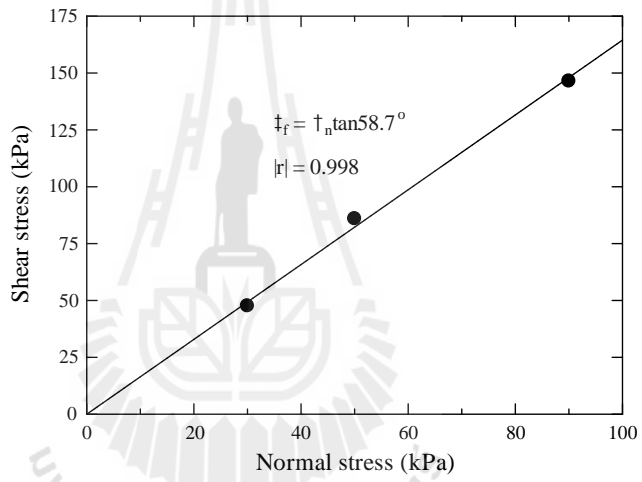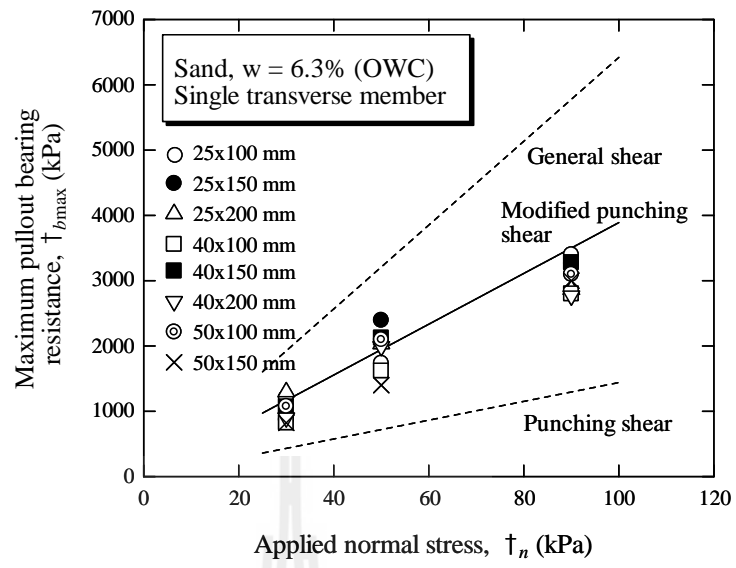
P_{bn}

is found that when S/B is larger than 25, there would be no more transverse member interference. Thus, this ratio is referred to as free interference spacing ratio. When S/B is less than 3.75, the shear surface caused by each transverse member joins together to form a rough shear surface and only the first transverse member causes bearing resistance. In this case, all the transverse members would act like a rough block. As such, the maximum pullout bearing resistance is determined from the sum of the friction on the block sides and the bearing capacity of the first transverse member. Since the bearing capacity is more dominant, the pullout bearing resistance is close to that of a single isolated transverse member. This S/B ratio is thus defined as a rough block spacing ratio. From this finding, the failure mechanism of the bearing reinforcement is classified into three zones, depending upon S/B ratio as shown in Figure 2.16. Zone 1 is referred to as block failure when $S/B \leq 3.75$. Zone 2 is regarded as member interference failure when $3.75 < S/B < 25$. Zone 3 ($S/B \geq 25$) is individual failure where soil in front of each transverse member fails individually.

The level of transverse member interference can be expressed by the interference factor, R. It is defined as the ratio of the average maximum pullout bearing force of the bearing reinforcement with n transverse members to that of a single isolated transverse member.

$$F = \frac{P_{bn}}{nP_{b1}}$$ (2.18)

The higher the level of transverse member interference (the lower the S/B), the lower the P_{bn}, and hence the lower the R. Based on the analysis of the test

data, it is found that the interference factor is mainly dependent upon S/B, and n, irrespective of L and applied normal stress. The following equation for interference factor is hence:

$$F = a + b \ln \left(\frac{S}{B} \right) \qquad (2.19)$$

These two constants, a and b can be obtained with the two physical conditions: 1) when S/B equals 3.75, the interference factor equals $1/n$ since P_{bn} and P_{b1} are the same, and 2) when S/B equals 25, the interference factor equals unity. These two conditions establish the lower and upper values of R at corresponding values of $S/B = 3.75$ and 25, respectively. From these two conditions, the constants a and b can be determined by the following equations:

$$b = 0.527 \left[1 - \frac{1}{n} \right] \qquad (2.20)$$

$$a = 1 - 3.219b \qquad (2.21)$$

As such, a and b values are 0.152 and 0.264, -0.132 and 0.351, and -0.273 and 0.395 for $n = 2$, 3, and 4, respectively. Using these a and b values for different n, the maximum pullout bearing resistance can be predicted as shown by the solid lines in Figure 2.16. The laboratory P_{b1} values ($P_{b1} = 6.4$, 12.7, and 19.7 kN for $n = 2$, 3, and 4, respectively) are used for this prediction.

Maximum pullout bearing force, P_{bn} (kN)

Spacing ratio, S/B

n = 2

$\sigma_n =$

90 kPa

Zone 1: Block failure

Zone 2: Member interference failure

Zone 3: Individual failure

P_{bI} (kN) =

19.7

12.7

6.4

50 kPa

30 kPa

$F = 0.152 + 0.264\ln(S/B)$

n = 3

$\sigma_n = 90$ kPa

$\sigma_n = 50$ kPa

$\sigma_n = 30$ kPa

$F = -0.132 + 0.351\ln(S/B)$

n = 4

$\sigma_n = 90$ kPa

$\sigma_n = 50$ kPa

$\sigma_n = 30$ kPa

$F = -0.273 + 0.395\ln(S/B)$

× L = 10 cm
▲ L = 15 cm
☐ L = 20 cm
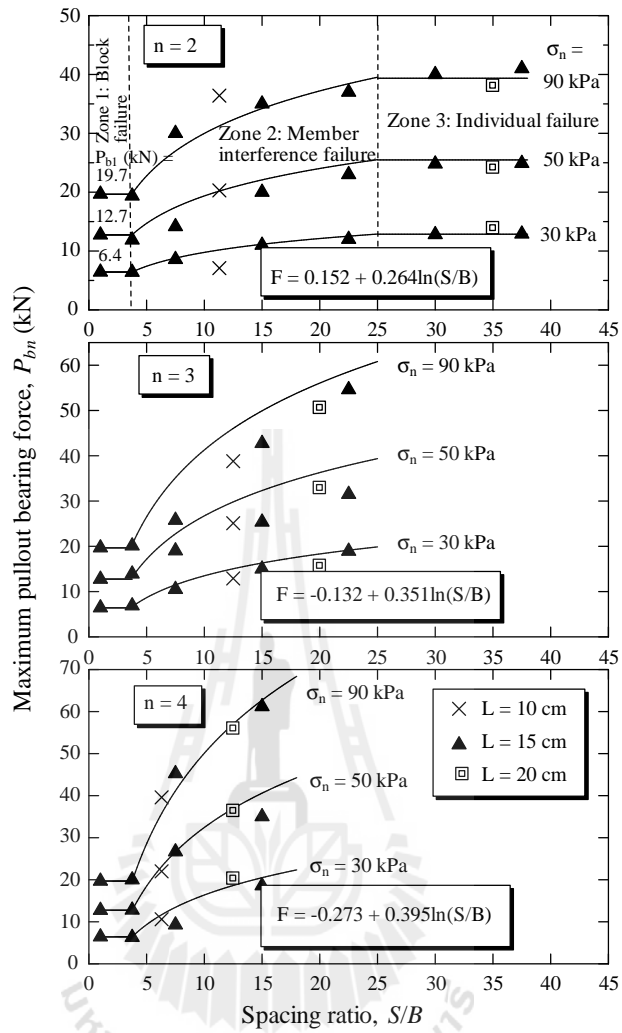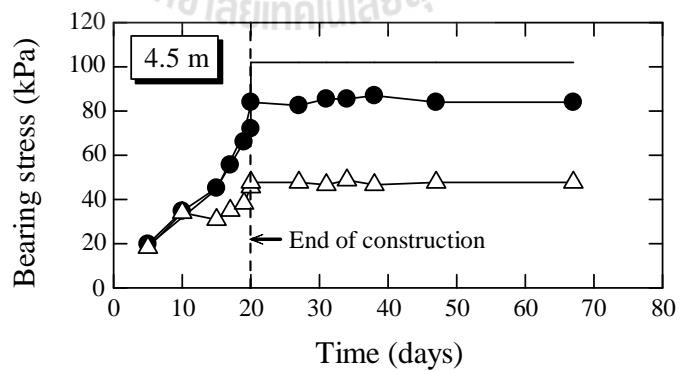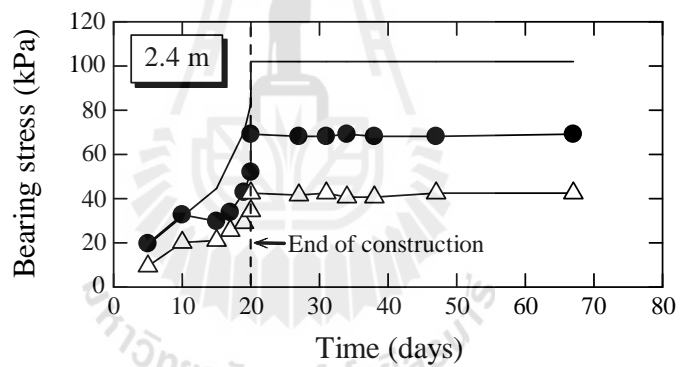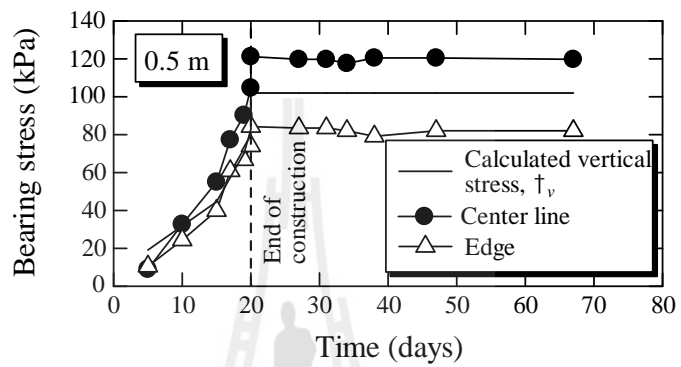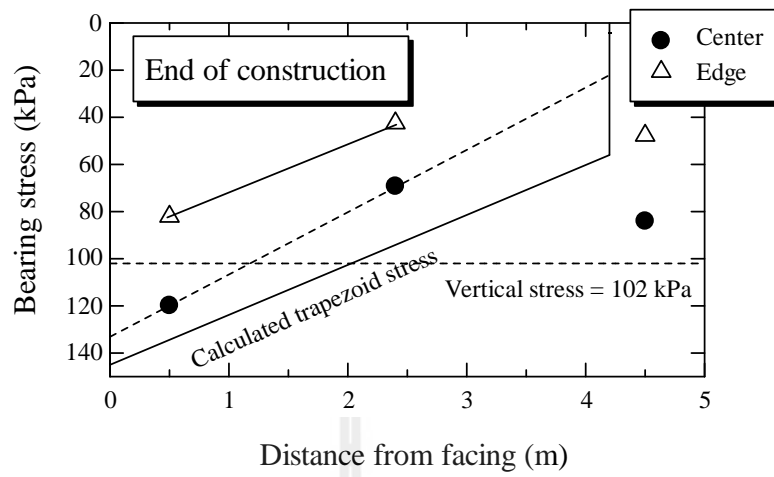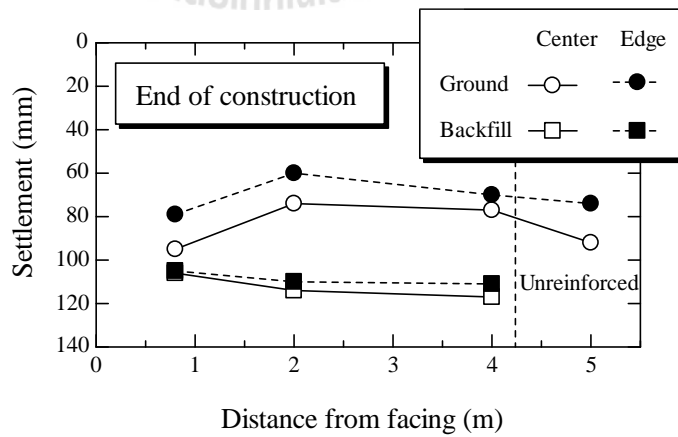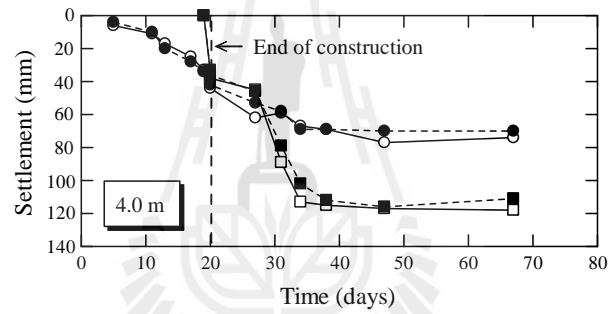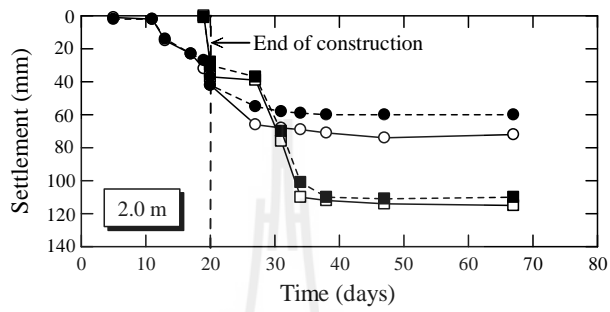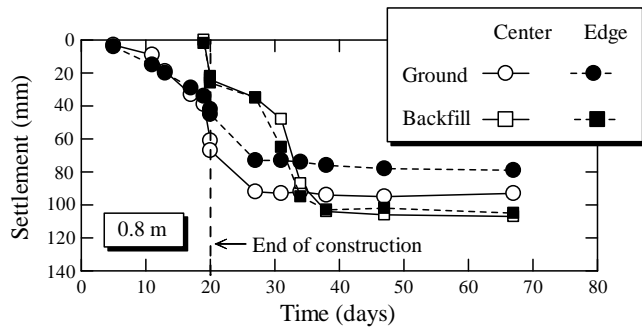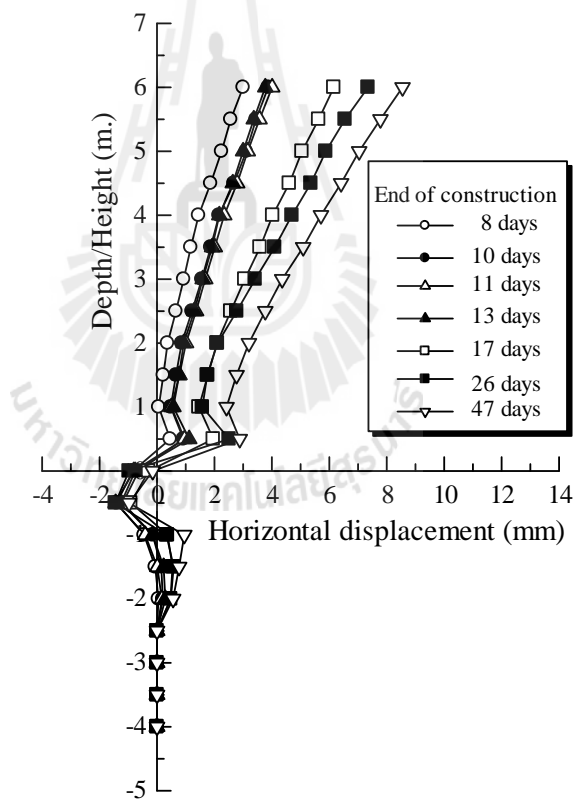
2.7.4 Coefficient of lateral earth pressure

The coefficients of lateral earth pressure for any backfill load were the ratios of the lateral earth pressure, $\dagger_h$, to the vertical pressure, $\dagger_v$. The lateral earth pressures at the maximum tension in reinforcement were determined from the strain gauges on the reinforcement and the lateral earth pressures at wall facing panels were measured from earth pressure gauges attached to the wall facing panels. The K for the maximum tension in reinforcement is used for designing the internal stability of the earth wall (pullout and rupture failure criteria) whereas the K at the wall facing panels is used for designing the tie points and facing panels.

Figure 2.22 shows the relationship between the wall depth (1/wall height) and the coefficients of lateral earth pressure at the maximum tension in the reinforcements after the completion of construction, compared with those for the other reinforcements (Christopher et al., 1990 and Bergado et al., 1999). Figure 2.22 shows the relationship between K and depth at the wall face and at maximum tension compared with that recommended by AASHTO (1996). ASSHTO (1996) recommends that at the maximum tension, the lateral earth pressure, $\dagger_h$, at each reinforcement level of an earth wall with inextensible reinforcements shall be calculated using $K = K_0$ at the top of the wall and decreases linearly to $K = K_a$ at 6 m depth. Below a 6 m depth, $K = K_a$ shall be used. It is found from Figure 2.23 that the measured K for the maximum tension in the bearing reinforcements is in agreement with this recommendation.
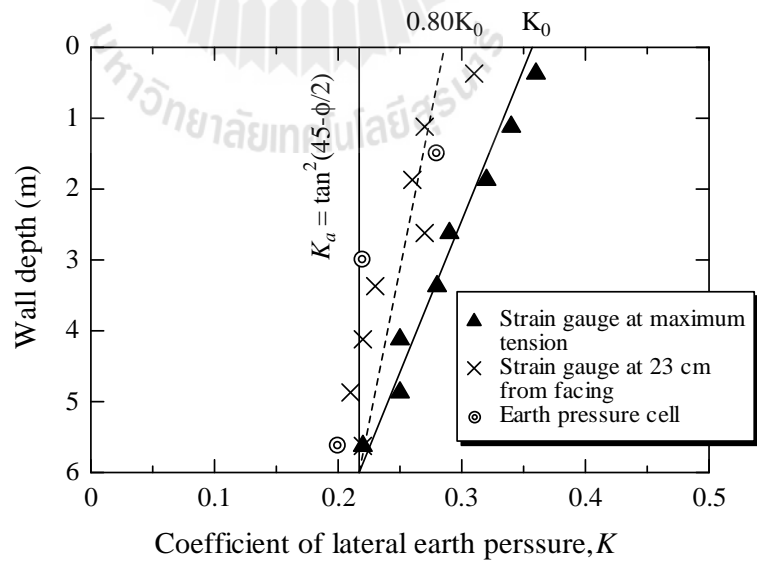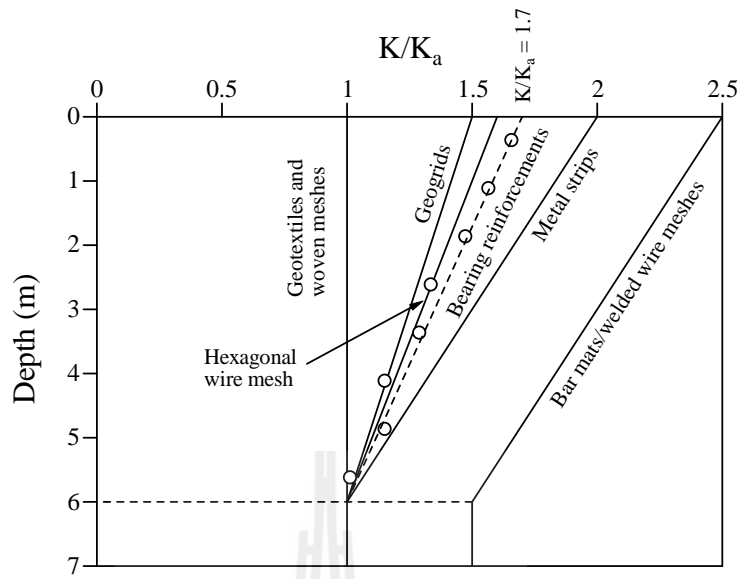
2.7.5 Possible failure plane

The initial reading on strain gage was taken from zero tension. Subsequent readings were then taken as that wall was constructed and past construction. From the strains calculate, the tensions in the wire can be computed as:

$$T = EA\vee \tag{2.22}$$

where T is axial tension in reinforcing wire, E is modulus of elasticity of steel, A is cross-sectional area of the reinforcing wire and $\vee$ is axial strain in the reinforcing wires.

Figure 2.24 illustrates the reinforcement tension measured at 14 days after the completion of construction and 10 days after additional surcharge load. The maximum tension line (possible failure plane) of the bearing reinforcement corresponds to the bilinear type of maximum tension line (coherent gravity structure hypothesis) as expected for metal strip and steel grids (AASHTO, 1996, 2002; and Anderson et al., 1987, Bergado et al., 1998; and Chai, 1992).
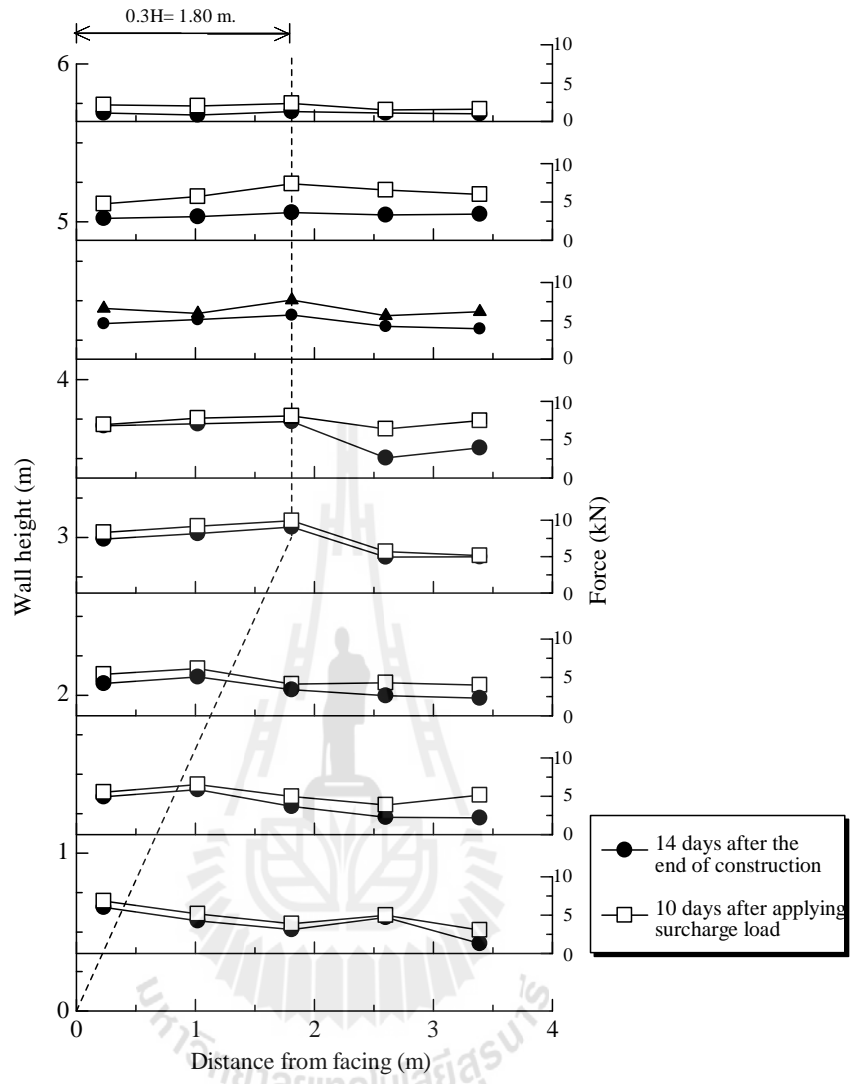
namely: discrete material and composite material. Although the discrete approach needs more computer time, it is preferable because the properties and responses of soil/reinforcement interaction properties are key factors that control its performance. Hence, the discrete approach is used in this research, and is discussed in detail in the following sections.

2.8.1 Elasto-plastic model

The elasto-plastic model is characterized by: the yield function, the flow rule, and the hardening law. The strain due to any increment of stress can be divided into two components: elastic strain and plastic strain. For conditions where the stress state is in yield locus, an increment stress can only cause elastic strain. If the stress conditions correspond to a point on the yield surface and if the material is stable, the increment of stress produces elastic and plastic strain. There are several elastoplastic models for soils as discussed below.

2.8.1.1   Elasto-perfectly-plastic Mohr Coulomb model

The relationship between effective stress rate and strain rate for elastoplasticity (Smith and Giffith, 1988) are given as follows:

$$\dagger^{'} = \left[D^e - \frac{r}{d} D^e \frac{\partial g}{\partial \dagger^{'}} \frac{\partial f^T}{\partial g} D^e \right] \vee \tag{2.23}$$

$$d = \frac{\partial f^T}{\partial \dagger^{'}} D^e \frac{\partial g}{\partial \dagger^{'}} \tag{2.24}$$

where f is yield function, g is plastic potential function, σ' is effective stress tensor, ε is strain tensor and D^e is elastic constitutive matrix.

The term λ is used as a switch. If material behavior is elastic which, the value of λ is zero. For plastic behavior, λ is unity.

The yield function for Mohr Coulomb model is defined as three yield functions, which are formulated in terms of principal stress (Smith and Griffith, 1988) as follows:

$$f_1 = \frac{1}{2}\left|\sigma_2 - \sigma_3\right| + \frac{1}{2}\left|\sigma_2 + \sigma_3\right|\sin\phi - c\cos\phi \geq 0 \tag{2.25}$$

$$f_2 = \frac{1}{2}\left|\sigma_3 - \sigma_1\right| + \frac{1}{2}\left|\sigma_3 + \sigma_1\right|\sin\phi - c\cos\phi \geq 0 \tag{2.26}$$

$$f_3 = \frac{1}{2}\left|\sigma_1 - \sigma_2\right| + \frac{1}{2}\left|\sigma_1 + \sigma_2\right|\sin\phi - c\cos\phi \geq 0 \tag{2.27}$$

where ϕ is friction angle of soil, c is cohesion intercept.

The plastic potential functions are defined as follows:

$$g_1 = \frac{1}{2}\left|\sigma_2 - \sigma_3\right| + \frac{1}{2}\left|\sigma_2 + \sigma_3\right|\sin\psi \tag{2.28}$$

$$g_2 = \frac{1}{2}\left|\sigma_3 - \sigma_1\right| + \frac{1}{2}\left|\sigma_3 + \sigma_1\right|\sin\psi \tag{2.29}$$

$$g_3 = \frac{1}{2}\left|\sigma_1 - \sigma_2\right| + \frac{1}{2}\left|\sigma_1 + \sigma_2\right|\sin\psi \tag{2.30}$$

where ψ is the dilation angle.

In order to model the influence of stress level on the material stiffness, a simple power law for the shear modulus is introduced (Vermeer and Brinkgreve, 1995):

$$G = G_{ref} \left(\frac{P^*}{P_{ref}} \right)^m \tag{2.31}$$

where $P^* = -\frac{1}{3}(\dagger_1 + \dagger_2 + \dagger_3) + c \cot w$, G_{ref} is reference shear modulus, corresponding to $P^* = P_{ref}$, P_{ref} is reference pressure model parameters for and m is power number.

Thus, the Mohr Coulomb model required a total of given parameters which are G_{ref}, P_{ref}, m, €, w, c, {, which are familiar to most geotechnical engineers.

2.8.2 Soil and reinforcement interface model

In PLAXIS program, the stress-strain behavior at soil-interface is simulated by elastic, perfectly-plastic interface model. The model parameters at soil-structure interface can be generated from that soil using the interface coefficient, R_{inter}, defined as the ratio of the shear strength of the interface to the corresponding shear strength of the soil (Vermeer and Brinkgreve, 1995) as follows:

$$\tan u = R_{inter} \tan w \tag{2.32}$$

$$c_i = R_{inter} c \tag{2.33}$$

$$G_i = R_{inter}^2 G \tag{2.34}$$

where G is shear modulus of soil that contacts with reinforcement, G_i is shear of

interface element, w is angular of friction of soil contacted with reinforcement and

u is angular of friction of interface element.

2.8.3   The influential parameters

There are many parameters that affect the behavior of reinforced wall

such as interaction between reinforcement and soil, angular friction of backfill soil

and stiffness of the reinforcement, etc. Alfaro (1996) has studied the effect of the

stiffness of the reinforcement to the behavior of reinforced soil wall using FEM. Two

embankments were constructed in the campus of the Asian Institute of Technology.

The reinforcement were steel grid (Bergado et al., 1991b) and Tenax geogrid

(Bergado et al., 1994). Back analysis and parametric study were done. The conclusion

was that the increase in stiffness or rigidity of reinforced soil system leads to smaller

lateral movements of soil foundation and provides higher settlement at or the near the

toe. On the other hand, lower reinforced soil system stiffness results in lower

settlement at the toe with its maximum value located away from the toe to the interior

portion. The role of reinforcement extensibility to tensions in the reinforcement is that

the stiff reinforcements exhibit high tensions under working conditions.

Rowe and Ho (1997) have studied the influential parameters based on

finite element analysis of the continuous wall on rigid foundation with full facing

panel and hinge toe. Granular backfill was used in the analysis. The effect of the

influential parameters on the horizontal and the vertical forces developed within the

reinforced soil system are shown in Figure 2.25, 2.26 and 2.27. The influential

parameters consist of reinforcement stiffness, backfill friction angle and facing/soil

Note: $\delta = 2/3\phi$ $\phi_{rs} = \phi$ $\gamma = 20 kN/m^3$ $J = 2000 kN/m$
$H = 6m$ $L/H = 0.708$ $S_v = 1m$ $n = 6$

■ 1: vertical reaction at toe of wall
□ 2: horizontal reaction at toe of wall
○ 3: sum of force at facing/reinforcement joint
● 4: sum of maximum force in reinforcement
▽ 5: sum of 2 and 3: (total force required for external equilibrium of facing)
▼ 6: sum of 2 and 4 (total force required for internal equilibrium of reinforced soil block)

Note: $\phi=35°$ $\phi_{rs}=35°$ $\gamma=20kN/m^3$ $J=2000kN/m$
$H=6m$ $L/H=0.708$ $S_v=1m$ $n=6$
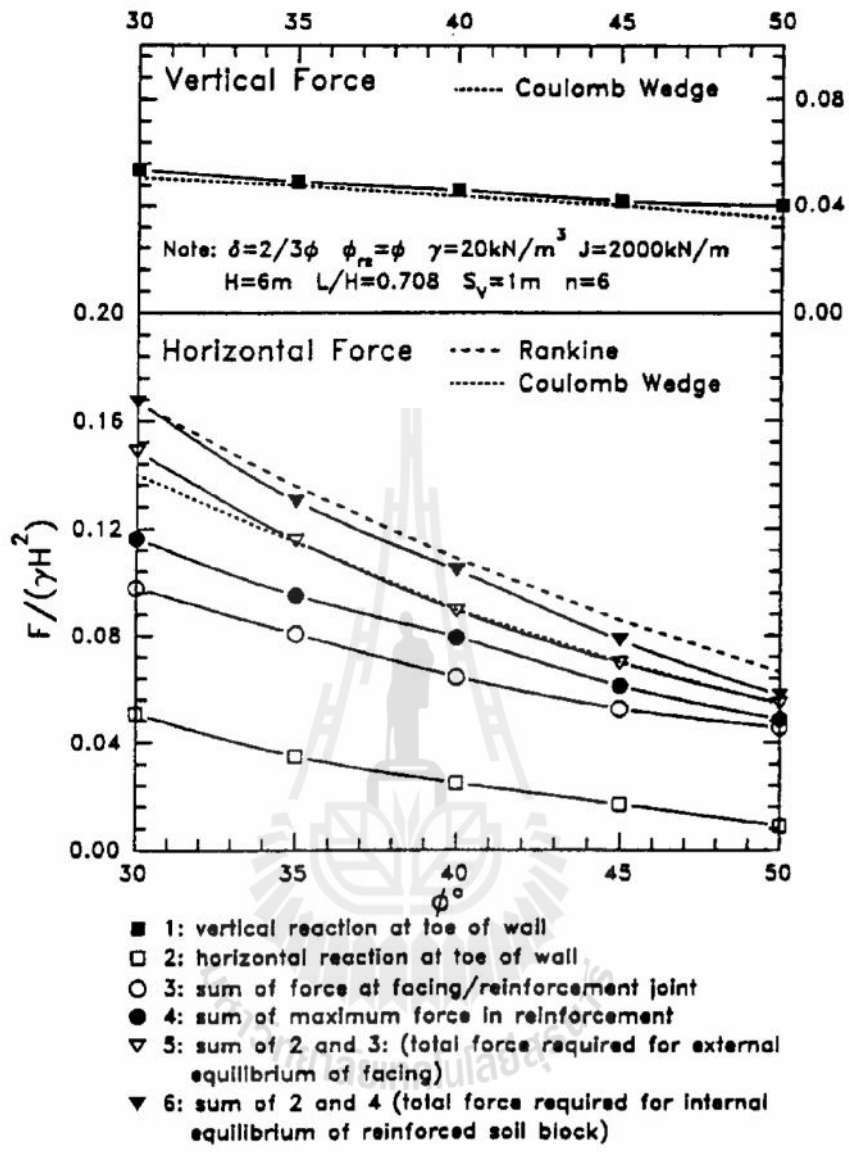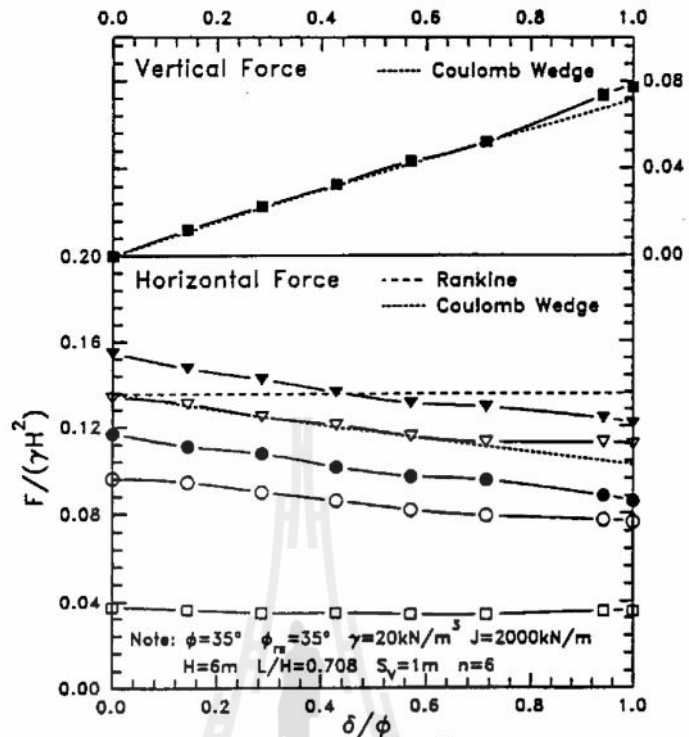
■ 1: vertical reaction at toe of wall
□ 2: horizontal reaction at toe of wall
○ 3: sum of force at facing/reinforcement joint
● 4: sum of maximum force in reinforcement
▽ 5: sum of 2 and 3: (total force required for external equilibrium of facing)
▼ 6: sum of 2 and 4: (total force required for internal equilibrium of reinforced soil block)

as an elastoplastic material with a Mohr-Coulomb yield function and a non-associated flow rule. It is indicated that internal equilibrium should be analyzed via Rankine state. Moreover, external equilibrium should be done by means of Coulomb active wedge analysis. Further study was carried out in Rowe and Ho (1998). As illustrated in Figure 2.29, it was clearly shown that the most important parameters were the reinforcement stiffness factor, $\wedge$, and the backfill soil friction angle, W. The other parameters (i.e., soil-facing interface angle, reinforcement-soil friction angle, soil Young's modulus and facing rigidity) are relatively less important. Rowe and Ho (1998) also demonstrated for a certain value of the reinforcement stiffness factor, as illustrated in Figure 2.30.

The reinforcement stiffness factor can be expressed as follows:

$$\wedge = \frac{J}{K_a x HS_v} \tag{2.35}$$

where $J = EA$ is the reinforcement stiffness, E is the Young's modulus of reinforcement, A is the cross section, K_a is the Rankine's active earth pressure coefficient, x is the unit weight of the soil, H is the wall height and S_v is the vertical spacing between layers of reinforcement.

$$u_r = \frac{PL}{EA} = \frac{PL}{J} \tag{2.36}$$

$$P = \left(\frac{J}{L}\right) u_r \tag{2.37}$$
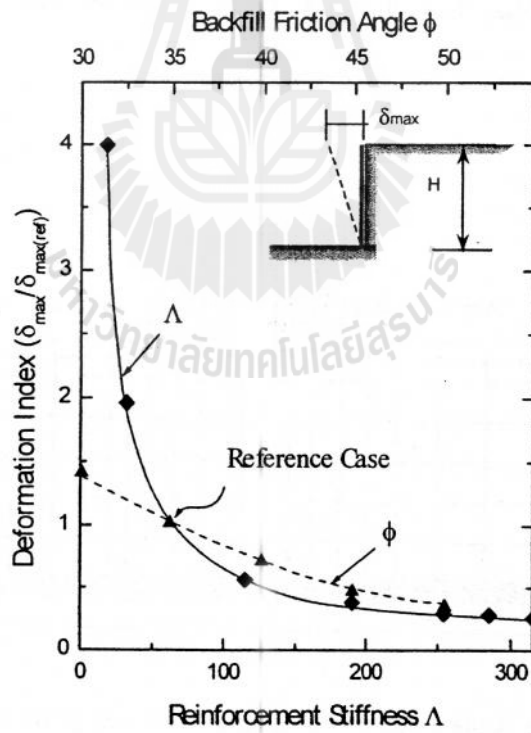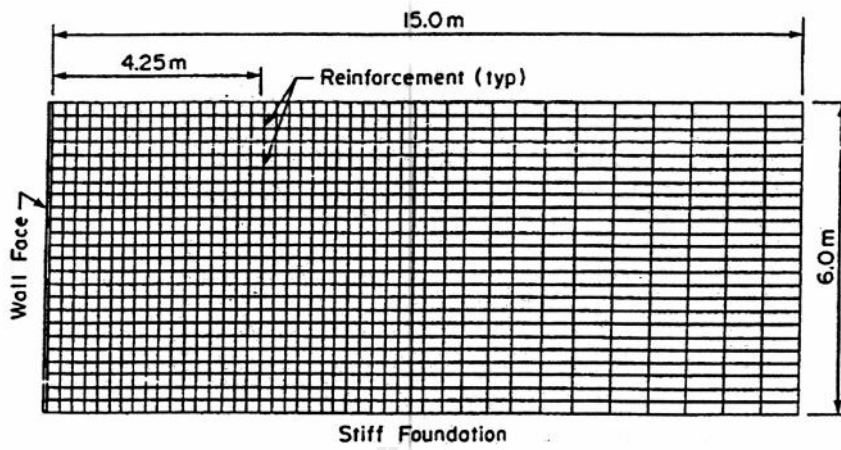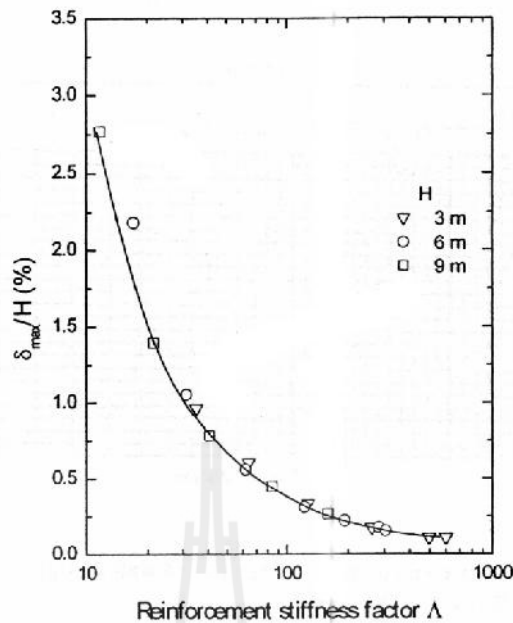
Figure 2.30   Effect of reinforcement stiffness factor, $\wedge$ on normalized maximum

deformation at wall face $\left(u_{max}/H\right)$ for three wall height, H

(Rowe and Ho, 1998)

Ling and Leshchinsky (2003) conducted a series of numerical studies using finite elements to investigate the effect of several design parameters on the performance of modular-block GRS-RWs. The main conclusions were: the response of the wall and reinforcement was not sensitive to the change in stiffness in the case of an elastic foundation; the length of reinforcement provided in the base case (L/H=0.5) gives a satisfactory performance; force distribution of reinforcement changed from a trapezoid to a parabola when the spacing was increased; lateral displacement of reinforcement shifted from parabolic to trapezoidal when stiffness increased. The width of the block affected the wall behavior in terms of lateral

displacement and the behavior did not seem sensitive to the variation in the friction angle between the block and the connection strength.

Hatami and Bathurst (2006) constructed four full-scale reinforced-soil segmental retaining walls and simulated using the FLAC program. Results of this study showed that it is important to include compaction effects in the simulations in order to accurately model the construction and the surcharge loading response of the reinforced soil walls. Comparison of predicted and measured results of reinforcement load and displacement suggested that the assumption of a perfect bond between the reinforcement and soil may not be valid. They suggested using and interface that accommodates potential slippage between the reinforcement and soil was warranted.

Yoo and Jung (2006) conducted a comprehension stress-pore pressure coupled finite element analysis to examined positive and negative pore pressures under the collapsed geosynthetic reinforced segmental remaining wall in Korea. A commercially available finite element package (ABAQUS) was used for analyses. The results from the FEM analyses were in accordance with the field observation. Also, the results from the global stability analysis and was effectively used to help identify the underlying mechanism of the effect of rainfall infiltration on slope stability problems.

2.9.2 Reinforced wall on soft foundation

Steel grid reinforced embankment: This fully instrumented embankment was constructed in the campus of Asian Institute of technology in March 1989 (Shivashanker, 1991). The height of this embankment is 5.7 m. The backfills of this reinforced wall were clayey sand, lateritic and weather clay. Chai (1992) performed

finite element analysis on this embankment by using CRISPAIT. The finite element

mesh is shown in Figure 2.31 with plane strain condition. The constitutive model for

the backfill material was elastic-perfactly plastic Mohr Coulomb model. The interface

face element between the reinforcement and the surrounding soil was joint element

(Goodman et al., 1968) with hyperbolic shear stiffness. The results of the analysis

were compared to the full scale test embankment behavior as shown in Figure 2.32

and 2.33. The calculated soil/reinforcement pullout and direct shear mode zones are

shown in Figure 2.34. It is shown that pullout interaction zone is only near the wall

face and at the bottom of the reinforced embankment.
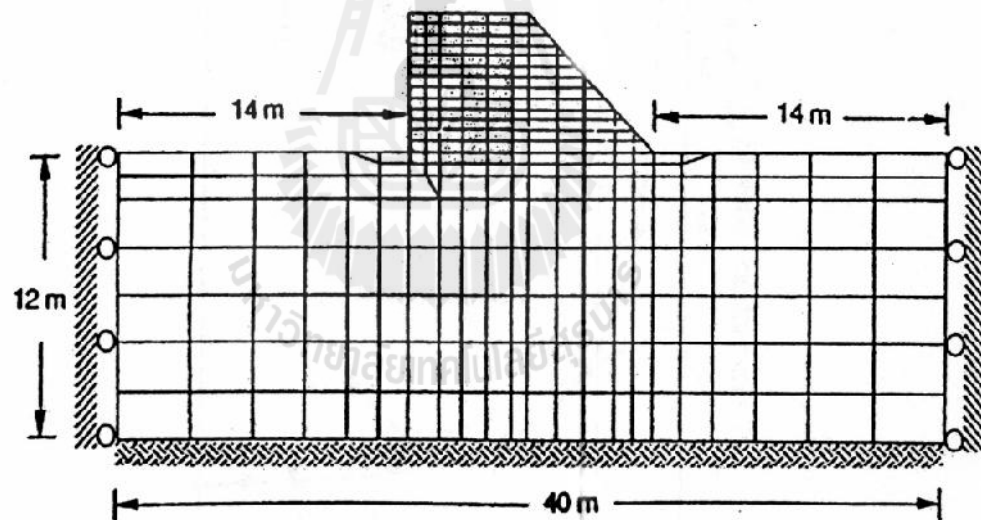
Figure 2.31 Finite element mesh for steel grid reinforced embankment (Chai, 1992)
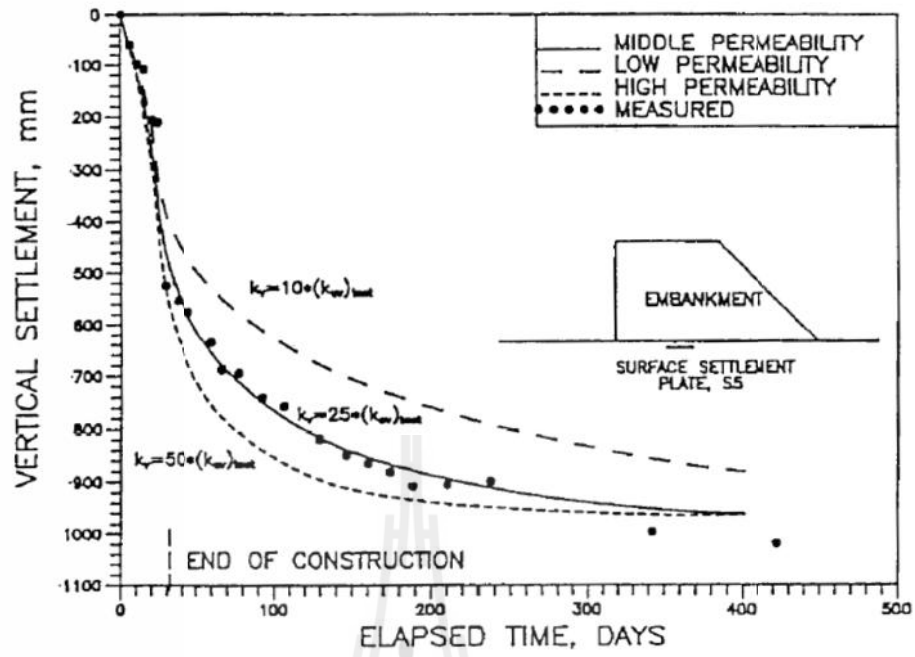
Figure 2.32 Measured and simulation settlement curves (Chai, 1992)
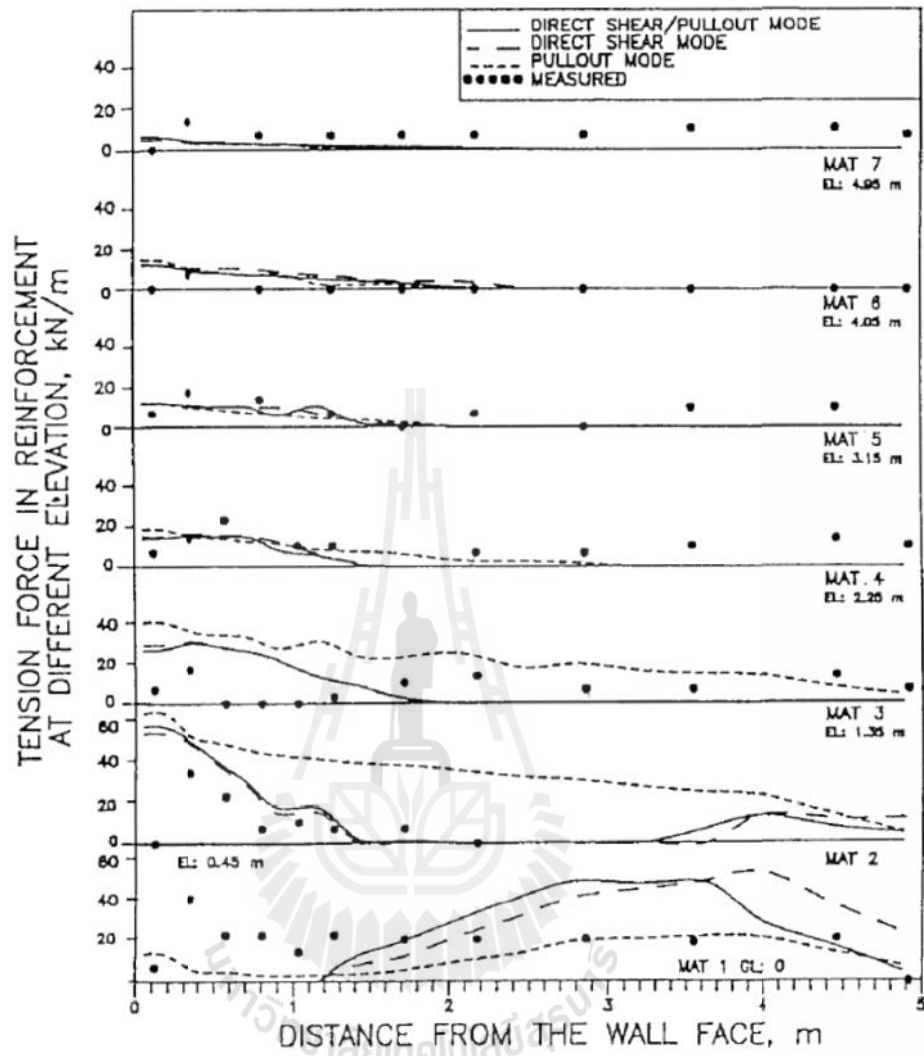
Figure 2.33 Measured and simulation reinforcement tensile force in steel grid reinforced embankment (Chai, 1992)

DIRECT SHEAR MODE

PULLOUT MODE

REINFORCEMENT

1 m
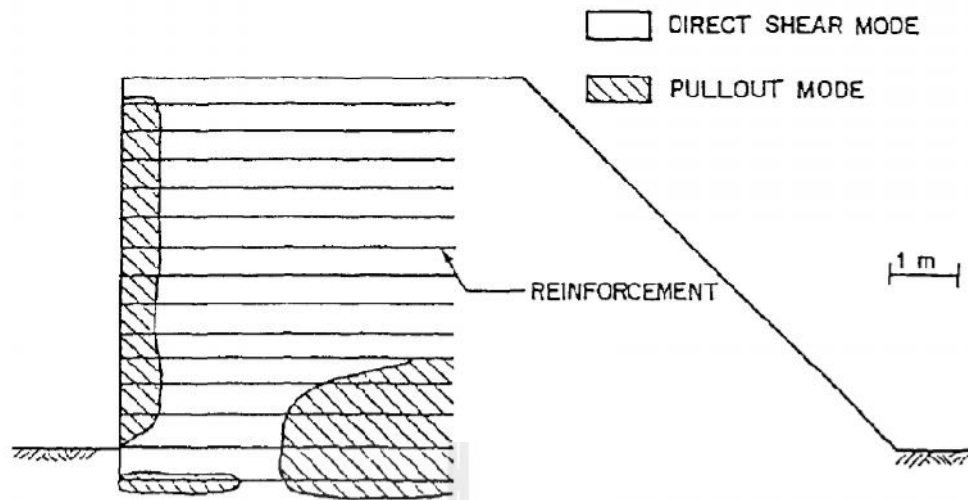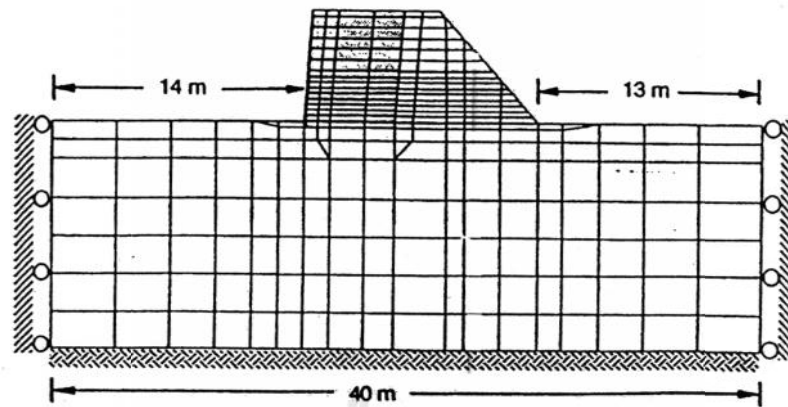
Figure 2.35 Finite element mesh for polymer grid reinforced embankment

(Alfaro, 1996)
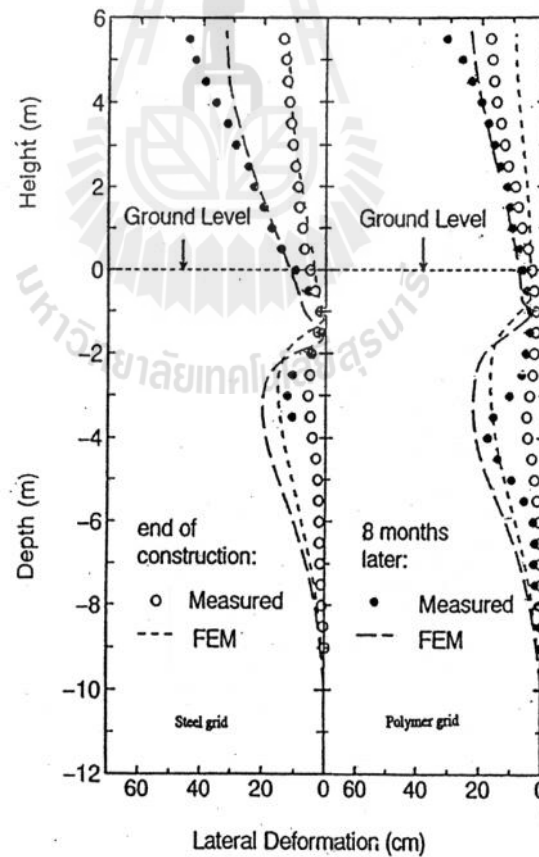
Figure 2.36 Measured and simulated lateral deformation (Alfaro, 1996)

Interaction Mode:
- Pullout
- Direct Shear

reinforcements

(a) end of construction

Interaction Mode:
- Pullout
- Direct Shear

reinforcements
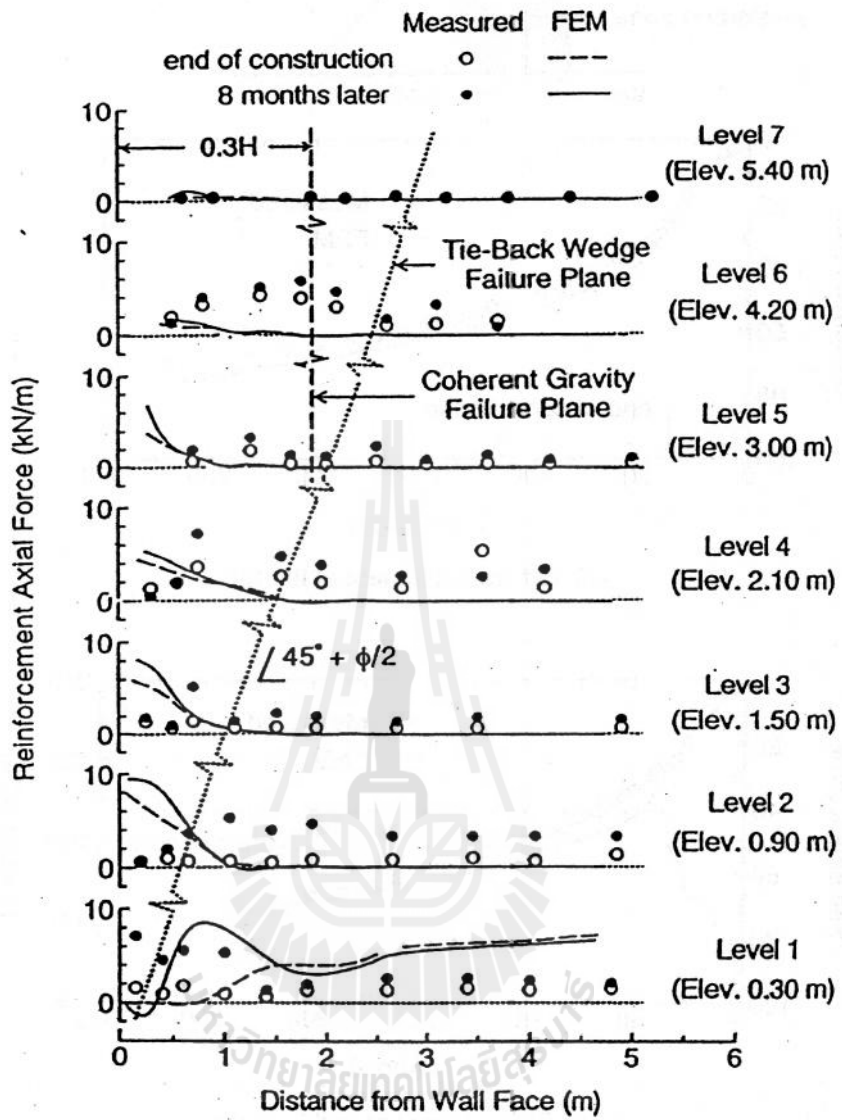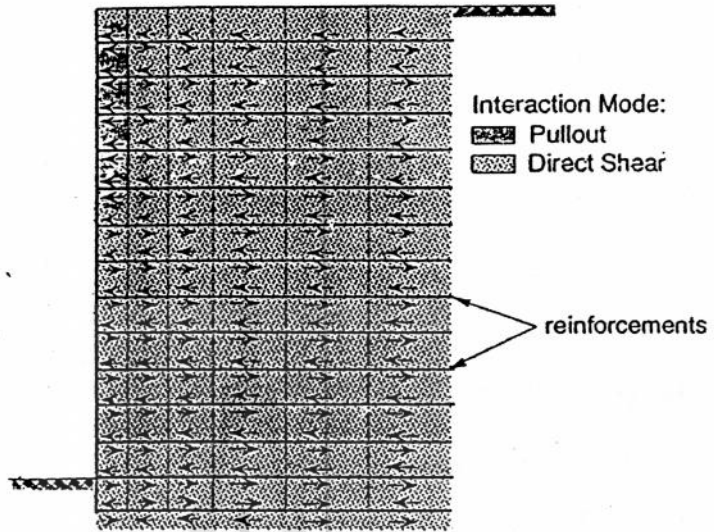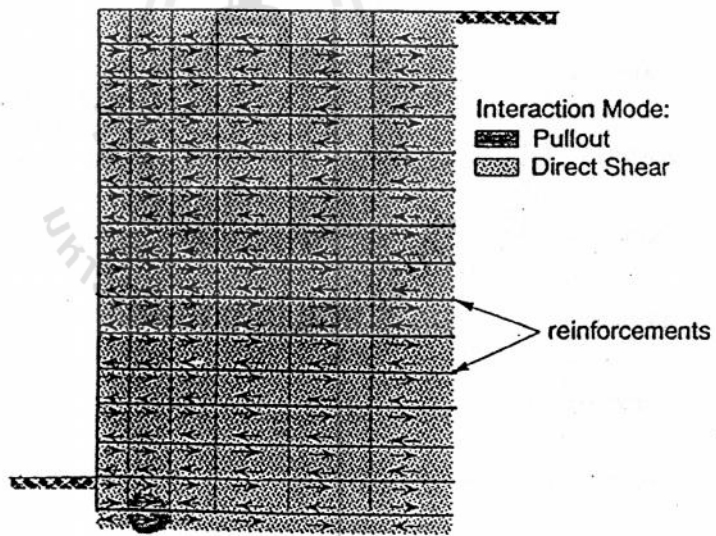
(b) 1 year after construction

Hexagonal wire mesh embankment: The hexagonal wire mesh wall-embankment system was built through the generous financial support of B.B Trading from Malaysia by using camel Brand twisted and coated wire mesh as the reinforcement and silty sand as backfill material (Bergado et al, 2000). The embankment was divided into two sections along its length. Each section was constructed with different types of hexagonal wire mesh, namely: zinc coated and PVC-coated. The construction of the wall involved the placement of the gabion facing unit with reinforcement attachment at very 0.5 m vertical spacing. The gabion facing were filled with boulders and inclined at 10 degree with respect to the vertical alignment. After the gabion wall was placed and filled with boulders, the first reinforcement was placed and instrumented. The backfill was compacted in 0.167 m lifts to a total thickness of 0.50 m with combination of roller compactor and hand compactor around the instrumentation such as settlement plate, standard piezometer, and inclinometer casing. After completion, the embankment was 6.0 m high, 6.0 m long, 6.0 m wide at the top and the base of embankment was 18 m wide. Additional surcharge of 1 m was added on the top of the embankment with one thousand plastic sand bags. Each bag was filled with 40 kgs of Ayutthaya sand and laid in one cubic meter of gabion cage. Thus, the unit weight of additional surcharge load was approximately equal to 16.7 kN/m^2. The behavior of the embankment, which was simulated by PLAXIS (Bergado et al, 2000) and the finite element meshes is shown in Figure 2.39. The properties of the interface element were based on the strength of the interface between reinforcement and surrounding soil. The comparison between the calculation and the field data of the surface settlement plate is shown in Figure 2.40. The comparison between the calculated settlement and the measured data from the

6 m

13. 0 m

20 m   12 m   20 m

Close Boundary for Consolidation
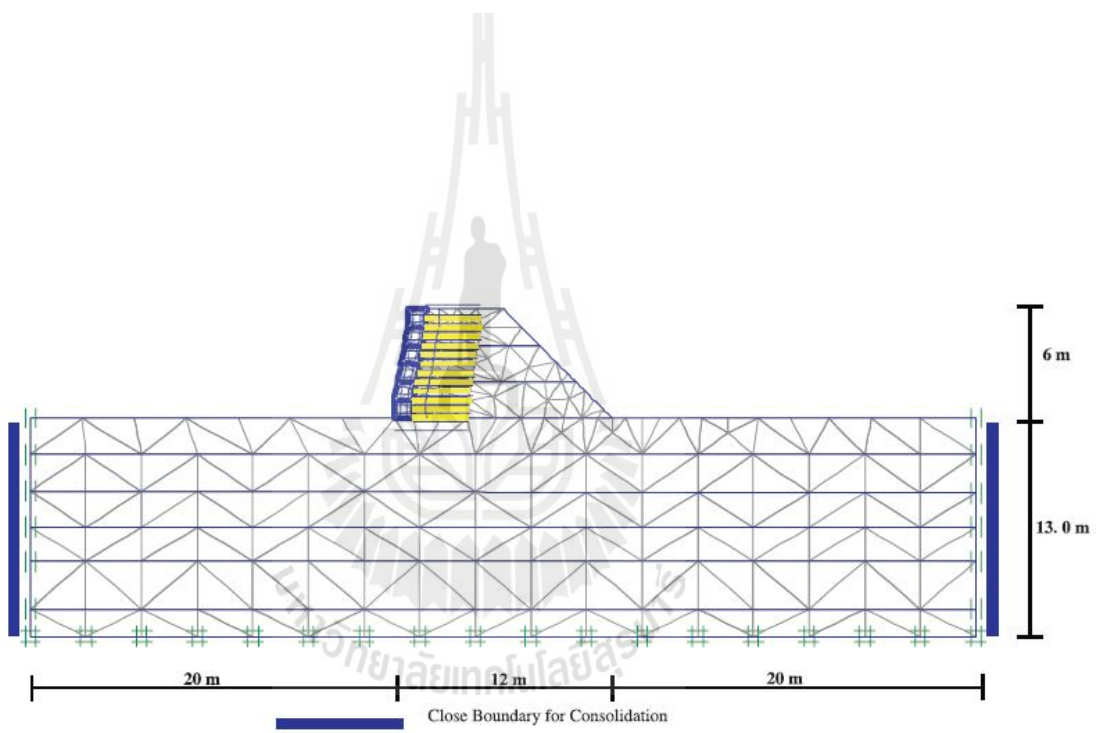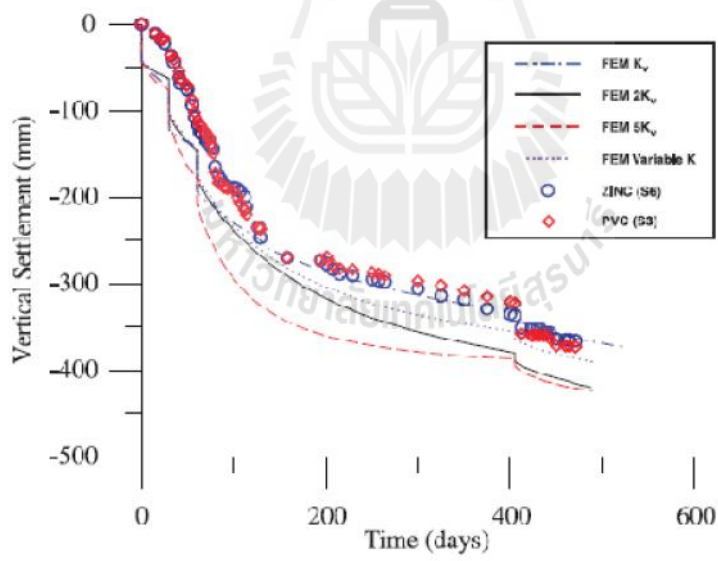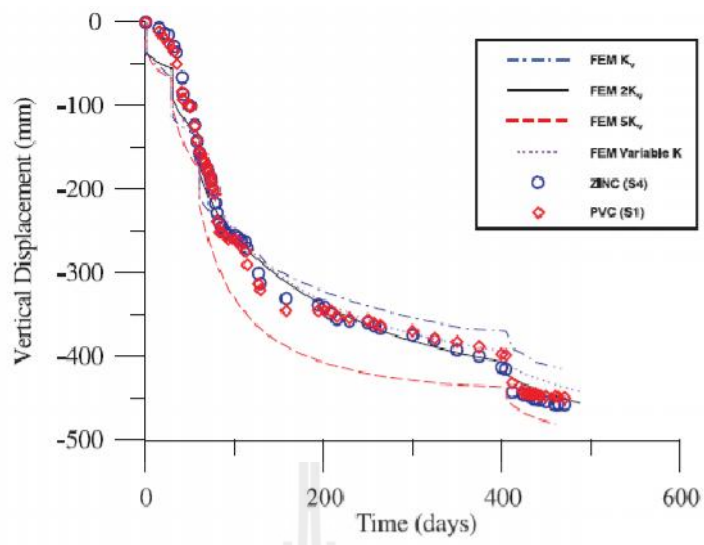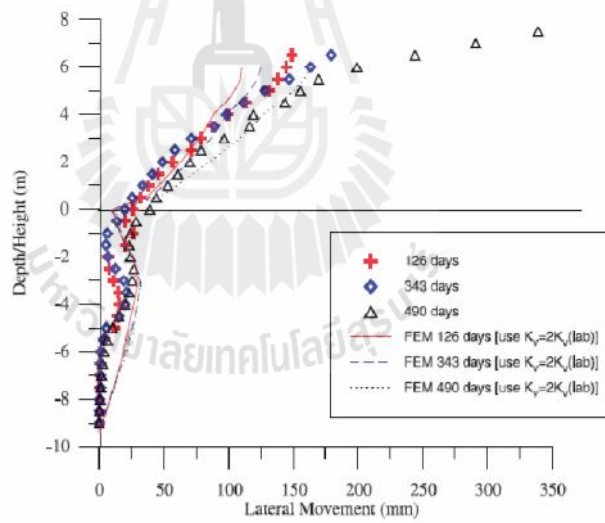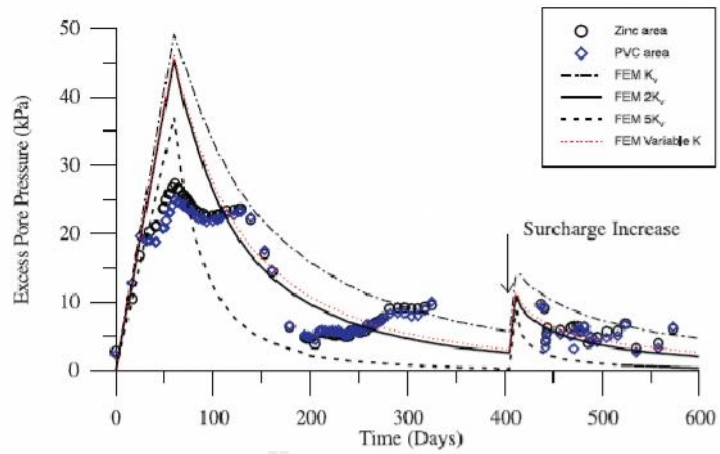
2.10 References

AASHTO (1996), Standard Specifications for Highway and Bridge, 1th edition. Washington D.C., **American Association of State Highway and Transportation Officials**.

AASHTO (2002), Standard Specifications for Highway and Bridge, 7th edition. Washington D.C., **American Association of State Highway and Transportation Officials**.

Abiera, H. O., 1991. Mechanically stabilized earth using TENSAR, bamboo and steel grid reinforcements with lateritic soil as backfill, **M. Eng Thesis GT-90-21**, Asian Institute of Technology, Bangkok, Thailand.

Alagiyawanna, A.M.N, Sugimoto, M., Sato, S., and Toyota, H., 2001. Influence of longitudinal and transverse member on geogrid pullout behavior during deformation. **Geotextiles and Geomembranes**, Vol. 19, pp. 483-507

Alfaro, M.C., 1996. Reinforced soil wall-embankment system on soft foundation using inextensible and extensible grid reinforcements. **Ph.D Dissertation**, Saga University, Japan.

Bergado D.T., Teerawattanasuk C., Youwai S. and Voottipruex P., 2000. FE modeling of hexagonal wire reinforced embankment on soft clay. **Canadian Geotechnical Journal**, Vol. 37, pp. 1209-1226.

Bergado D.T., and Chai J.C, 1994. Pull-out force/displacement relationship of extensible grid reinforcements, **Geotextiles and Geomembranes**, Vol. 13,pp. 295-316.

Bergado D.T., Long,P. V., Loke, K.H. and Werner, G., 1994. Performance of reinforced embankment on soft Bangkok clay with high-strength geotextile reinforcement, **Geotextiles and Geomembranes**, Vol. 13, pp. 403-420

Bergado D.T., Sampaco, C. L., Shivashankar, R., Alfaro, M. C., Anderson, L. R. and Balasubramaniam, A.S., 1991b. Performance of welded wire wall with poor quality backfills on soft clay, **ASCE Geotechnical Engineering Congress**, Boulder, Colorado, U.S.A. pp. 909-922.

Bernal, A., Salgado, R., Swan, R. and Lovell, C., 1997. Interaction between tire shreds, rubber-sand and geosynthetics. **Geosynthetics International**, Vol. 4, No. 6, pp. 623-643.

Biot, M. A., 1941. General theory of three dimensional consolidation, **Journal of Applied Physics**, Vol. 12, pp. 155-164

Chai, J. C. (1992), "Interaction between grid reinforcement and cohesive-frictional soil and performance of reinforced wall/embankment on soft ground", **D.Eng. Dissertation**, Asian Institute of Technology, Bangkok, Thailand.

Chen, R.H., and Chiu, Y.M. (2008), "Model tests of geocell retaining structures", **Geotextiles and Geomembranes**, Vol.25, No.1, pp.56-70.

Hird, C. C. and Jewell, R. A., 1990. Theory of reinforced embankment, Reinforced Embankments- Theory and Practice, **Shercliff, D.A. Ed., Thomas Telford Ltd**., London, UK,pp.117-142.

Hird, C.D, and Kwok, C,M.,1989. FE studies of interface behavior in reinforced embankments on soft ground, **Computers and Geotechnics**, Vol. 8, pp.111-131.

Holtz, R. D., Christopher, B.R. and Berg, R. R., 1995. **Geotextile Design & Construction Guidelines**, Publication No. FHWA HI-1995-038.

Ingold, T.S., 1982a Reinforced Earth, **Thomas Telford**, London.

Ingold, T.S., 1982b. An analytical study of geotextile reinforced embankment, **second international Conference of Geotextile**, Las Vegas. U.S.A., Vol. 3,pp. 683-688.

Jewell, R.A., 1986.The mechanics of reinforced embankments on soft soils, Proceeding of the Prediction Symposium on a Reinforced Embankments on Soft Ground, 17-18th Sept., 1986, **King's College**, Strand, London, pp. 159-163.

Jewell, R. A., Milligan, G. W. E., Sarsby, R. W. and Dubois, D., 1984 Interaction between soil and geogrids, Proc. Of the Symp. on Polymer Grid Reinforcement in Civil Eng., **Thomas Telford Limited**, London, U.K., pp. 19-29

Kaniraj, S.R., 1994. Rotational stability of unreinforced and reinforced embankments on soft soils. **Geotextiles and Geomembranes**, Vol. 13,pp. 707-726

Kondner, R. L. and Zelasko, J.S., 1963. A hyperbolic stress-strain formulation of sand, **Proc. Of Second Pan American Conf**. on Soil Mech. and Foundation Eng'g.

Kongkitkul. W., 2001. Nummerical and analytical modeling of interaction between hexagonal wire mesh reinforcement and silty sand backfill during in-soil pullout tests, **M. Eng. Thesis No. GE 00-18**, Asian Institute of Technology, Bangkok, Thailand.

Ling, H. I. and Leshchinsky, D., 2003. Finite element parametric study of the behavior of segmental block reinforced-soil retaining walls. **Geosynthetics International**, Vol. 10, No.3, pp.77-94.

Long, P.V., 1996. Behavior of geotextile-reinforced embankment on soft ground. **Doctoral Dissertation No. GT 96-1**, Asian Institute of Technology, Bangkok, Thailand.

Low, B. K., Wong, K.S., Lim, C. and Broms, B.B.,1990. Slip circie analysis of reinforced embankments on soft ground, **Geotextiles and Geomembranes**, Vol. 9, pp. 165-181

Mandel, J. and Salencon, J., 1969. Force portance d'un sol sur une asssie rigid. **Proc. 7th ICSMFE**, Vol. 2., pp.157-164

Milligan and Busbridge, J. R., 1983. Guideline for the use of Tensar geogrids in reinforcement of fill over weak foundation, **Golder Associate Report to the Tensar Corporation**, Mississaaupa, Ontario.

Mitchell, J.K. and Villet, W.C.B., 1987.Reinforcement of Earth Slopes and Embankments. **Nationnal Cooperative Highway Research Program Report No. 290**, Washington, D.C., Transportation Research Board, 323 P.

Palmeira, E.M., 2009. Soil–geosynthetic interaction: Modelling and analysis. Geotextiles and Geomembranes 27, 368-390.

Palmeira, E.M. and Milligan, G. W. E., 1989. Scale and other factors affecting the results of pullout tests of grids buried in sand. **Geotechnique**, Vol. 39, No. 3,pp. 511-524.

Prandtl, L. 1920. Eindringungs fesligkeit und fesligkeit von schneiden, **Mathemtik und Mechanik**, Vol. 1, p. 15.

Roscoe, K. H. and Burland, J. B., 1968. On the generalized stress-strain behavior of wet clays, **Proceeding of Engineering Plasticity**, Cambridge University Press, pp. 539-609

Rowe, R. K., 1992. Reinforced embankments on soft cohesive deposits. **Proc. of the Int'l Symposium on Applications of Geosynthetics Technology**, Jakarta, pp.1-19.

Rowe, R. K., 1984 Reinforced embankment, analysis and design, **Journal of Geotechnical Engineering Division, ASCE**, Vol. 110, No. 2, pp. 231-246

Rowe, R. K. and Ho, S. K., 1998. Horizontal deformation in reinforced soil walls. **Canadian Geotechnical Journal**, Vol.35, pp. 312-327

Rowe, R. K. and Ho, S. K., 1997.Continuous panel reinforced soil walls on rigid foundation. **Journal of Geotechnical and Geoenvironmental Engineering, ASCE**, Vol. 123, No 10, pp. 912-920.

Rowe, R. K. and Soderman, K. L., 1987 Reinforcement of embankment on soils whose strength increases with depth. **Proceeding of Geosynthetics' 87**, New Orleans, pp. 266-277.

Schlosser, F. and Long N. T. 1973. Etude du comportement cu maeriau teree armee, **Annles De L'Inst Techq Du Battiment Et Des Trav Publ**., Suppl. No. 304, Ser Mater. No. 45

Shivashankar, R., 1991. Behavior of Mechanically Stabilized Earth (MSE) Embankment with Poor Quality Backfills on Soft Clay Deposits, Including a Study of the Pullout Resistances. **D. Eng. Dissertation**, Asian Institute of Technology. Bangkok, Thailand

Smith I .M. and Griffith D. V., 1988. Programming the Finite Element Method, **Second Edition, John Will and Sons**, Chichester, U. K.

Srikongsri, A., 1999. Analytical model for interaction between hexagonal wire mesh and silty sand backfill. **M. Eng. Thesis No. GE-98-14**, Asian Institute of Technology, Bangkok Thailand.

Tatlisoz, N., Edil T. B. and Benson, C. H., 1998. Interaction between reinforcing geosynthetics and soil-tire chip mixtures. **Journal of Geotechnical and Geoenvironmental Engineering, ASCE**, Vol.124. NO. 11, pp. 1109-1119.

Vermeer, P. A. and Brinkgreve, R. B. J. (Editor), 1995. Finite Element Code for Soil and Rock Analysis, **A. A. Balkema, Rotterdam**, Netherland.

Vidal, H., 1969. The principle of reinforced earth. Highway Research Record No. 282, **Highway Research Board, National Research Council**, Washington D. C., pp. 1-16.

Wongsawanon, T., 1998, Interaction between hexagonal wire mesh reinforcement and silty sand backfill. **M. Eng. Thesis No. GE 97-14**, Asian Institute of Technology, Bangkok, Thailand.

Yang, 1972. Strength and deformation characteristics of reinforced sand**, Ph. D. Thesis**, UCLA.

Yoo, C. and Jung, H. Y., 2006 Case history of geosynthetic reinforced segmental retaining wall failure. **Journal of Geotechnical and Geoenvironmental Engineering**, Vol. 132, No. 12, pp 1538-1548.

Yuan, Z . and Chua, K. M., 1991. Analytical model for pullout of soil reinforcement, **Transportation Research Record**, No. 1320, pp. 64-71.

CHAPTER III

PULLOUT RESISTANCE OF BEARING

REINFORCEMENT EMBEDDEDIN

COARSE-GRAINED SOILS

3.1 Statement of problem

The maximum bearing stress, $\dagger_{b\max}$, of a single transverse member for the bearing reinforcement embedded in a poorly graded sand can be predicted satisfactorily based on the modified punching shear mechanism (Horpibulsuk and Neramitkornburee, 2010). The proposed equation was applicable to a particular compacted sand with small particles. The applicability of the proposed equation for different coarse-grained soils, which are commonly used as backfill materials, thus required examination. It was revealed that the soil particle size controls the pullout bearing mechanisms. Therefore, this chapter aims to study the pullout resistance mechanism of the bearing reinforcement embedded in different coarse-grained soils with different dimensions of transverse member, gradations, average grain sizes, D_{50}, and friction angles. The knowledge gained from this study is useful for the internal stability analysis of the BRE wall based on the limit equilibrium analysis.

3.2 Laboratory investigation

3.2.1 Soil samples

The tested soils consisted of 3 soil types with different grain size distributions and friction angles. The soils were collected from different locations in Nakhon Ratchasima, Thailand. They were well-graded gravel (GW), well-graded sand (SW) and crushed rock (GP) according to the Unified Soil Classification System (USCS). The average grain sizes, D_{50} were 5.7, 1.0 and 7.0 mm for GW, SW and GP, respectively. The compaction characteristics based on standard Proctor energy are optimum water content, OWC = 3.9 and 6.3% and maximum dry unit weight, $1x_{d\max} =$ 20.15 and 18.15 kN/m^3 for GW and SW, respectively. The crushed rock (GP) is not compacted to obtain a friction angle lower than that of the GW and SW. The tested water content was 0.31% and the tested dry unit weight was 16.64 kN/m^3. Strength parameters of all tested soils were obtained from a large direct shear apparatus with a diameter of 35 cm. The friction angles were 45, 42 and 40 degrees, for GW, SW and GP, respectively. The high friction angles (greater than 36 degrees) are acceptable for MSE wall construction in Thailand. In addition to these three soils, the test results of the poorly-graded sand (SP) obtained from Horpibulsuk and Niramitkornburee (2010) were also used for this study. The average grain size, D_{50} of SP was 0.31 mm. The optimum water content, OWC was 6.3%; the maximum dry unit weight, $x_{d\max}$ was 16.80 kN/m^3; and the friction angle, w, was 40 degrees. The crushed rock (GP) and the poorly-graded sand (SP) have the same friction angle but different grain size distributions and average grain sizes, D_{50}. These two soils were used to study the effect of D_{50} on the pullout bearing mechanism. The index properties of all the tested

Type	Average grain size, D_{50} (mm)	Specific gravity, G_s	Tested water content, OWC (%)	Tested dry unit weight, $\gamma_{d,max}$ (kN/m^3)	Friction angle, φ ($^\circ$)
Well- graded gravel (GW)	5.7	2.73	3.9	20.15	45
Well- graded sand (SW)	1	2.69	6.3	18.15	42
Poorly-graded sand (SP)	0.31	2.77	6.3	16.8	40
Crushed rock (GP)	7	-	0.31	16.64	40

3.2.2   Methodology

The pullout test apparatus used in this investigation is made of rolled steel plates, angles, channels, and H-sections welded or bolted together to give an inside dimension of 2.6 m in length by 0.6 m in width by 0.8 m in height as shown in Figure 3.2. The front wall contains upper and lower parts with a slot in between for the reinforcement specimen. Friction between the tested soils and the side walls of the apparatus was minimized by the use of a lubricated rubber member as done by Horpibulsuk and Niramitkornburee (2010). During the pullout of the reinforcement, due to an arching effect of the front wall, the normal stress on the reinforcement near the front wall may increase (dilate) or decrease (contract). To reduce this effect, a sleeve was installed inside the slot opening, which was 150 mm in horizontal width and 100 mm in height to isolate the bearing reinforcement near the front wall. The compacted sand thickness of 300 mm was maintained above and below the reinforcement.

For any model test, the boundary effect cannot be completely avoided. One of the boundary effects for the pullout test is the effect of front wall of the pullout test apparatus. For investigating the pullout force of a single transverse member, the effect of front wall was avoided by placing the transverse member far away from the front wall. However, for investigating the influence of the spacing between the transverse members, the effect of front wall could not be completely avoided. When the spacing between the first transverse member and the front wall is equal to or smaller than the spacing between the transverse members, S, the effect of the front wall may increase or decrease (in case the slot on the wall for a tested reinforcement to pass through is too large) the pullout bearing resistance of the first transverse

member. If the spacing between the front wall and the first transverse member is larger than the *S* value, the pullout bearing resistance of the first transverse member may be higher than other members (less interaction effect). As for the effect of the side walls and the upper and the bottom boundaries, considering the size of the tested reinforcements, it is believed that the pullout test apparatus is large enough to avoid considerable boundary effects.

Figure 3.2 Schematic diagram of pullout test apparatus

(Horpibulsuk and Niramitkornburee, 2010).

Normal stress was applied with a pressurized air bag positioned between the compacted soil and the top cover of the apparatus. Before installing the air bag, a 30 mm thick layer of soil was placed on the top of the compacted soil and covered by a 4 mm thick steel plate. The purpose of this procedure was to try to produce a uniformly distributed normal stress on the top of the backfill soil (Figure 3.2). The pullout force was applied by a 200 kN capacity electro-hydraulic controlled jack. The pullout displacement at the front of the pullout apparatus was monitored by a linear variation differential transformer (LVDT). The maximum applied pullout displacement (end of test) is 40 mm, which is approximately 10% of the leg length (B) of the transverse member. The applied normal stress was 30, 50 and 90 kPa. These different applied normal stresses were considered to simulate total vertical stress (due to dead and live loads) on the bearing reinforcement at different depths. The pullout rate of 1 mm/min was adopted throughout the tests.

3.2.3 Bearing Reinforcement

To understand the role of the influential factors (dimension, spacing, number of transverse members, normal stress and average grain size) on the pullout mechanism, the pullout tests on the bearing reinforcements with different dimensions, number, and spacing of transverse members embedded in the tested soils (different grain size) were conducted under different applied normal stresses. The leg length, B, and the length, L, of the tested transverse members (steel equal angles) were 25, 40 and 50 mm and 100, 150 and 200 mm, respectively; all are generally used for MSE walls. The B/L values for the tested transverse members are between 0.13 and 0.5. Although during pullout of the bearing reinforcement, the deformation around the

bearing member is three-dimensional, Horpibulsuk and Niramitkornburee (2010) reported that within this B/L range the bearing capacity of the single transverse member embedded in poorly-graded sand can be predicted by the modified plane strain punching shear failure model successfully, i.e. the three-dimensional effect has been inexplicitly considered by the proposed plane strain failure model. The spacing between transverse members, S, varies from 150 to 1500 mm, depending upon the number of transverse members. In this study, the number of transverse members, n, ranged from 1 to 4, which is generally the case in practice. The pullout friction resistance of a longitudinal member is investigated from the pullout test on a single longitudinal member with a diameter of 16.0 mm and length of 2.6 m.

3.3 Test results and discussion

3.3.1 Pullout Friction Resistance

Figure 3.3 shows the pullout friction force and displacement relationship of a longitudinal member with a diameter of 16 mm and length of 2.6 m for well-graded gravel (GW), well-graded sand (SW), poorly-graded sand (SP) and crushed rock (GP). For a particular soil, the maximum pullout friction force, $P_{f,\max}$ increases with the increase in normal stresses, σ_n. The displacement at peak failure is insignificantly affected by the normal stress; it is approximately 3 to 5 mm for all the applied normal stresses and tested soils. The well-graded gravel (GW) gives the highest pullout friction force because it has the highest friction angle. The crushed rock (GP) and the poorly-graded sand (SP) give the same the friction pullout force, P_f, for the same normal stress, σ_n even with different grain size distributions and

D_{50} values, possibly because they have the same friction angle. Figure 3.6 shows the failure envelope of all tested soils where δ is the apparent interface friction angle between soils and the steel longitudinal member. The shear stress, τ was determined from $P_{f\max}/f\,DL$ where D and L are the diameter and length of the longitudinal member, respectively. The $\tan\delta$ values are very high and are larger than the $\tan\phi$ values for all tested soils because the roughness of the steel deformed bar increases the failure friction plane during pullout (i.e., the failure friction diameter is greater than the measured diameter of the longitudinal member) (Horpibulsuk et al., 2011). The higher $\tan\delta$ value is also due to the arching effect caused by the stress concentration on the steel bar as consequence of the higher stiffness of the steel bar compared to that of the surrounding soil. Even with the differences in $\tan\delta$ and $\tan\delta$ /$\tan\phi$ values for the different soils, their δ/ϕ values are essentially the same, approximately 1.47. To conclude, the maximum friction pullout force, $P_{f,\max}$, and δ are mainly controlled by the friction angle and are independent upon grain size.

Top-left plot:

Friction pullout force, P_f (kN)

Longitudinal bar (16 mm diameter)
Well-graded gravel (GW)

τ_n = 90 kPa
τ_n = 50 kPa
τ_n = 30 kPa

Displacement, d (mm)

Top-right plot:

Friction pullout force, P_f (kN)

Well-graded sand (SW)

τ_n = 90 kPa
τ_n = 50 kPa
τ_n = 30 kPa

Displacement, d (mm)

Middle-left plot:

Friction pullout force, P_f (kN)

Poorly graded sand (SP)
(Horpibulsuk and Neramitkornburee, 2010)

τ_n = 90 kPa
τ_n = 50 kPa
τ_n = 30 kPa

Displacement, d (mm)

Middle-right plot:

Friction pullout force, P_f (kN)

Crushed rock (GP)

τ_n = 90 kPa
τ_n = 50 kPa
τ_n = 30 kPa

Displacement, d (mm)

Bottom plot:

Shear stress, τ (kPa)

Poorly-graded sand (SP), $\tau_f = \tau_n \tan 58.7^o$
(Horpibulsuk and Neramitkornburee, 2010)

Well-graded gravel (GW), $\tau_f = \tau_n \tan 67.9^o$

Well-graded sand (SW), $\tau_f = \tau_n \tan 61.66^o$

Crushed rock, $\tau_f = \tau_n \tan 58.0^o$

Normal stress, τ_n (kPa)

3.3.2 Pullout Bearing Mechanism of a Single Isolated Transverse Member ($n = 1$)

The pullout bearing force at any displacement is the difference between the total pullout force and the pullout friction force. Figure 3.5 shows the total pullout force and displacement relationship of the bearing reinforcement with a 1.0 m longitudinal member and a 40x150 (BxL) mm transverse member for all tested soils. It is notable that initially, the pullout resistance sharply increases with displacement and then gradually increases until failure at a large displacement of approximately 40 mm, which is the end of the test. The initial sharp increase is caused by the pullout friction resistance, which fully mobilizes at small displacement while the soil-bearing capacity fully mobilizes at large displacement. The total pullout force, P_t, increases with the increase in the normal stresses, σ_n, for all tested soils. It increases as the friction angle increases for a particular normal stress. Although the crushed rock (GP) and poorly-graded sand (SP) give the same the pullout friction force, P_f, for the same normal stresses, σ_n, the total pullout force, P_t, of the crushed rock (GP) is higher than that of poorly-graded sand (SP). In other words, the pullout bearing force of the crushed rock is larger. This higher pullout bearing force is caused by the larger grain size.

The influence of grain size on the pullout bearing resistance is expressed by the ratio of the leg length of the transverse member, B, to the average grain size, D_{50} (B/D_{50}). Figure 3.6 shows the bearing stress, σ_b and displacement, d, relationship of the transverse member with different B values for all tested soils. The measured bearing stress is obtained from the assumption that the soil in the angle leg

acts as a rigid block (Horpibulsuk and Niramitkornburee, 2010). The bearing stress is thus determined from the ratio of the pullout force to the area of transverse member, $B \times L$. It is found that the failure bearing stresses, $\dagger_{b\max}$, for large D_{50} soils (the well-graded gravel and the crushed rock) increase as the B/D_{50} value decreases. The $\dagger_b$ versus d relationships for both the SW and SP soils are independent of the B/D_{50} value because the grain sizes of both soils (SW and SP) are much smaller than B ($B/D_{50} > 25$). The well-graded sand (SW) exhibits slightly higher failure bearing stresses than the poorly-graded sand (SP) because of a higher friction angle, W. Thus, the pullout bearing resistance is dependent upon the average grain size, D_{50}, the leg length, B, and the friction angle, W, irrespective of gradation (well-graded and poorly graded).
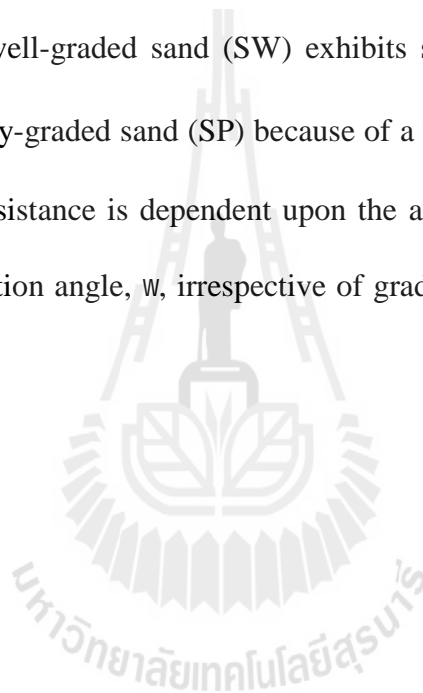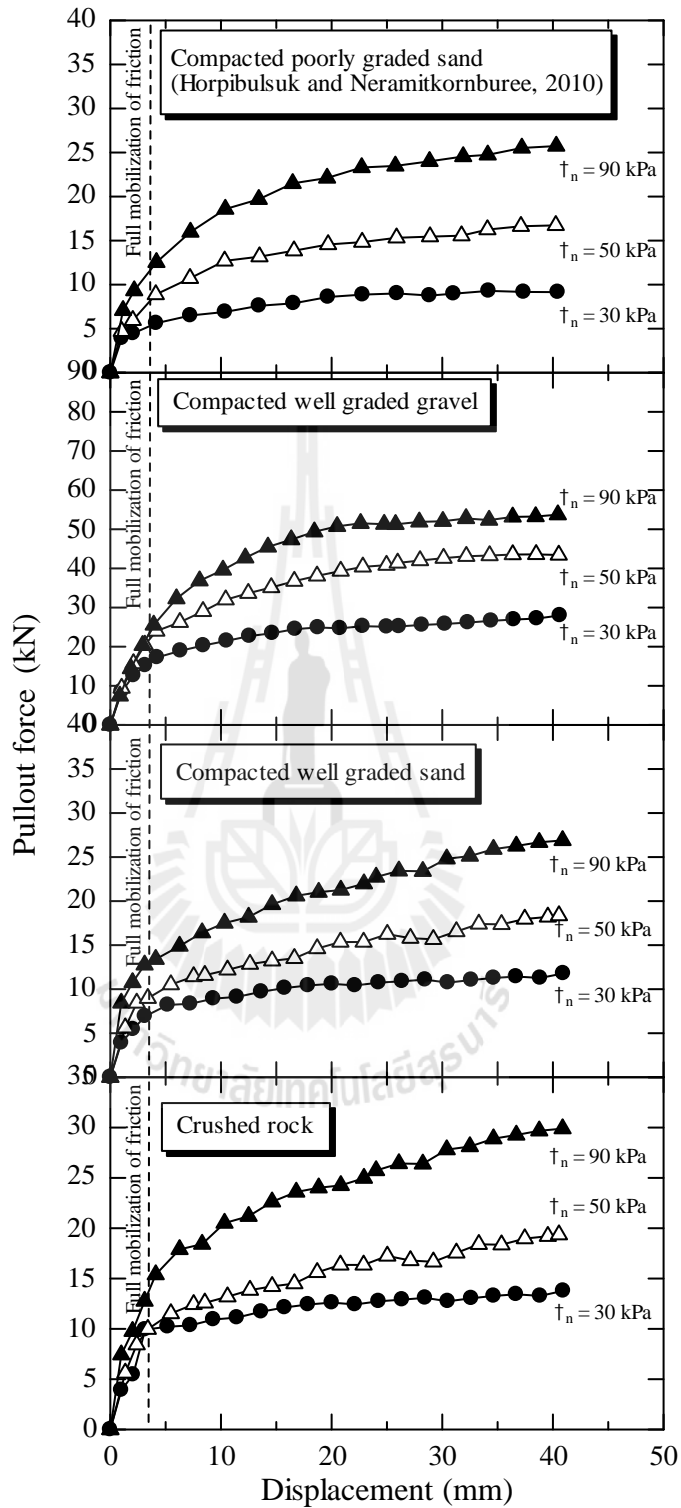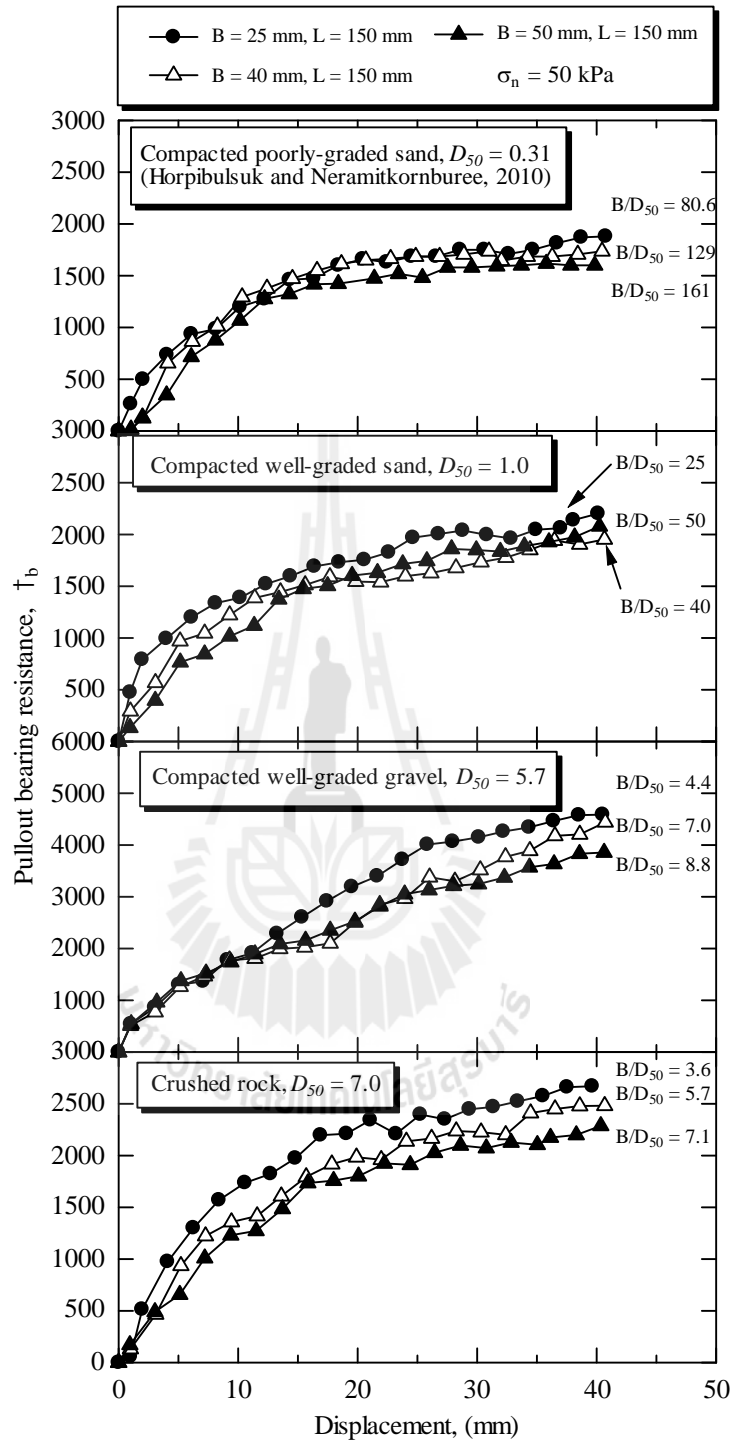
Legend:
- ● B = 25 mm, L = 150 mm
- △ B = 40 mm, L = 150 mm
- ▲ B = 50 mm, L = 150 mm
- σ_n = 50 kPa

Panel 1 (top): Compacted poorly-graded sand, D_{50} = 0.31 (Horpibulsuk and Neramitkornburee, 2010)
- B/D_{50} = 80.6
- B/D_{50} = 129
- B/D_{50} = 161

Panel 2: Compacted well-graded sand, D_{50} = 1.0
- B/D_{50} = 25
- B/D_{50} = 50
- B/D_{50} = 40

Panel 3: Compacted well-graded gravel, D_{50} = 5.7
- B/D_{50} = 4.4
- B/D_{50} = 7.0
- B/D_{50} = 8.8

Panel 4 (bottom): Crushed rock, D_{50} = 7.0
- B/D_{50} = 3.6
- B/D_{50} = 5.7
- B/D_{50} = 7.1

Y-axis: Pullout bearing resistance, t_b

X-axis: Displacement, (mm)

B

The maximum pullout bearing resistance can be determined from the plasticity solutions. Using the proposed equations (Eqs. 1 to 4), the comparison between the measured and predicted maximum bearing stresses are shown in Figure 3.7. For the well-graded gravel (GW) and the crushed rock (GP), with large average grain size, D_{50}, the maximum bearing stress, $\dagger_{b\max}$, at low normal stress of approximately 30 kPa was close to that predicted by the general shear mechanism. However, the measured maximum bearing stress, $\dagger_{b\max}$, at high normal stress of 90 kPa was very close to that predicted by the modified punching shear mechanism. The same is not true for the small D_{50} soils (SP and SW). The measured pullout bearing stress is predicted satisfactorily based on the modified punching shear mechanism for the different tested normal stresses. As the bearing reinforcement is pulled out and shear displacement occurs along the interface, the zone of soil surrounding the reinforcement tends to dilate. However, the volume change is restrained by the surrounding non-dilating soil, resulting in an increase in normal stress on the soil-reinforcement interface (interlocking effect). The interlocking effect is significant for the large particle soils and can be ignored for the small particle soils. Hence, the pullout mechanism of the bearing reinforcement embedded in the gravelly soils (both well-graded and poorly graded) under low normal stress approaches the general shear failure. This effect decreases as the normal stress increases.

To understand the development in the bearing capacity with the friction angle, which is used as an engineering parameter in practice, the measured bearing capacity factor, N_q, and friction angle, w, relationship for all tested soils is plotted and shown in Figure 3.8, where N_q is the measured $\dagger_{b\max}/\dagger_n$. The measured N_q

values were compared with the values predicted by the three mechanisms. It is found from Figures 3.7 and 3.8 that the modified punching shear mechanism can be used to predict the pullout bearing stress of different transverse member dimensions for the small particle soils (SP and SW), regardless of the gradation (either well-graded or poorly graded), and that the general shear N_q is the upper boundary for the two large particle soils (GP and GW).

The effect of B/D_{50} on the pullout bearing mechanism for large D_{50} soils is illustrated in Figure 3.9, which is the relationship between $N_q/N_{q(\text{modified})}$ and B/D_{50} of single isolated transverse member for all tested soils. For the small particle soils (SW and SP), $N_q/N_{q(\text{modified})}$ is close to unity (the N_q value can be approximated from Eq. (2.13)). However, for the large particle soils (both well-graded and poorly graded), $N_q/N_{q(\text{modified})}$ decreases as the B/D_{50} value increases and tends to approach unity when the B/D_{50} value is close to 12, which agrees well with the pullout results of the grid reinforcement reported by Palmeira (2009). The failure mechanism of bearing reinforcement is classified into two zones, which is dependent upon the B/D_{50} value, regardless of gradation (well-graded or poorly graded). Zone 1, where $B/D_{50} \leq 12$, is the interlocking induced failure while Zone 2, where $B/D_{50} \geq 12$, is the modified punching shear failure.
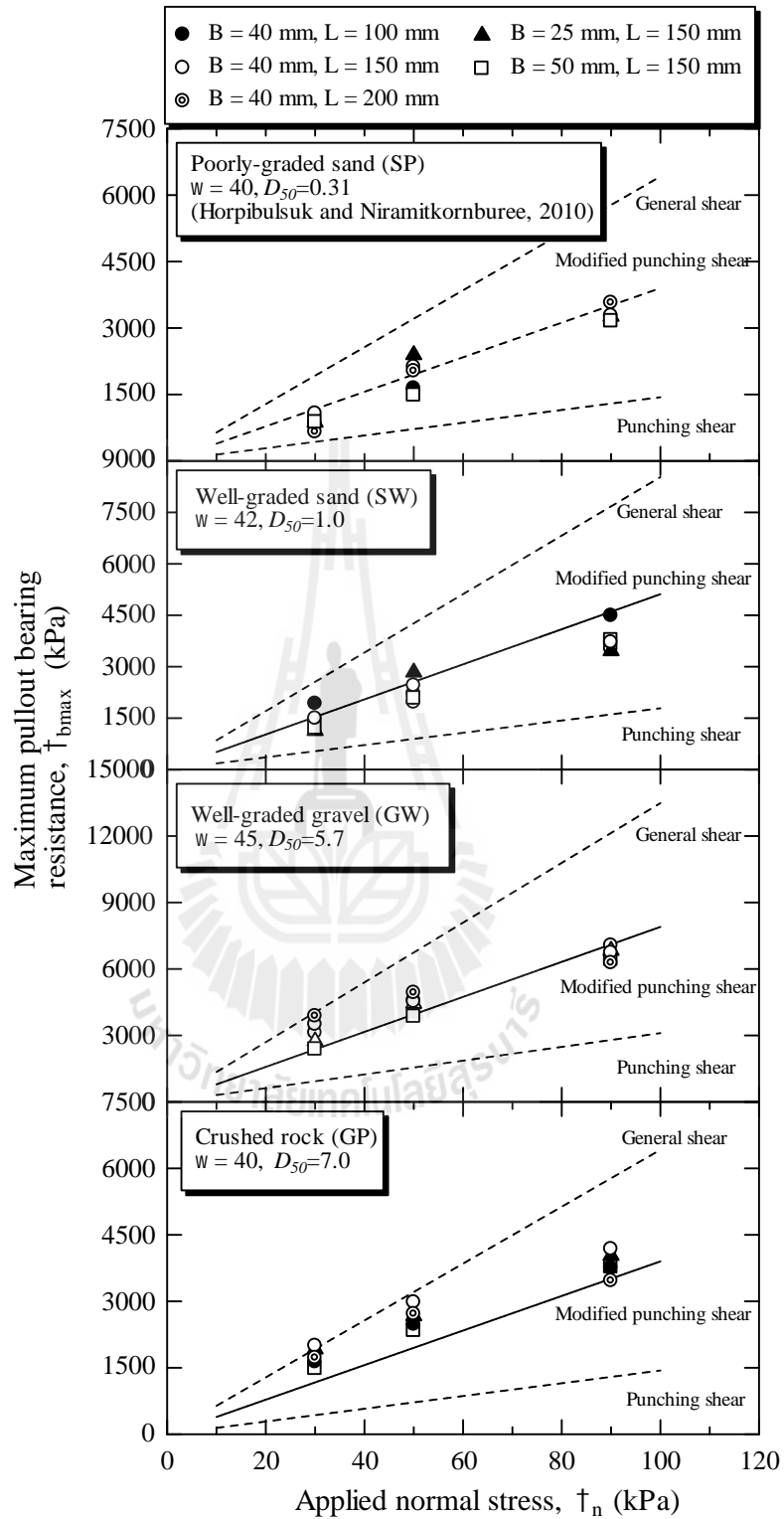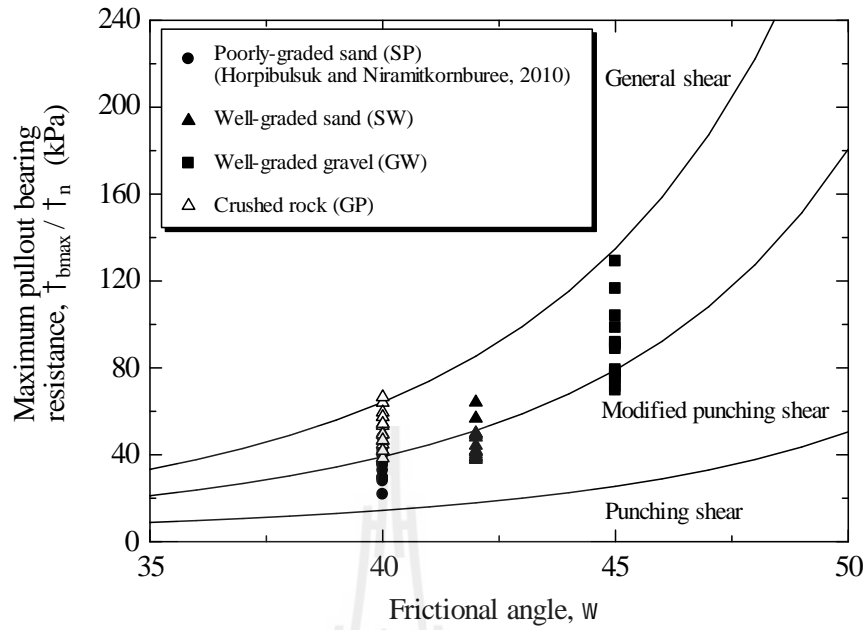
N_q
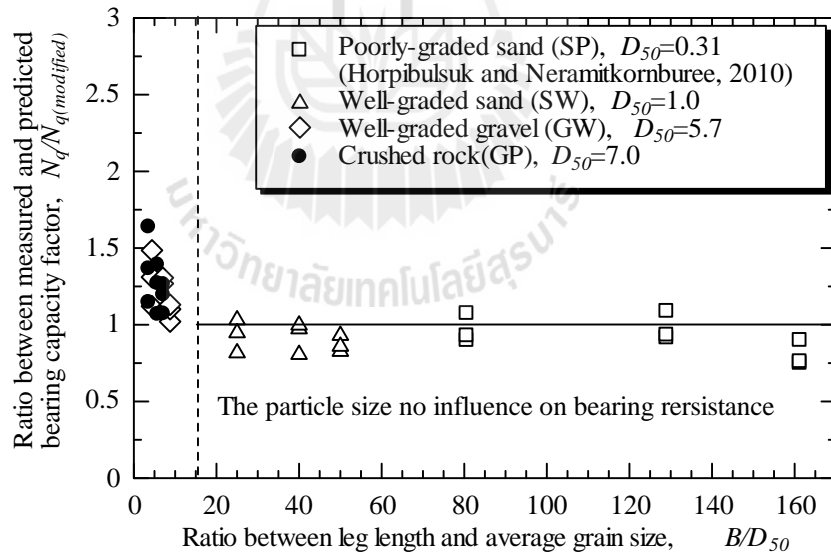
$N_q/N_{q(\text{modified})}$ B/D_{50}

the N_q value for different B/D_{50} values is depicted in Figures 3.10 and 3.11. Assuming that general shear and modified punching shear solutions are the upper and lower boundaries, the N_q values for all tested soils (different friction angles) at $B/D_{50} = 12$ under different normal stresses are approximated from Eq.(2.13). At a B/D_{50} of 3, the N_q value at $\sigma_n < 30 \, \text{kPa}$ can be approximated by Eq.(2.9); additionally, the N_q value decreases with increasing normal stress and is determined by Eq.(2.13) when $\sigma_n > 120$. This premise yields the following equations for predicting the N_q value for different normal stresses and B/D_{50} values:

$$N_{q1}/N_{q(\text{modified})} = a + b \ln\left(\frac{B}{D_{50}}\right) \qquad \text{for } 3 \leq B/D_{50} \leq 12 \qquad (3.1)$$

$$N_{q2}/N_{q(\text{modified})} = c + d \ln\left(\sigma_n\right) \qquad \text{for } 30\,\text{kPa} \leq \sigma_n \leq 120\,\text{kPa} \qquad (3.2)$$

where N_{q1} is the N_q value at $\sigma_n = 30$ kPa for $3 \leq B/D_{50} \leq 12$ and N_{q2} is the N_q value at the required B/D_{50} value and normal stress. The a, b, c and d are constants, depending upon the normal stress, σ_n; B/D_{50}; and the friction angle, φ. The constants a and b in Eq. (3.1) can be obtained with the two physical conditions at $\sigma_n = 30$ kPa: 1) when B/D_{50} equals 3, $N_{q1} = N_{q(\text{general})}$ and 2) when B/D_{50} equals 12, $N_{q2} = N_{q(\text{modified})}$ equals 1. The constants a and b are thus determined by the following equations:

$$b = 0.722\left(1 - \frac{N_{q(\text{general})}}{N_{q(\text{modified})}}\right) \qquad (3.3)$$

$$a = 1 - 2.485b$$

$$30\,\text{kPa} \leq \dagger_n \leq 120\,\text{kPa}$$

$$\dagger_n$$

$$\dagger_n$$

$$d = 0.722\left(1 - \frac{N_{q1}}{N_{q(\text{modified})}}\right)$$

$$c = 1 - 4.787d$$
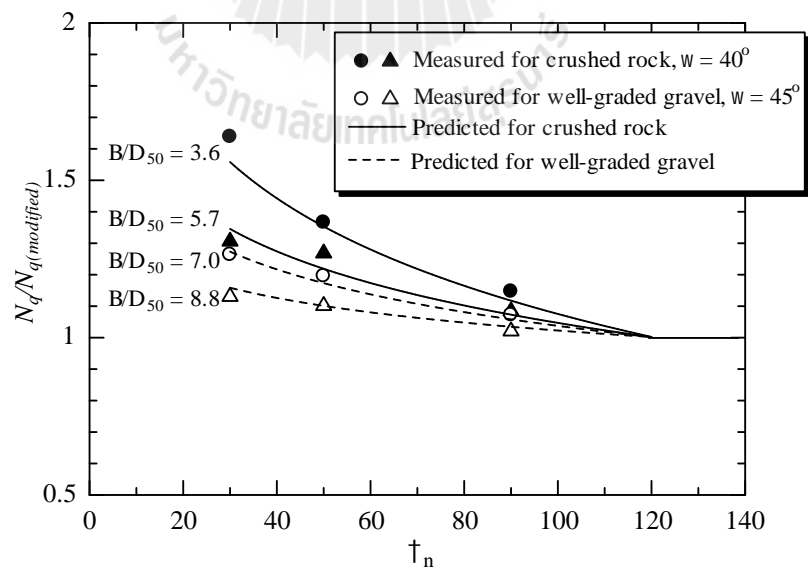
$$N_q / N_{q(\text{modified})} \qquad \dagger_n$$

$$N_q / N_{q(\text{modified})} \qquad B/D_{50}$$
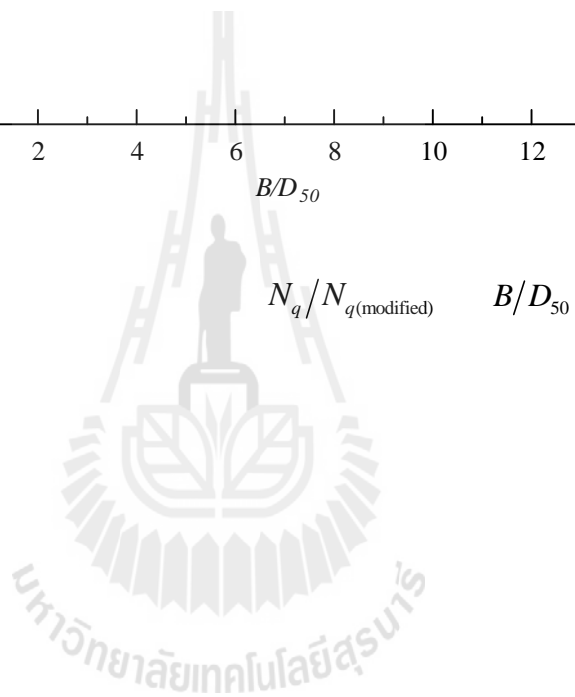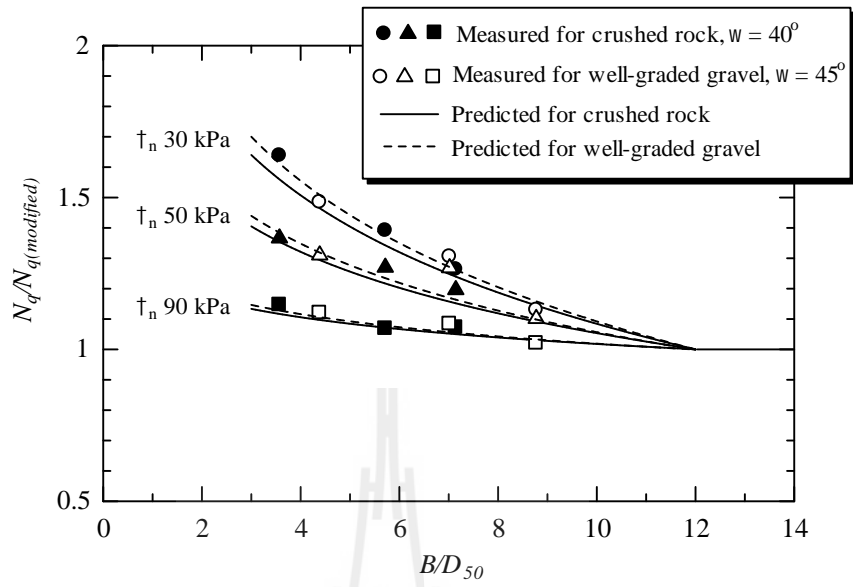
(Palmeira and Milligan, 1989; Plameira, 2009; Bergado and Chai, 1994; and Bergado et al., 1996). Similarly, Horpibulsuk and Niramitkornburee (2010) demonstrated that the transverse member interference for the bearing reinforcement is controlled by the spacing of transverse members and the leg length of transverse member, *B*, regardless of the length of the transverse member, *L*. During the pullout of the bearing reinforcement, the transverse members interfere with each other. A dimensionless parameter, the transverse member spacing ratio, *S*/*B*, was introduced to investigate the influence of spacing, *S*, and the dimension (*B* and *L*) of transverse members on the pullout bearing characteristics. Generally, the larger the *S*/*B* is, the higher the pullout bearing resistance up to a certain maximum value, due to less interference among transverse members.

Figure 3.12 shows the typical relationship between the maximum pullout bearing force, P_{bn}, and transverse member spacing ratio, *S*/*B*, for 40x150 mm transverse members ($n = 2$ to 4) under different applied normal stresses compared with maximum pullout bearing force of a single isolated transverse member ($n = 1$), P_{b1}, for all tested soils. The result is in agreement with that reported by Horpibulsuk and Niramitkornburee (2010), indicating that the failure mechanism of the bearing reinforcement is classified into three zones, depending on the S/B value. Zone 1 is referred to as block failure when the $S/B \leq 3.75$. Zone 2 is regarded as member interference failure when $3.75 < S/B < 25$. Zone 3 ($S/B > 25$) is individual failure where soil in front of each transverse member fails individually. The interference factor, *F* was proposed as follows (Horpibulsuk and Niramitkornburee, 2010):

$$F = \frac{P_{bn}}{nP_{b1}} = e + f \ln\left(\frac{S}{B}\right) \tag{3.7}$$

where e and f are constant, depending on n. These two constants can be obtained from two physical conditions: 1) when S/B equals 3.75, the interference factor equals $1/n$ because P_{bn} and P_{b1} are the same, and 2) when S/B equals 25, the interference factor equals unity. These two conditions establish the lower and upper values of F at corresponding values of $S/B = 3.75$ and 25, respectively. From these two conditions, the constants e and f can be determined by the following equations:

$$f = 0.527\left[1 - \frac{1}{n}\right] \tag{3.8}$$

$$e = 1 - 3.219f \tag{3.9}$$

It is found that the interference factor, F, predicted by Eqs.(3.8) and (3.9) can fit the experimental data. Based on the previous (Horpibulsuk and Niramitkornburee, 2010) and present studies, it is concluded that the member interference is dependent on only S/B, irrespective of grain size distribution and friction angle for the soils investigated. These two factors play a great role in determining P_{b1}. As such, even with the same S/B (same F), the P_{bn} values would be different for different grain size distributions and friction angles.

average grains and gradations. Finally, the procedure for examining the internal stability against pullout failure of the BRE wall is suggested. The conclusions can be drawn as follows:

1. The pullout friction resistance of the bearing reinforcement is mainly controlled by only the friction angle, irrespective of grain size distribution. The apparent friction between soil and the longitudinal member, μ, is greater than the soil friction angle because of the roughness and the rigidity of the steel deformed bar. The μ/ψ ratio is approximately 1.47 for all tested soils.

2. The pullout bearing mechanism is essentially controlled by B/D_{50} and normal stress, regardless of gradation (well-graded and poorly graded). As the bearing reinforcement is pulled out and shear displacement occurs along the interface, the zone of soil surrounding the reinforcement tends to dilate. However, the volume change is restrained by the surrounding non-dilating soil, resulting in an increase in normal stress on the soil-reinforcement interface (interlocking). The interlocking effect is significant for B/D_{50} values less than 12 and decreases as the normal stress increases.

3. By assuming that the general shear and modified punching shear mechanisms are the upper and lower boundaries, the equations of predicting N_q for $3 \le B/D_{50} \le 12$ and $30 \le \dagger_n \le 120$ are proposed and verified. Consequently, the maximum pullout bearing force of the bearing reinforcement with a single transverse member, P_{b1}, can be approximated.

4. The member interference is essentially dependent on S/B, irrespective of grain size distribution and friction. The transverse member interference zones are

classified into three zones. Zone 1 $(S/B \le 3.75)$ is block failure where all transverse members act like a rough block. Zone 2 $(3.75 < S/B < 25)$ is member interference failure. Zone 3 $(S/B > 25)$ is individual failure. Because the friction angle and B/D_{50} play a great role in determining P_{b1}, even with the same S/B (same F), the P_{bn} values would be different for different grain size distributions and friction angles.

3.5 References

AASHTO (2002). Standard specifications for highway and bridge, 7th edition. Washington D.C., **American Association of State Highway and Transportation Officials**.

Abdi, M.R. and Arjomand, M.A. (2011), "Pullout tests conducted on clay reinforced with geogrid encapsulated in thin layers of sand", **Geotextiles and Geomembranes**, Vol.29, pp. 588-595.

Alfaro, M.C. and Pathak, Y. P. (2005), "Dilatant stresses at the interface of granular fills and geogrid strip reinforcement", **Geosynthetics International**, Vol.12, No.5, pp. 239-252.

Alfaro, M.C., Hayashi, S., Miura, N. and Watanabe, K., 1995. Pullout interaction mechanism of geogrid strip reinforcement. **Geosynthetics International**, Vol.2, No.4, pp. 679-698.

Athanasapoulos, G.A. (1993), "Effect of particle size on the mechanical behavior of sand-geotextile composites", **Geotextiles and Geomembranes**, Vol.12, pp. 252-273.

Bergado, D.T. and Chai, J.C. (1994), "Prediction of pullout load-displacement relationship for extensible reinforcement", **Geotextiles and Geomembranes**, Vol.30, No.5, pp. 295-316.

Bergado, D.T., Sampaco, C.L., Alfaro, M.C., and Balasubramaniam, A. (1988), "Welded-Wire Reinforced Earth (Mechanically Stabilized Embankments) With Cohesive Backfill On Soft Clay", **2nd Progress Report Submitted to USAID Bangkok Agency**.

Bergado, D.T., Chai, J.C., and Miura, N. (1996), "Prediction of pullout resistance and pullout force-displacement relationship for inextensible grid reinforcements", **Soils and Foundations**, Vol.36, No.4, pp.11-22.

Bergado, D.T., Teerawattanasuk, C. and Long, P.V. (2000), "Localized mobilization of reinforcement force and its direction at the vicinity of failure surface", **Geotextiles and Geomembranes**, Vol.18, pp. 311-331.

Chai, J. C. (1992). Interaction between grid reinforcement and cohesive-frictional soil and performance of reinforced wall/embankment on soft ground, **D.Eng. Dissertation**, Asian Institute of Technology, Bangkok, Thailand.

Hayashi, S., Shaha, J. T. and Watanabe, K. (1999), "Change in interface stress during pullout test on grid strip reinforcement", **Geotechnical Testing Journal**, **ASTM**, Vol.22, pp. 32-38.

Horpibulsuk, S., and Niramitkornburee, A. (2010), "Pullout resistance of bearing reinforcement embedded in sand", **Soils and Foundations**, Vol.50, No.2, pp.215-226.

Horpibulsuk, S., Suksiripattanapong, C., and Niramitkornburee, A. (2010). "A method of examining internal stability of the bearing reinforcement earth (BRE) wall." **Suranaree Journal of Science and Technology**. Vol.17, No.1, pp.1-11.

Horpibulsuk, S., Suksiripattanapong, C., Niramitkornburee, A., Chinkulkijniwat, A., and Tangsuttinon, T. (2011), "Performance of earth wall stabilized with bearing reinforcements", **Geotextiles and Geomembranes**, Vol.29, No.5, pp.514-524.

Jewell, R.A., Milligan, G.W.E., Sarsby, R.W. and Dubois, D. (1984), "Interaction between soil and geogrids", **Proceedings of the Symposium on Polymer Grid Reinforcement in Civil Engineering**, Thomas Telford Limited, London, UK, pp.11-17.

Khedkar, M.S. and Mandal, J.N., (2009), "Pullout behavior of cellular reinforcements." **Geotextiles and Geomembranes**, Vol.27, No.4, pp.262-271.

Kumar, P.V.S.N.P. and Madhav, M.R. (2009), "Analysis of reinforced soil wall considering oblique pull: bilinear failure mechanism – Linear subgrade response", **Lowland Technology International**, Vol.11, No.1, pp.1-11.

Leschinsky, D. and Reinschmidt, A.J. (1985), "Stability of membrane reinforced slopes", **Journal of Geotechnical Engineering**, ASCE, Vol.115, pp.1285-1300.

Madhav, M.R. and Umashankar, B. (2003), "Analysis of inextensible sheet reinforcement subjected to transverse displacement/force: Linear subgrade response", **Geotextiles and Geomembranes**, Vol.21, pp.69-84.

Palmeira, E.M. (2009), "Soil–geosynthetic interaction: Modelling and analysis", **Geotextiles and Geomembranes**, Vol.27, pp.368-390.

Palmeira, E.M. and Milligan, G.W.E. (1989), "Scale and other factors affecting the results of pull-out tests of grids buried in sand", **Geotechnique**, Vol.39, No.3, pp. 511–524.

Peterson, L.M. and Anderson, L.R. (1980), "Pullout resistance of welded wire mats embedded in soil", **Research Report Submitted to Hilfiker Co, from the Civil and Environmental Engineering Department**, Utah State University, USA.

Rowe, R.K. and Ho, S.K. (1997), "Continuous panel reinforced soil walls on rigid foundations", **Journal of Geotechnical and Geoenvironmental Engineering**, Vol.123, No.10, pp.912-920.

Skinner, G. D., and Rowe, R. K. (2005). "Design and behavior of a geosynthetic reinforced retaining wall and bridge abutment on a yielding foundation." **Geotextitles and Geomembranes**, Vol.23, No.4, pp.234-260.

Madhav, M.R. and Umashankar, B. (2003), "Analysis of inextensible sheet reinforcement subjected to transverse displacement/force: Linear subgrade response", **Geotextiles and Geomembranes**, Vol.21, pp. 69-84.

Shewbridge, S.E. and Sitar, N. (1989), "Deformation characteristics of reinforced sand in direct shear", **Journal of Geotechnical Engineering**, ASCE, Vol.115, pp. 1134-1147.

Shivashankar, R. (1991), "Behaviour of mechanically stabilized earth (MSE) embankment with poor quality backfills on soft clay deposits, including a Study of the pullout resistance", **D.Eng. Dissertation**, Asian Institute of Technology, Bangkok, Thailand.

Suksiripattanapong, C., Chinkulkijniwat, A., Horpibulsuk, S., Rujikiatkamjorn, C. and
Tangsuttinon, T. (2012), "Numerical analysis of bearing reinforcement earth (BRE) wall", **Geotextiles and Geomembranes**, Vol.32, pp. 28-37.

Tin, N., Bergado, D.T., Anderson, L.R. and Voottipruex, P. (2011), "Factors affecting kinked steel grid reinforcement in MSE structures" **Geotextiles and Geomembranes,** Vol.29, pp.172-180.

CHAPTER IV

THE FINITE ELEMENT ANALYSIS OF THE BEARING

REINFORCEMENT EARTH WALL

4.1 Statement of problem

The performance of MSE walls was extensively studied using the full-scale, laboratory model tests and numerical simulation (Bergado et al., 2000; Bergado and Teerawattanasuk, 2007; Park and Tan, 2005; Skinner and Rowe, 2005; Al Hattamleh and Muhunthan, 2006; Hatami and Bathurst, 2005 and 2006; and Abdelouhab et al., 2011). ThePLAXIS program has been proved as a powerful and precise tool for predicting the performance of the MSE walland pullout test results (Bergado et al., 2003; and Khedkar and Mandal, 2007 and 2009). This chapter presentsa a finite element simulation of the performance of the BRE wall during and after construction,which includes settlement, bearing stress, lateral movement, lateral earth pressure and tension force in the reinforcements. The full-scale test results by Horpibulsuk et al. (2011) were taken for this simulation. The simulation was performed using the finite element code (PLAXIS 2D). The bearing reinforcement was modeled as the geotextile with an equivalent friction resistance. Finally, the knowledge gained from this simulation provides useful information for further analysis and design of the other BRE walls with different wall heights, ground conditions and features of bearing reinforcement.

4.2 Full scale test of Bearing Reinforcement Earth (BRE) wall

4.2.1 Subsoil investigation

A full-scale test on a bearing reinforcement earth wall was performed at the campus of Suranaree University of Technology (SUT) on 20 July 2009. The general soil profile consisted of weathered crust layer of silty sand over the top 2.0 m. This layer was underlain by medium dense silty sand down to about 6 m depth. Below the medium dense sand layer was the very dense silty sand. The ground water was not observed even up to 8 meter depth (end of boring). Figure 4.1 shows the soil profile of the site. The in-situ strength of the subsoil was measured using the standard penetration test.
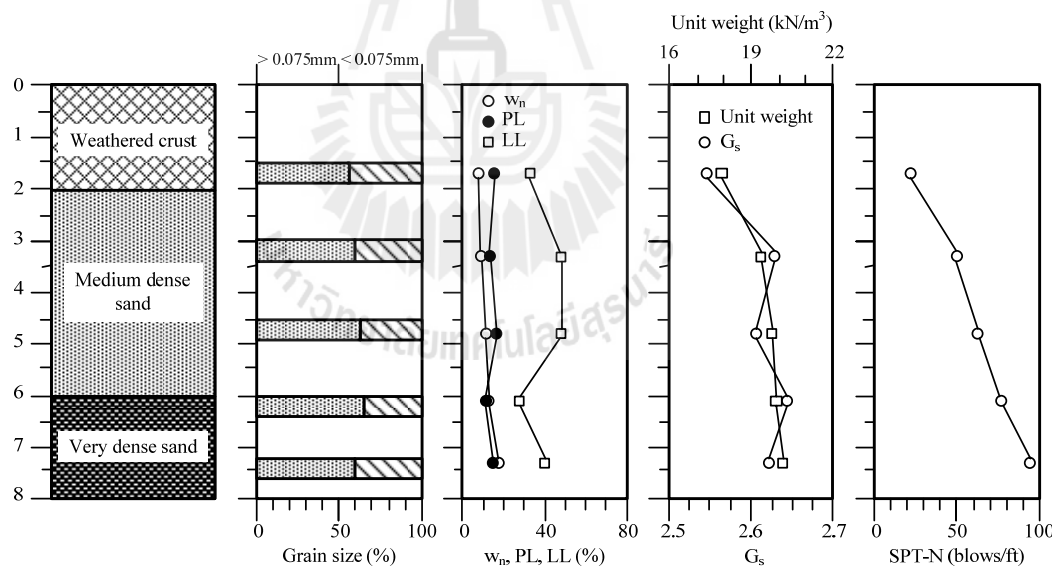
Figure 4.1 General soil profile

4.2.2 Feature of the test Bearing Reinforcement Earth wall

The wall was 6 m high, 9 m long and 6 m wide at the top, and 21 m long and 12 m wide at the base, as illustrated in Figures 4.2 and 4.3. The side and back slopes were 1:1. The BRE wall was designed based on the limit equilibrium analysis.

The detailed design was explained elsewhere by Horpibulsuk et al. (2010 and 2011). The ground was first excavated to 0.5 m depth below the original ground where the wall base was located. The wall facing panels were placed on a lean concrete leveling pad (0.15 m width and 0.15 m thickness) after 2 days of curing. The leveling pad was at 0.15 m depth below the excavated ground. The wall face was made of segmental concrete panels (1.50 x 1.50 x 0.14 m^3). In this construction, 4 facing panels were installed in the middle zone of the wall width (9 x 6 x 6 m^3) with 8 reinforcement levels. The longitudinal members for all layers were 12 mm diameter and 4.2 m long. The transverse members were equal steel angles with 25 mm leg length (B) and 180 mm length (L). The transverse member spacing was 750 mm for all transverse members. The vertical spacing between each reinforcement level was 750 mm. The horizontal spacing was 750 mm for levels 4 to 8 and 0.50 for levels 1 to 3. The details of the bearing reinforcement for each layer are summarized in Table 4.1. The backfill was compacted in layers of approximately 0.15 m thickness to a dry density of about 90% the standard Proctor density. The compaction was carried out with a hand compactor. The degree of compaction and water content were checked regularly at several points for all the compaction layers by the sand cone method. Construction sequence is illustrated in Figure 4.4. The total time spent for the construction was 20 days. At 47 days after the completion of construction, the top of the embankment was raised by 1.2 m as additional surcharge to simulate the surcharge load of about 20 kPa.

(a) Plan view

(b) Section view
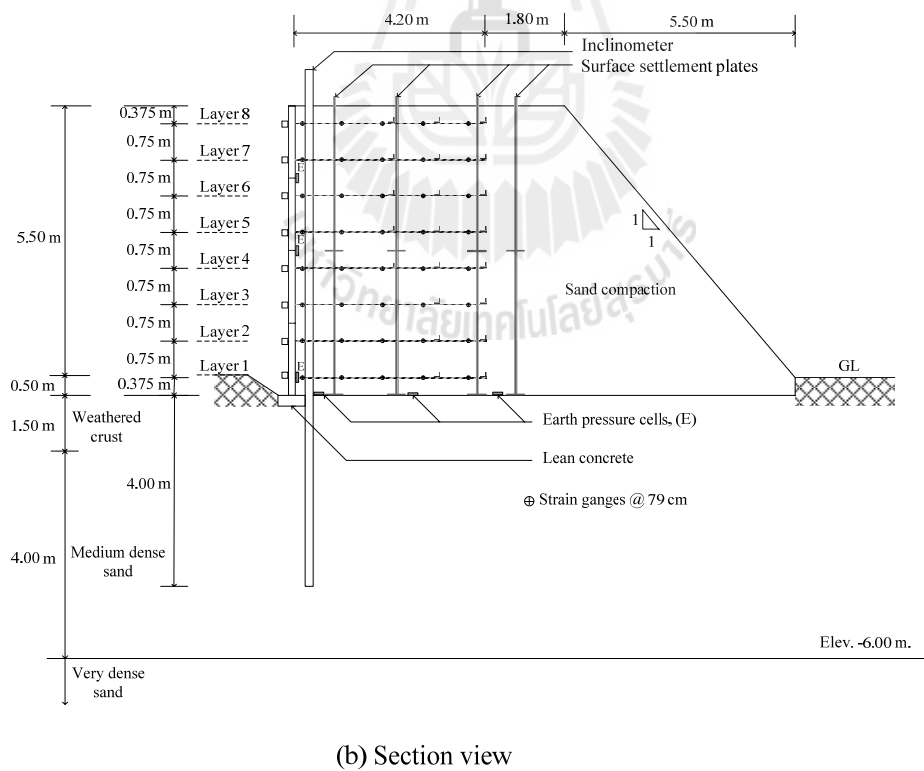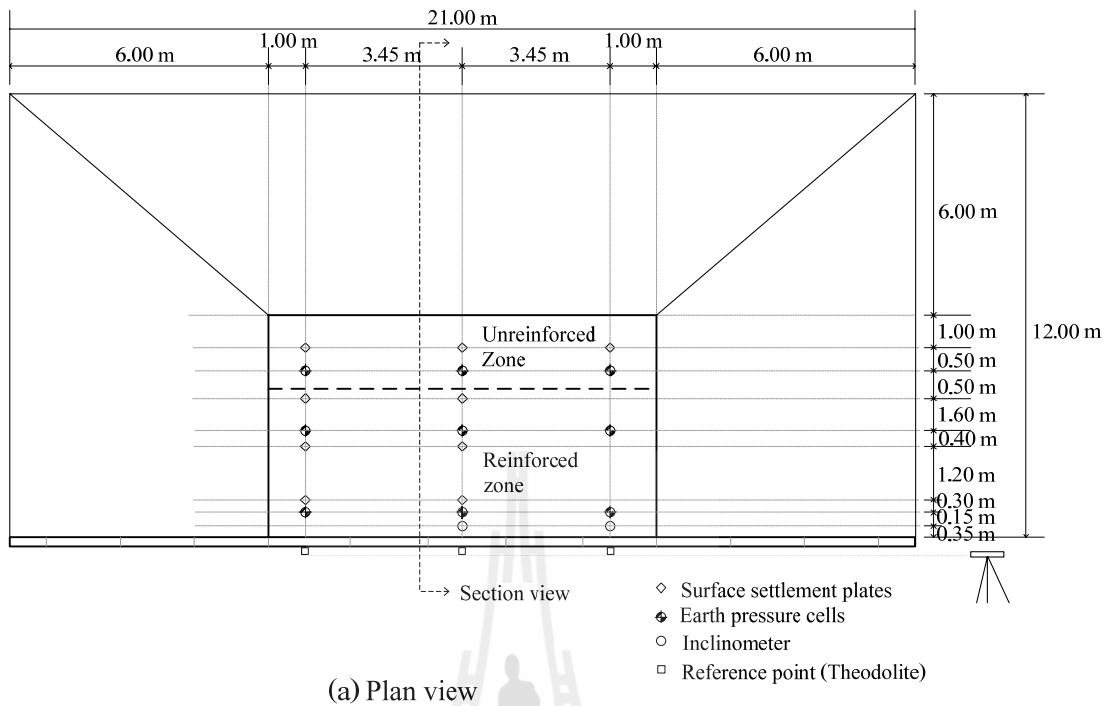
Figure 4.2 Schematic diagram of the test wall with instrumentation

Figure 4.3 Full-scale test BRE wall
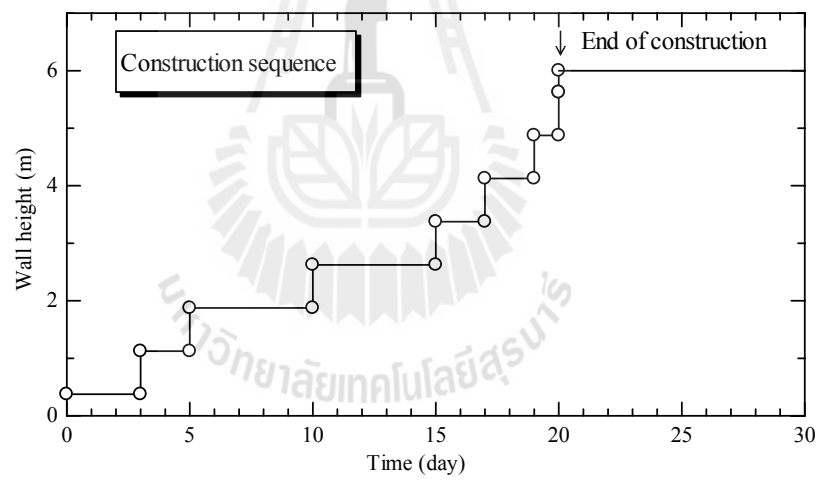
Figure 4.4 Construction sequence of BRE wall

Table 4.1 Reinforcement details for the test wall (Horpibulsuk and

Niramitkornburee, 2010).

Facing panel	Reinforcement layers	Spacing between longitudinal members (12 mm deformed bar)	Number of transverse members (25x25x3 mm equal angle)
1	1 (bottom)	500 mm	2
	2	500 mm	2
2	3	500 mm	2
	4	750 mm	3
3	5	750 mm	3
	6	750 mm	3
4	7	750 mm	3
	8 (Top)	750 mm	3

4.2.3 Instrumentation program

The BRE wall was extensively instrumented both in the subsoil and within the wall itself.The ground water table observation well and piezometer were not used in this investigation because the ground water was deeper than 8 m depth (end of boring). The settlement plates were installed in the subsoil and backfill. The earth pressure cells were installed in the subsoil andfacing panels. Lateral movements of each segmental panel during construction were recorded by a theodolite with reference to the benchmark.Lateral movements after the end of construction were measured from digital inclinometers. The inclinometer casing was installed from top of wall down to the medium dense sand about 4 m below the wall base. The strains and tensile forces along the longitudinal members were measured by outdoor

waterproof type strain gauges. The measurement points were located at 0.23, 1.02, 1.81, 2.60 and 3.39 m distance from the wall. The strain gauges were installed at all eight layers of the bearing reinforcement in the middle zone of the wall.

4.3 Model parameters

The bearing reinforcement earth wall was modeled as a plane strain problem. The finite element mesh and boundary condition are shown in Figure4.5. The finite element mesh involved 15-node triangular elements for the backfill and the foundation.The nodal points at the bottom boundary were fixed in both directions and those on the side boundaries were fixed only in the horizontal direction. The simulation was performed in drained condition because the groundwater was not detected during the study. The model parameters related to the compressibility were obtained from the conventional laboratory test that did not consider the time dependent behavior such as creep. The creep model is not within the scope of this study because this paper aims to simulate the wall behavior with the simple and well-known soil models for practical design.
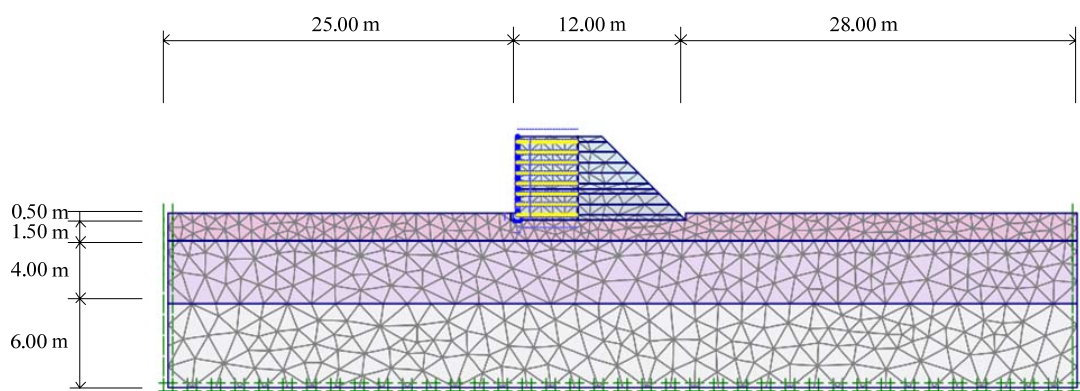
Figure 4.5 Finite element model of BRE wall

4.3.1 Backfill

The backfill was a clean sand, which consists of 0.3% gravel, 97% sand and 2.7% silt. This sand is classified as poorly graded sand (SP), according to the Unified Soil Classification System (USCS). The backfill material was modeled as a linear elastic–perfectly plastic material with the Mohr–Coulomb failure criteria. The apparent cohesion and the friction angle were determined from a large direct shear apparatus with the diameter of 35 cm and they are $c' = 0$ and $\phi' = 40$ degrees. This high friction angle (greater than 36 degrees) is acceptable for MSE wall construction. Considering the average normal pressure at mid-height of the backfill (3 m high), the average normal pressure was calculated to be about 60 kPa. The input parameter of sand at the average normal pressure of 60 kPa was selected to represent the backfill material properties of the BRE wall. The material properties of the backfill used for the finite element simulation are shown in Table 4.2.

4.3.2 Weathered crust

The weathered crust layer was a silty clay. The water content was 12% and the dry unit weight, γ_d was 17 kN/m³. The apparent cohesion and the friction angle were determined from drained direct shear tests and equal to $c' = 20$ kPa and $\phi' = 26$ degrees. An elastic, perfectly plastic Mohr-Coulomb model was used to simulate the behavior of the weathered crust layer. The material properties of the weathered crust layer used for the finite element simulations are also shown in Table 4.2.

Table 4.2 Model parameters for backfill and subsoil

Item	Backfill soil	Weathered crust	Medium dense sand	very dense sand
Material model	Mohr-Coulomb	Mohr-Coulomb	Mohr-Coulomb	Mohr-Coulomb
Material type	Drained	Drained	Drained	Drained
γ_{dry}	17 kN/m^3	17 kN/m^3	17.15 kN/m^3	18 kN/m^3
γ_{wet}	18.15 kN/m^3	18 kN/m^3	18.15 kN/m^3	19 kN/m^3
k_x	1 m/day	1 m/day	1 m/day	1 m/day
k_y	1 m/day	1 m/day	1 m/day	1 m/day
E_{ref}	35000 kN/m^2	1875 kN/m^2	40000 kN/m^2	50000 kN/m^2
ν	0.33	0.30	0.25	0.30
c'	1kPa	20 kPa	1kPa	1kPa
ϕ'	40°	26°	35°	38°

4.3.3 Medium to very dense sand

The medium to very dense sand layer was classified as clayey sand, according to the USCS. It consisted of 15-18% gravel, 48-60% sand, 8-10% silt and 16-23% clay. The natural water content was 12-20% and the dry unit weight, $\gamma_{d\,max}$ was 17-19 kN/m^3. Based on a drained direct shear test, the strength parameters were $c'= 0$ and $\phi'= 37$ degrees. This is typical of the residual soil in the SUT campus (Horpibulsuk et al., 2008). An elastic, perfectly plastic Mohr-Coulomb model was used to simulate the behavior of this medium to very dense sand. The material properties used for the finite element simulations are shown in Table 4.2.

4.3.4 Bearing reinforcement and interface parameter

Thegeotextile elements, which cannot resist the bending moment, were employed to model the bearing reinforcement, even though it is composed of longitudinal and transverse members. This modeling converts the contribution of both the friction and bearing resistances to the equivalent friction resistance. The equivalent friction resistance is represented by the interface factor, R. The input parameter for this element is an axial stiffness, AE, where A is the cross-sectional area of longitudinal member and E is the modulus of elasticity of the material (steel). The test longitudinal member was 12 mm diameter and 2.6 m length. The axial stiffness of bearing reinforcement used in laboratory model test is shown in Table4.3.The width of the transverse member in the laboratory model test was 0.15 m.The soil/bearing reinforcement interface parameter, R, was from the back analysis of the laboratory pullout tests by Horpibulsuk and Neramitkornburee (2010) (Figure 4.6). The elastic perfectly-plastic model was used to simulate the constitutive relation of the interface between soil and bearing reinforcement. Transverse members are rigid and there was no evidence of the bending of the transverse members from the retrieved bearing reinforcements. It is thus assumed that the pullout displacement and pullout force mobilized insignificantly varies over the length of the reinforcement and the R value is dependent on only the numbers of transverse member, n. As n increases, the R value increases (stiffness increases). The $n = 2$ and 3 were considered to determine the R that are the same as the full-scale BRE wall. The laboratory pullout test was modeled as a plane strain problem. The nodal points at the bottom boundary were fixed in both directions and those on the side boundaries were fixed only in the horizontal direction. The finite element mesh was comprised of 15-nodes triangular

elements. The finite element mesh consisted of 558 triangular soil elements not including interface elements.The parameters for bearing reinforcement used in the BRE wall model test are tabulated in Table 4.4.

Table 4.3 Model parameters for bearing reinforcement in laboratory model test

Type	Modulus of elasticity (GPa)	Axial stiffness, EA (kN/m)
Bearing reinforcement	200	150796
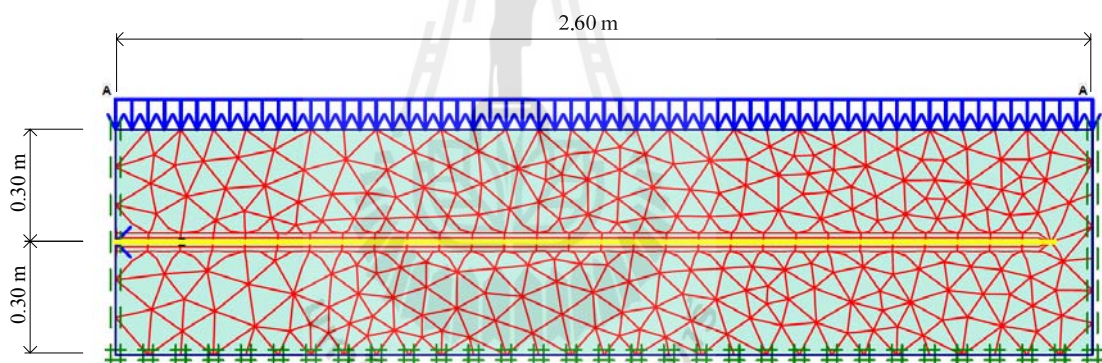
Figure 4.6 Finite element model for pullout tests.

Table 4.4 Model parameters for reinforced element structure

Item	Bearing reinforcement	Facing concrete
Material model	Elastic	Elastic
EA	4.5E+4 kN/m	3.556E+7 kN/m
EI	-	5808 kNm^2/m
w	-	3.36 kN/m/m
υ	-	0.30

4.3.5 Facing concrete panels

The facing panels were made of segmental concrete panel, which measured 1.50 x 1.50 x 0.14 m in dimension. The facing panel was modeled as a beam element. The values for the strength parameters and the modulus of elasticity are shown in Table 3. The soil/facing panel interface, R, was taken as 0.9, which is generally used for concrete panels (Bathurst, 1993)

4.4 Finite element analyses

4.4.1 Soil-reinforcement interface coefficient, R

Figures 4.7 to 4.10 show the measured and simulated total pullout force and displacement relationship of the 2.6 m length bearing reinforcements with 1 to 4 transverse members (n = 1 to 4), respectively. The test results within a small displacement of less than 5 mm were considered to determine the interface coefficient, R which is consistent with the field wall movement. The small lateral wall movement is caused by the base restriction effect of the hard stratum (Rowe and Ho, 1997). The interface coefficient, R, was derived by back analysis varied until the modeled curves coincided with the laboratory curves. It is found that the R values of 0.55, 0.65, 0.75 and 0.85 provide the best simulation for 1, 2, 3 and 4 transverse members, respectively. This method of determining, R is analogous to that by Bergado et al., (2003); and Khedkar and Mandal (2007 and 2009) for hexagonal wire mesh and cellular reinforcement. Figure 4.11 shows the effect of S/B on the R value. It is found that the relationship between R and S/B is in similar pattern to the relationship between F and S/B. In the interference zone, the R value increases with S/B up to S/B value of 25.
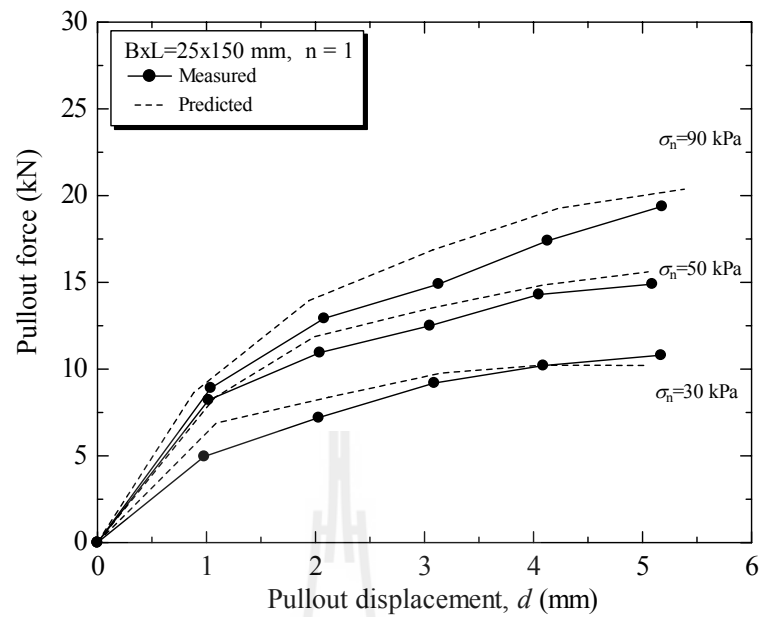
Figure 4.7 Comparison between the simulated and measured pullout test result of the

bearing reinforcement with a transverse members
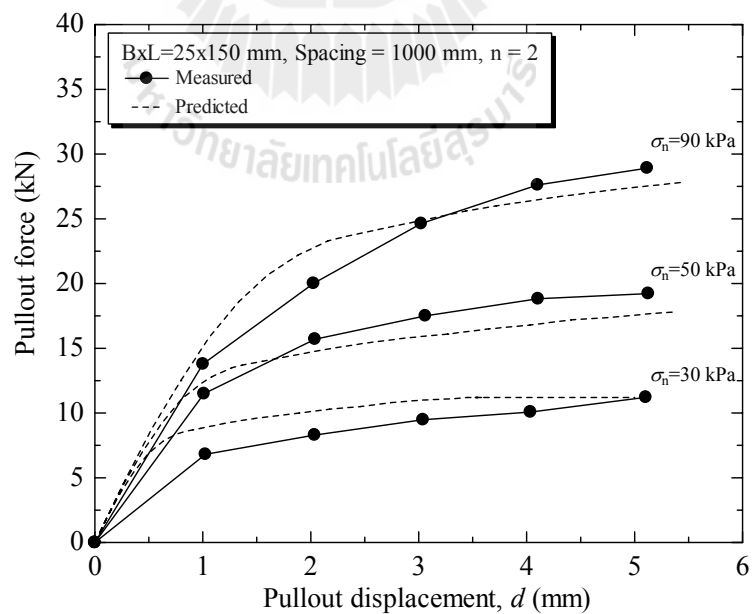
Figure 4.8 Comparison between the simulated and measured pullout test result of the

bearing reinforcement with two transverse members
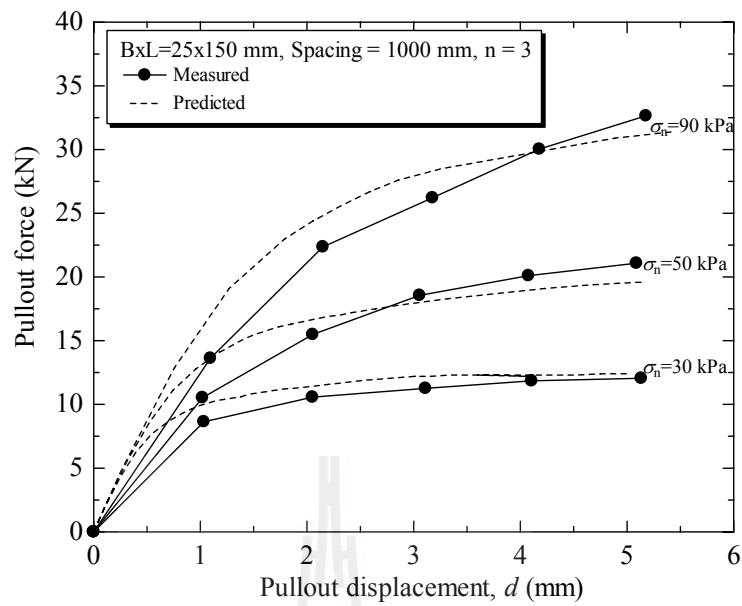
Figure 4.9 Comparison between the simulated and measured pullout test result of the

bearing reinforcement with three transverse members
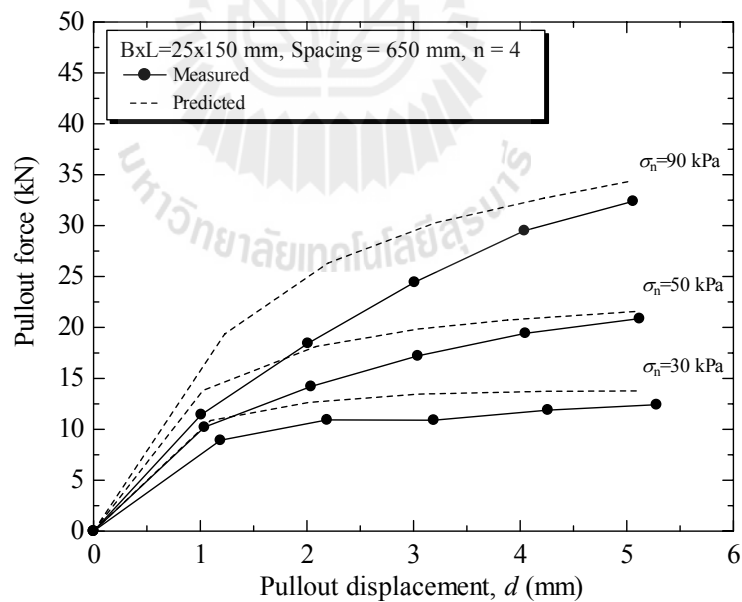
Figure 4.10 Comparison between the simulated and measured pullout test result of

the bearing reinforcement with four transverse members
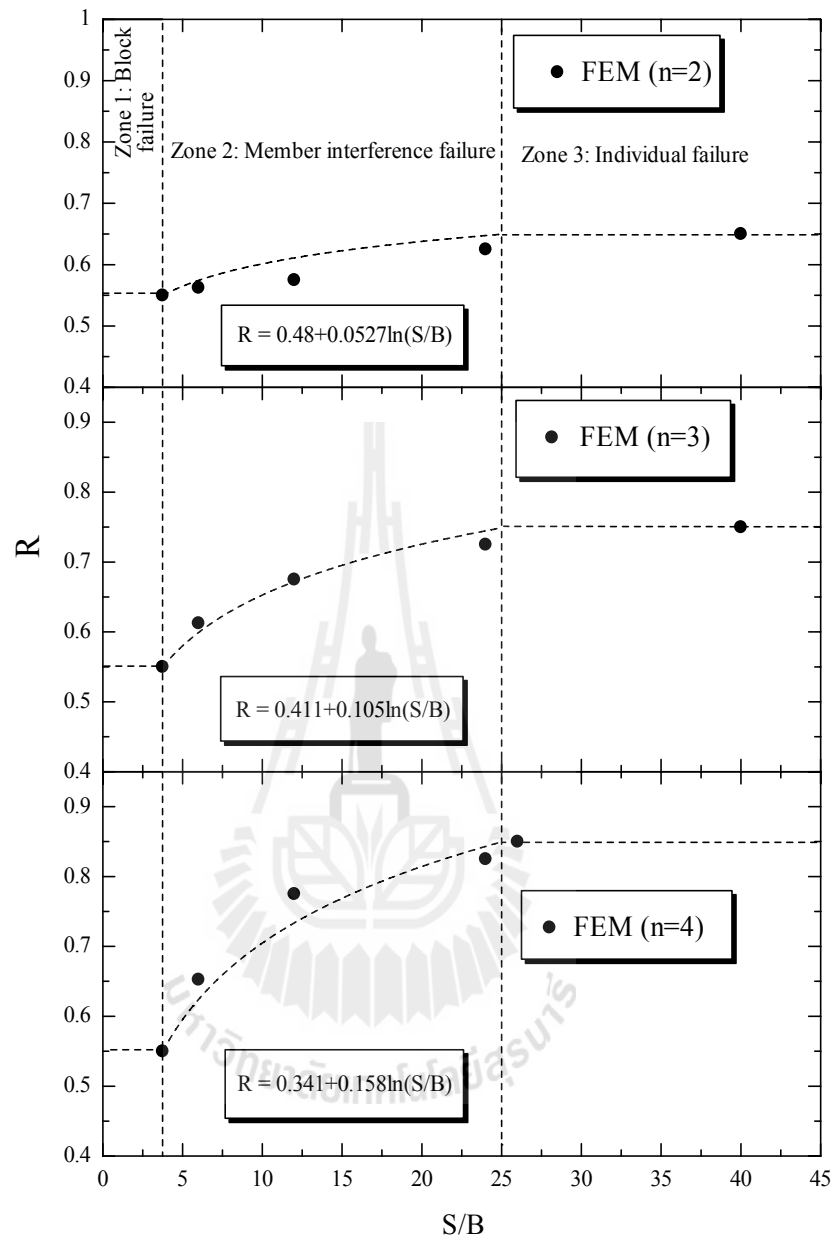
Figure 4.11 Effect of S/B on R value.

4.4.2 Bearing stress

Figure 4.12 shows the relationship between bearing stress and construction time in both reinforced (0.5 and 2.4 m from wall facing) and unreinforced (4.5 m from facing) zones. The bearing stresses increase during

construction due to the construction load. The bearing stress changes insignificantly with time after the completion of construction. The simulated bearing stresses for both front and back are very good in agreement with the measured ones. At 2.4 m from the wall face, the bearing stresses during 10 days (1st and 2nd loading) of construction are very close to the measured ones but beyond the 2nd loading, the simulated bearing stress is lower than the measured one, and hence the simulated final bearing stress is lower. The difference between the simulated and measured might be due to the non-uniformity of compaction at this particular location; therefore, the earth pressure cell sank into the ground at about 32 kPa vertical pressure (2nd loading). The bearing stress could be again recorded after the 3rd loading that the earth pressure cell sat on the hard compacted foundation. Figure 4.13 shows the measured and the simulated distribution of bearing stresses at the end of construction from the front to back. The simulated and measured bearing stresses patterns are in good agreement. Within the reinforced zone, the bearing stress distribution is essentially uniform even with the eccentric load from the backfill, which is typical of rigid foundation. The maximum bearing stress at front is due to a eccentric load caused by the lateral thrust from the unreinforced backfill and the vertical load from the weight of segmental panels. The bearing stress insignificantly changes with distance in the unreinforced zone and being equal to that at the end of bearing reinforcement.
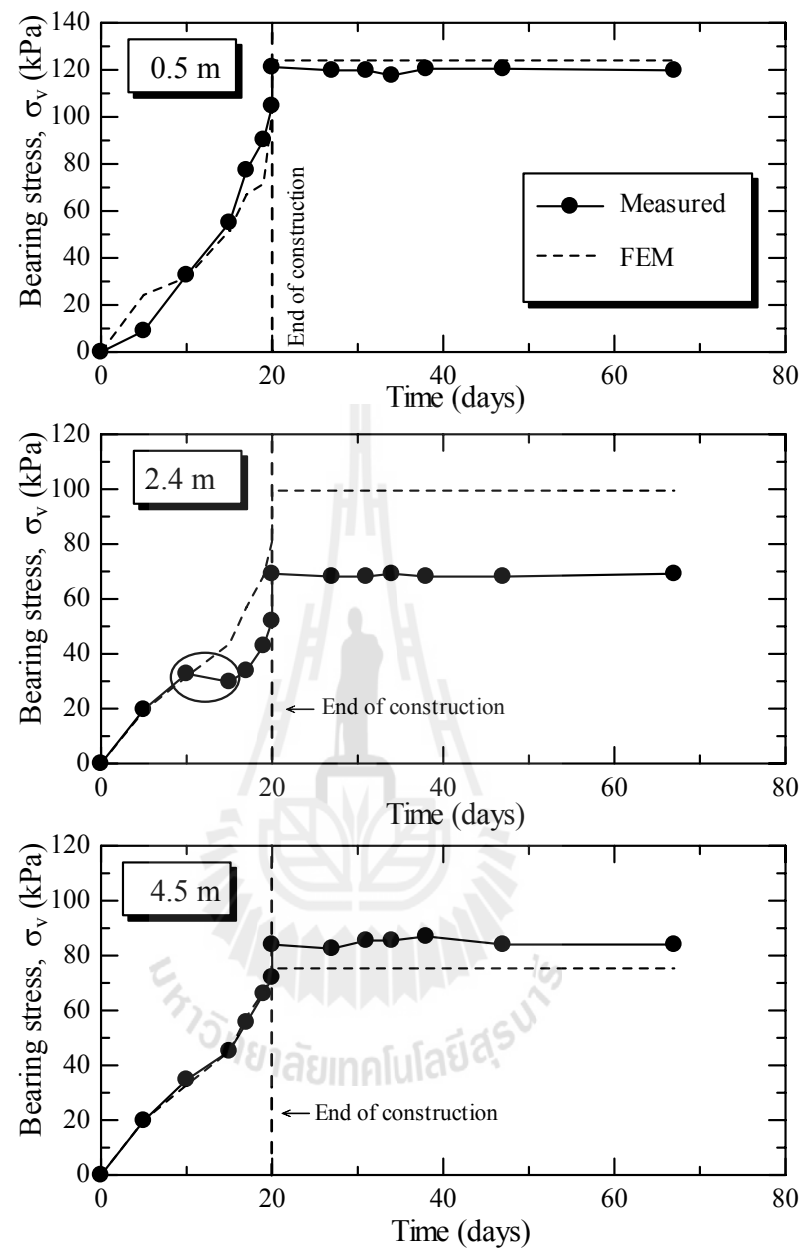
Figure 4.12 Comparison between the simulated and measured bearing stress change

with construction time.
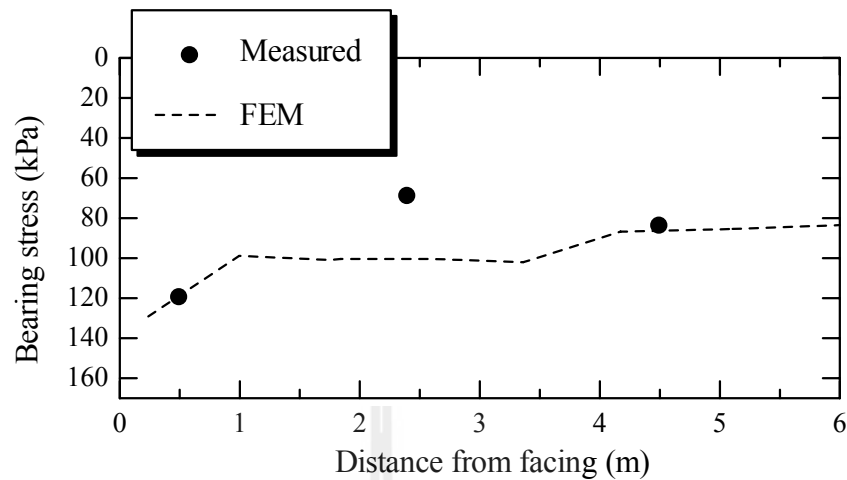
Figure 4.13 Comparison between the simulated and measured bearing stress distribution.

4.4.3 Settlement

The measured and simulated settlements of the BRE wall are illustrated in Figures 4.14 and 4.15. The observed data from the four settlement plates at the center of the BRE wall were compared with the simulation. The settlement increased with construction time (Figures 4.14). Because the wall was founded on the relatively dry and hard stratum, the immediate settlement was dominant (insignificant consolidation settlement). The simulated settlements during construction are very close to the measured ones. The simulated settlements decrease from front that is close to the facing panel (82 mm) to back (77 mm) (*vide* Figure 4.15). The settlement is almost uniform which is due to the uniform bearing stress distribution. Among the four measuring points, 2 measured data divert from the simulation results: at 0.8 m and 5 m (unreinforced zone) from the facing. The measured settlement at 0.8 m from the facing is slightly higher than the simulated one possibly because the foundation

might be disturbed during the foundation excavation for making the leveling pad. The measured settlement in unreinforced zone (5 m from facing) is higher than the simulated one because the stiffness of the foundation in the unreinforced zone is lower than that in the reinforced zone (the foundation in the reinforced zone was compacted before constructing the BRE wall). In this simulation, the same modulus of elasticity, E was applied to both unreinforced and reinforced zones for simplicity. A better simulation could be found if different E is used for the simulation. Overall speaking, the computed settlements in the reinforced zone from the FEM analysis agree reasonably well with the measured ones.
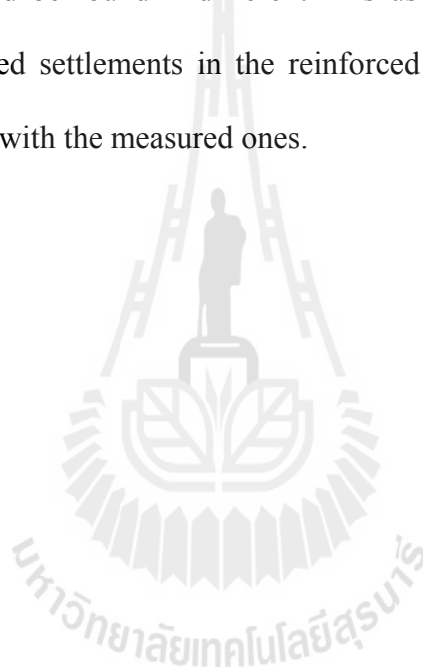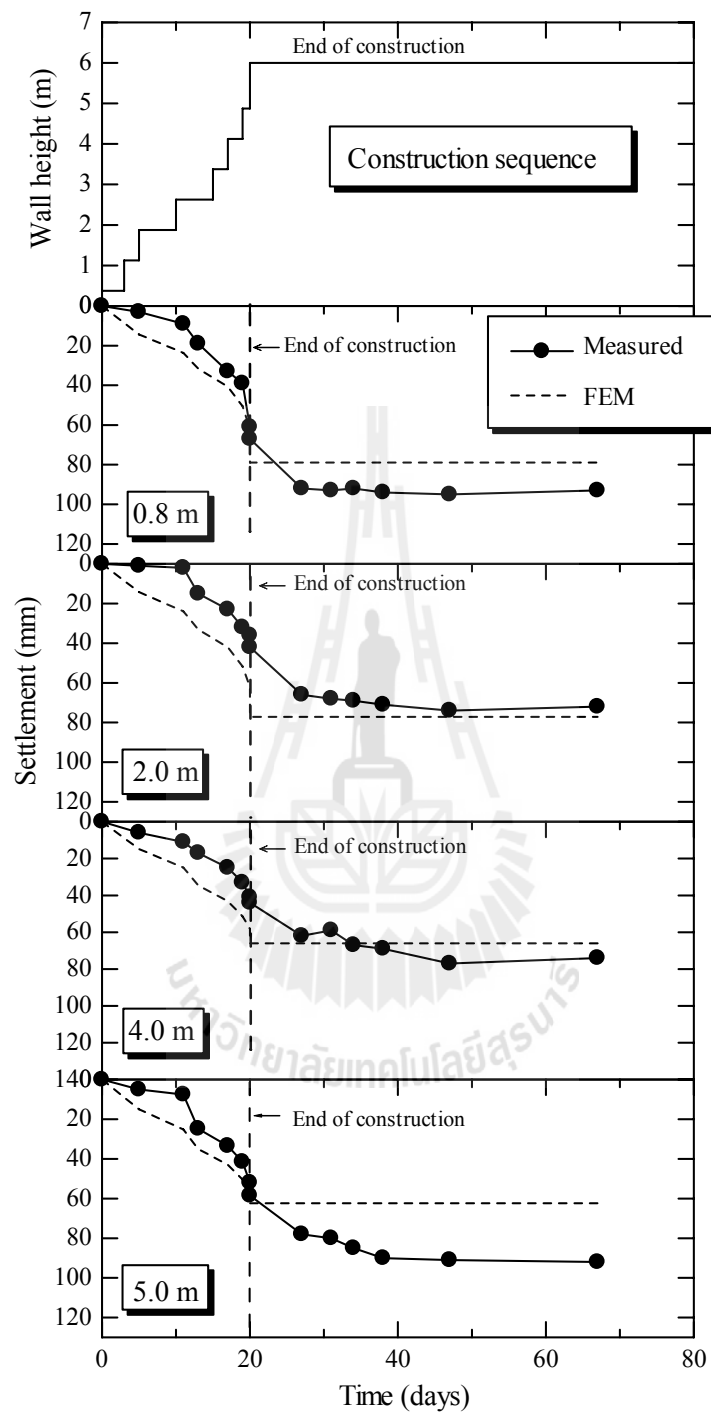
Figure 4.14 Comparison between the simulated and measured settlement change

with construction time.
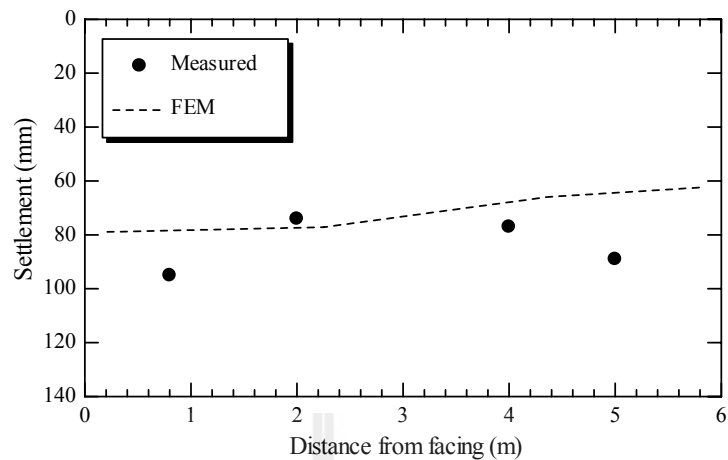
Figure 4.15 Comparison between the measured and computed settlements

4.4.4 Lateral movement

The simulated and measured lateral movements are compared and shown in Figure 4.16. The measured lateral movement was the sum of the lateral movements during construction (measured by a theodolite) and after end construction (measured by digital inclinometers). The measured lateral movement is slightly lower than the simulated one. However, based on the R values obtained from the simulation, the patterns of the lateral movement from both the simulation and measurement are almost the same. Lateral movement is caused by the wall settlement and pullout displacement of the reinforcement, which is governed by the R value. The R value also controls the tension in the reinforcement. The lower the R value, the greater the lateral movement and the lower the tension in reinforcement. The obtained R values are considered as suitable because both the simulated lateral movement and the simulated tension in the reinforcement (presented in the following section) are in good agreement with the measured ones. The simulated maximum lateral movement in the

subsoil occurs between 0.5-1.5 m depth below original ground surface corresponding to the weathered crust. The simulated maximum wall movement occurs at about the mid-height with a small magnitude of 23.5 mm. Although the BRE wall rotated about the toe, at a certain stage of deformation process, a crack developed at about the middle of the wall height and the wall started to deform as two rigid panels with a progressive opening of the crack. This finding is in agreement with that by Pinto and Cousens (1996 and 2000).
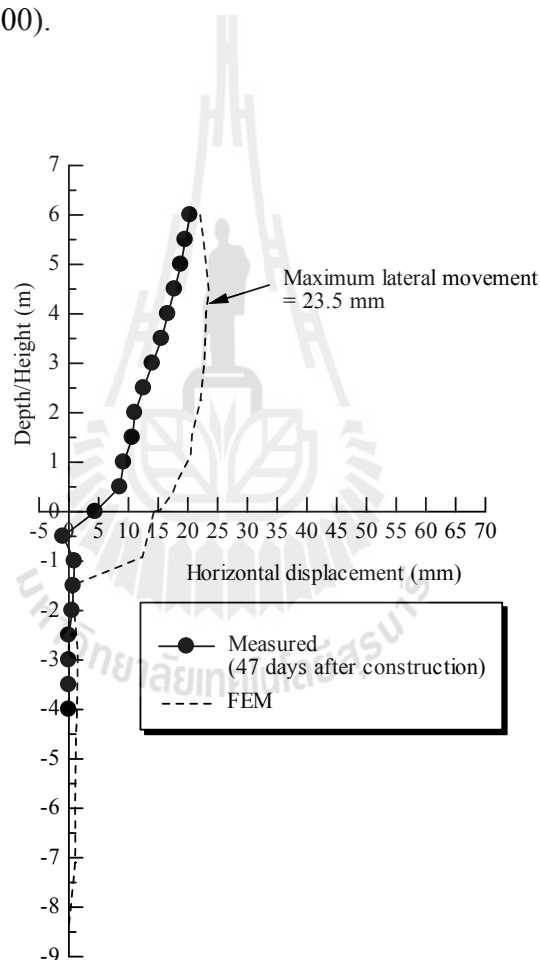
Figure 4.16 Comparison between the simulated and measured lateral movements

4.4.5 Lateral earth pressure

The measured and simulated lateral earth pressures during construction at wall face are depicted in Figure 4.17. The lateral earth pressures at wall facing panels were measured from earth pressure cells attached to the wall facing panels. The lateral earth pressure, σ_h at the wall facing panels is useful for designing the tie points and facing panels. The simulated lateral earth pressure increases during construction due to construction load (caused by the backfill). The simulated lateral earth pressures during construction were close to the measured ones for the three measurement points (0.375, 3.0 and 4.5 m from the wall base). The lateral earth pressures, σ_h are initially close to the at-rest value, $K_0 \sigma_v$. With the increase in the backfill load, the lateral earth pressures, σ_h reduce and tend to approach the active value, $K_a \sigma_v$. Both K_0 and K_a were calculated from the Rankine's theory that the friction between wall and soil is ignored. At 0.375 m, the simulated σ_h is lower than the calculated $K_a \sigma_v$ due to the effect of the soil/wall interface. This finding is the same as that by Rowe and Ho (1997).
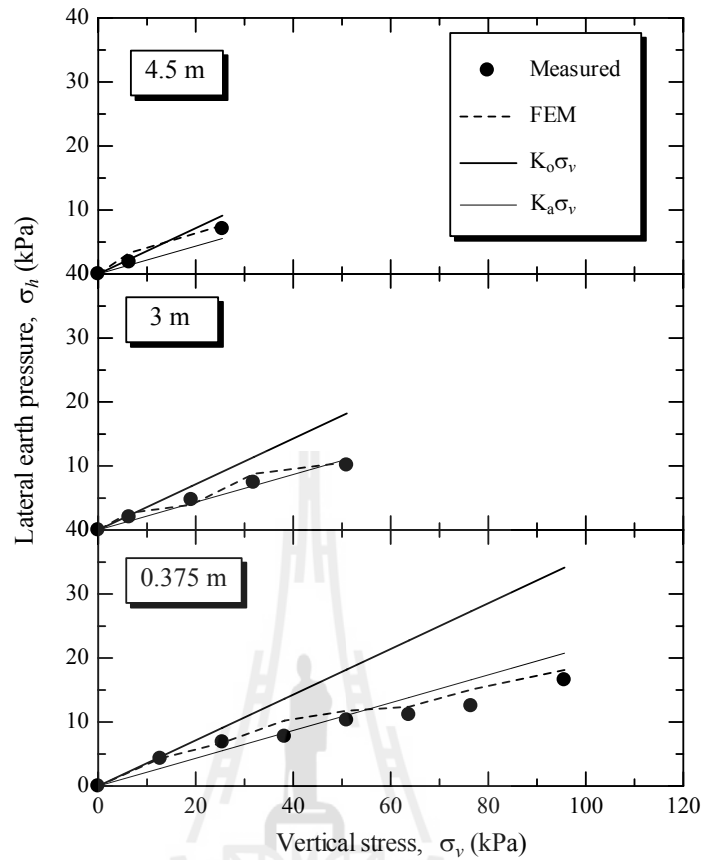
Figure 4.17 Comparison between the simulated and measured lateral earth pressures
at different depths and applied vertical stresses

4.4.6 Tensions in the bearing reinforcement

The simulated and measured tensions during construction at the points
0.23, 1.81 m distance from the wall face are shown in Figure 4.18. The simulated
tension forces are in good agreement with the measured ones. The tension forces for
both points increased with the vertical stress.Figure 4.19 shows the comparison
between the simulated and the measured tension forces in the bearing reinforcements
at 14 days after the completion of construction and 10 days after additional surcharge
load 20 kPa. The smooth relationships between tension and distance are found for

both the measured data and simulation results. The smooth curves from the measured data are because all the strain gauges were attached to the longitudinal members. In fact, the sharp peaks might be recorded if the strain gauges were attached close to the transverse members. The possible failure plane recommended by AASHTO (2002) for inextensible reinforcements is also shown in the figure by a dash line. Most of the simulated maximum tension forces lie on the recommended possible failure plane. In practice, the maximum tension (possible failure) plane recommended by AASHTO (2002) can be thus used to examine the internal stability of the BRE wall using the limit equilibrium analysis. This simulated maximum tension pattern is approximate bi-linear and similar to the previous studies for different types of reinforcement (Chai, 1992; Bergado et al., 1995; Alfaro et al., 1997; and Bergado and Teerawattanasuk, 2007). This approximate bi-linear maximum tension plane is caused by the lateral movement of two facing panels at about the mid-height of the wall.
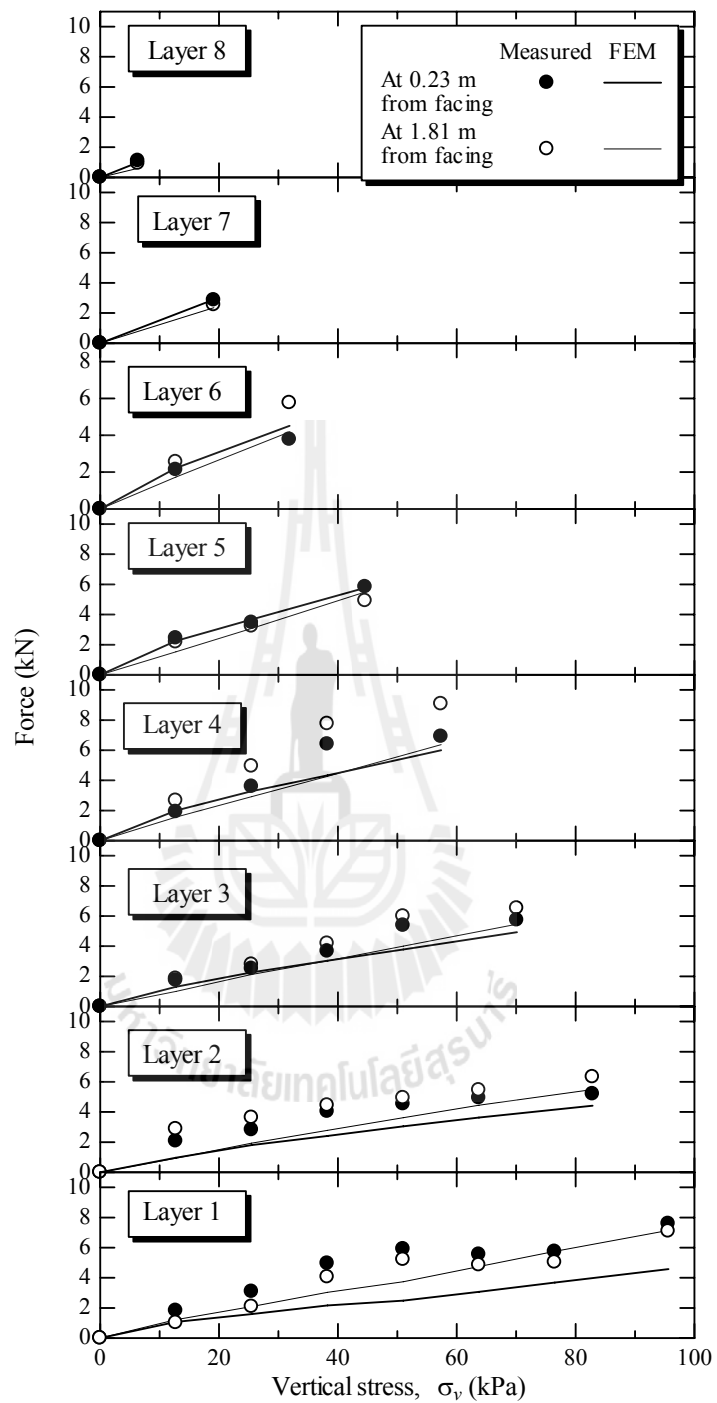
Figure 4.18 Comparison between the simulated and measured tension forces and for

different reinforcement layers and applied vertical stresses at 0.23 and

1.81 m from the wall face.
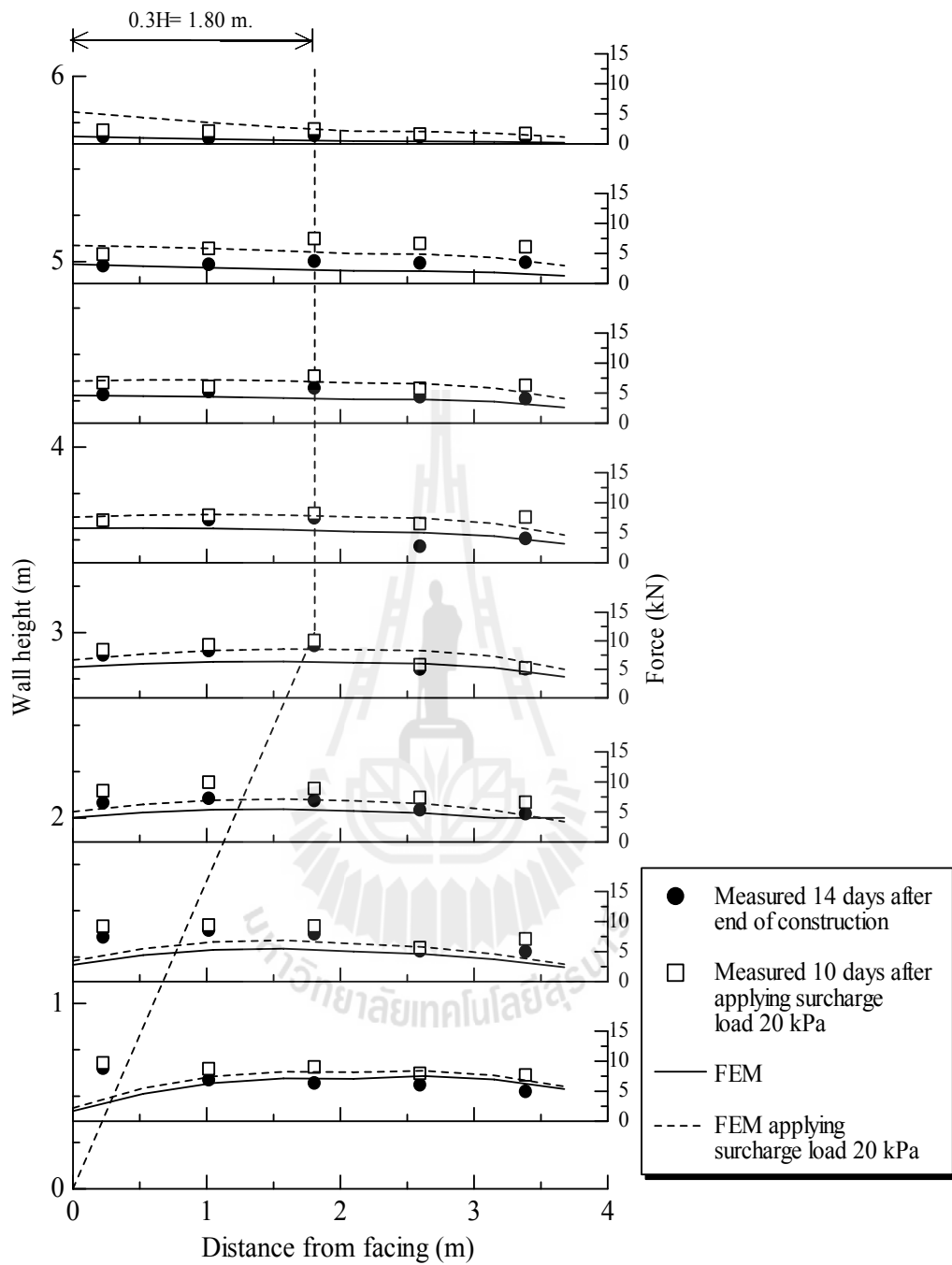
Figure 4.19 Comparison between the simulated and measured tension forces in the

reinforcements

4.5 Conclusions

This chapter presents a numerical analysis of the bearing reinforcement earth (BRE) wall constructed on the hard stratum by PLAXIS 2D. The goetextile elements, which cannot resist the bending moment, were used to model the bearing reinforcements by converting the contribution of both the friction and bearing resistances to the equivalent friction resistance. This modeling is considered to be applicable and practical for working state (small pullout displacement). The equivalent friction resistance is represented by the interface factor, R, which was determined from the back analysis of the laboratory pullout test. The R values of 0.65 and 0.75 were obtained for the bearing reinforcements with 2 and 3 transverse members, respectively. The BRE wall was modeled under a plane strain condition and the reinforcements were modeled using geotextile elements, which cannot resist the bending moment. Overall, the behavior of the BRE wall is simulated satisfactorily and agreed well with the predictions. The changes in foundation settlements, bearing stresses, lateral earth pressures and tensions in the reinforcements during and after construction are in good agreement with the measured ones. The bearing stress distribution is approximately trapezoid shape as generally observed for embankments found on hard stratum. The foundation settlement is almost uniform due to the effect of high stiffness of the foundation and reinforcements. The simulated lateral earth pressures for different depths are initially close to the at-rest Rankine lateral earth pressure. During construction, the simulated lateral earth pressures approach the active Rankine lateral earth pressure and are lower than the active Rankine lateral earth pressure especially at about wall base because of the effect of the wall/soil interface. The simulated maximum lateral wall movement occurs at about the mid-

height. Although the BRE wall rotates about the toe, at a certain stage of deformation process, a crack develops at the middle of the wall height and the wall starts to deform as two rigid blocks with a progressive opening of the crack. This results in the approximate bilinear maximum tension (possible failure) plane. This maximum tension (possible failure) plane is very close to that recommended by AASHTO (2002) for inextensible reinforcements. In practice, this recommended maximum tension plane is acceptable to examine the internal stability of the BRE wall. The simulation approach presented was successfully applied to investigate the performance of the BRE wall in Thailand.

4.6 References

AASHTO (1996). Standard specifications for highway and bridge, 1th edition. Washington D.C., **American Association of State Highway and Transportation Officials**.

AASHTO (2002). Standard specifications for highway and bridge, 7th edition. Washington D.C., **American Association of State Highway and Transportation Officials**.

Alforo, M.C., Hayashi, S., Miura, N., Bergado, D.T. (1997), "Deformation of reinforced soil-embankment system on soft clay foundation, **Soils and Foundations**, Vol.37, No.4, pp.33-46.

Al Hattamleh, O., Muhunthan, B. (2006), "Numerical procedures for deformation calculations in the reinforced soil walls", **Geotextitles and Geomembranes**, Vol.24, No.1, pp.52-57.

Bathurst, R.J. (1993), "Investigation of footing resistant on stability of large-scale reinforced soil wall tests", **Proceedings of 46th Canadian Geotechnical Conference**.

Bergado, D.T., Chai, J.C., Miura, N., 1995. "FE analysis of grid reinforced embankment system on soft Bangkok clay." **Computers and Geotechnics**, Vol.17, pp.447–471.

Bergado, D.T., Chai, J.C., and Miura, N. (1996), "Prediction of pullout resistance and pullout force-displacement relationship for inextensible grid reinforcements", **Soils and Foundations**, Vol.36, No.4, pp.11-22.

Bergado, D.T., Teerawattanasuk, C., 2007. "2D and 3D numerical simulations of reinforced embankments on soft ground." **Geotextiles and Geomembranes**, Vol.26, No.1, pp.39–55.

Bergado, D.T., Teerawattanasuk, C., Youwai, S., Voottipruex, P., 2000. "FE modeling of hexagonal wire reinforced embankment on soft clay." **Canadian Geotechnical Journal**, Vol.37, No.6, pp.1–18.

Bergado, D.T., Youwai, S., Teerawattanasuk, C., Visudmedanukul, P., 2003. "The interaction mechanism and behavior of hexagonal wire mesh reinforced embankment with silty sand backfill on soft clay." **Computers and Geotechnics**, Vol.30, pp.517–534.

Chai, J. C. (1992). Interaction between grid reinforcement and cohesive-frictional soil and performance of reinforced wall/embankment on soft ground, **D.Eng. Dissertation**, Asian Institute of Technology, Bangkok, Thailand.

Hatami, K., Bathurust, R.J. (2005), "Development and verification of numerical model for the analysis of geosynthetic-reinforcement soil segmental wall

under working stress condition", **Canadian Geotechnical Journal**, Vol.42, pp.1066-1085.

Hatami, K., Bathurust, R.J. (2006), "Numerical model for the analysis of geosynthetic-reinforced soil segmental wall under surcharge loading", *Journal of* **Geotechnical and Geoenvironmental Engineering**, Vol.136, No.6, pp.673-684.

Horpibulsuk, S., and Niramitkornburee, A. (2010), "Pullout resistance of bearing reinforcement embedded in sand", **Soils and Foundations**, Vol.50, No.2, pp.215-226.

Horpibulsuk, S., Kumpala, A., and Katkan, W. (2008), "A case history on underpinning for a distressed building on hard residual soil underneath non-uniform loose sand", **Soils and Foundations**, Vol.48, No.2, pp.267-286.

Horpibulsuk, S.,Suksiripattanapong, C., and Niramitkornburee, A. (2010). "A method of examining internal stability of the bearing reinforcement earth (BRE) wall." **Suranaree Journal of Science and Technology**. Vol.17, No.1, pp.1-11.

Horpibulsuk, S., Suksiripattanapong, C., Niramitkornburee, A., Chinkulkijniwat, A., and Tangsuttinon, T. (2011), "Performance of earth wall stabilized with bearing reinforcements", **Geotextiles and Geomembranes**, Vol.29, No.5, pp.514-524.

Khedkar, M.S., Mandal, J.N., (2007), "Pullout response study for cellular reinforcement." In: **Proceedings of Fifth International Symposium on Earth Reinforcement, IS Kyushu '07, November 14–16, 2007**, Fukuoka, Japan, pp. 293–298.

Khedkar, M.S., Mandal, J.N., (2009), "Pullout behavior of cellular reinforcements." **Geotextiles and Geomembranes**, Vol.27, No.4, pp.262-271.

Park, T., and Tan, S. A. (2005). "Enhanced performance of reinforced soil walls by the inclusion of short fiber." **Geotextiles and Geomembranes**, Vol.23, No.4, pp.348-361.

Pinto, M. I. M. and Cousens, T.W. (1996). "Geotextile reinforced brick faced retaining walls." **Geotextiles and Geomembranes**, Vol.14, No.9, pp.449-464.

Pinto, M. I. M. and Cousens, T.W. (2000). "Effect of the foundation quality on a geotextile-reinforced brick-faced soil retaining wall." **Geosynthetics International**, Vol.7, No.3, pp.217-242.

Rowe, R.K. and Ho, S.K. (1997), "Continuous panel reinforced soil walls on rigid foundations", **Journal of Geotechnical and Geoenvironmental Engineering**, Vol.123, No.10, pp.912-920.

Skinner, G. D., and Rowe, R. K. (2005). "Design and behavior of a geosynthetic reinforced retaining wall and bridge abutment on a yielding foundation." **Geotextitles and Geomembranes**, Vol.23, No.4, pp.234-260.

CHAPTER IV

THE PARAMETRIC STUDY ON PERFORMANCE OF

BEARING REINFORCEMENT EARTH WALL

5.1 Statement of problem

The performance of MSE walls was extensively studied using the full-scale, laboratory model tests and numerical simulation (Bergado et al., 2000; Bergado et al., 2003; Bergado and Teerawattanasuk, 2007; Park and Tan, 2005; Skinner and Rowe, 2005; Rowe and Ho, 1997; Al Hattamleh and Muhunthan, 2006; Hatami and Bathurst, 2005 and 2006; Abdelouhab et al., 2011 and Khedkar and Mandal, 2007 and 2009). In Chapter 4,the PALXIS program with the simplified method was used successfully to simulate the performance of BRE wall. The understanding of the performance of BRE wall is useful information for effective design in terms of engineering and ecconomic viewpoints. Thus, thischapter aims to carry out the parametric studies onthe performance of the BRE wall by varying the foundation conditions (thickness and modulus of elasticity of the weathered crust) and the BRE wall properties (number of transverse members, reinforcement length, wall height and reinforcement vertical spacing).

5.2 Methodology

The bearing reinforcement earth wall was generally constructed on the weathered crust layer which is more compressible. Therefore, the thickness and modulus of weathered crust layer affect BRE wall. The modulus of elasticity of the

weathered crust is directly related to the strength of soil. Higher shear strength is associated with higher modulus. The parametric studies on settlement, bearing stress, lateral movement and tension forces in the bearing reinforcements were performed by varying the thickness, T and modulus, E of the weathered crust while other parameters of BRE wall properties were kept constant. The thicknesses of the weathered crust were 1.5, 2.0 and 2.5 m, which are commonly found in the field. The E values were 1,575, 1,875 and 2,175 kPa, which are representatives of weathered crust. The parametric studies were performed with 5 cases that the parameters for each case were shown in Table 5.1. The effect of geometry on BRE wall was performed by varying the number of transverse members, reinforcement length, wall height and vertical spacing. The interaction coefficient of bearing reinforcement and backfill soil, R were varied based on the laboratory model test. The R values of 0.65 and 0.75 were represented for 2 and 3 transverse members, respectively (Suksiripattanapong et al., 2012). It was shown that the R value increases with number of transverse members. In this parametric study, the R values of 0.55, 0.65, 0.75 and 0.85 were considered for 1, 2, 3 and 4 transverse members, respectively (*vide* Figures 4.7 to 4.9). The influence of R values on the lateral movement and tensions in the bearing reinforcement will be examined. The effect of reinforcement length on the performance of BRE wall wasillustrated by comparisons of simulation results of cases 31 to 32. The reinforcement lengths were varied between 4.2 and 6 m. The effect of wall height on the performance of BRE wall was depicted by comparisons of simulation results of cases 31, 35 and 39. The wall heights were 6.0, 7.5 and 9.0 m. In the parametric study, all parameters were kept constant except the wall height and reinforcement length. The minimum reinforcement length for the simulationwas70% of the wall

height as recommended for designing of MSE walls by AASTHO (2002). Therefore, the studied reinforcement lengths were 4.2, 5.25 and 6.3 m. The variations of vertical spacing were 0.5, 0.75 and 1.0 m (cases 31, 43 and 55). 44 cases of the parametric studies onthe BRE wall properties to the wall performance. Table 5.1 shows the detailed BRE wall properties for each case.

Table 5.1 Foundation conditions and BRE wall properties.

Item	E_{ref} (kPa)	T (m)	n	L (m)	H (m)	S_v(m)	Remark
Case 1	1,575	2.0	2,3	4.2	6.0	0.75	
Case 2	1,875	2.0	2,3	4.2	6.0	0.75	
Case 3	2,175	2.0	2,3	4.2	6.0	0.75	
Case 4	1,875	1.5	2,3	4.2	6.0	0.75	
Case 5	1,875	2.5	2,3	4.2	6.0	0.75	
Case 6	1,575	2.5	2,3	4.2	6.0	0.75	
Case 7	2,175	2.5	2,3	4.2	6.0	0.75	Parameters for backfill, medium and very dense sand are constant
Case 8	1,575	1.5	2,3	4.2	6.0	0.75	
Case 9	2,175	1.5	2,3	4.2	6.0	0.75	
Case 10	1,575	1.5	2,3	5.25	7.5	0.75	
Case 11	1,575	2.0	2,3	5.25	7.5	0.75	
Case 12	1,575	2.5	2,3	5.25	7.5	0.75	
Case 13	1,875	1.5	2,3	5.25	7.5	0.75	
Case 14	1,875	2.0	2,3	5.25	7.5	0.75	
Case 15	1,875	2.5	2,3	5.25	7.5	0.75	
Case 16	2,175	1.5	2,3	5.25	7.5	0.75	

Table 5.1 Foundation conditions and BRE wall properties (Continued).

Item	E_{ref} (kPa)	T (m)	n	L (m)	H (m)	S_{v}(m)	Remark
Case 17	2,175	2.0	2,3	5.25	7.5	0.75	
Case 18	2,175	2.5	2,3	5.25	7.5	0.75	
Case 19	1,575	1.5	2,3	6.3	9.0	0.75	
Case 20	1,575	2.0	2,3	6.3	9.0	0.75	
Case 21	1,575	2.5	2,3	6.3	9.0	0.75	
Case 22	1,875	1.5	2,3	6.3	9.0	0.75	
Case 23	1,875	2.0	2,3	6.3	9.0	0.75	
Case 24	1,875	2.5	2,3	6.3	9.0	0.75	
Case 25	2,175	1.5	2,3	6.3	9.0	0.75	
Case 26	2,175	2.0	2,3	6.3	9.0	0.75	Parameters for backfill, medium and very dense sand are constant
Case 27	2,175	2.5	2,3	6.3	9.0	0.75	
Case 28	1,875	2.0	1,2	4.2	6.0	0.75	
Case 29	1,875	2.0	2,3	4.2	6.0	0.75	
Case 30	1,875	2.0	3,4	4.2	6.0	0.75	
Case 31	1,875	2.0	2,3	4.2	6.0	0.75	
Case 32	1,875	2.0	2,3	4.8	6.0	0.75	
Case 33	1,875	2.0	2,3	5.4	6.0	0.75	
Case 34	1,875	2.0	2,3	6.0	6.0	0.75	
Case 35	1,875	2.0	2,3	5.25	7.5	0.75	
Case 36	1,875	2.0	2,3	6.0	7.5	0.75	
Case 37	1,875	2.0	2,3	6.75	7.5	0.75	
Case 38	1,875	2.0	2,3	7.5	7.5	0.75	

Table 5.1 Foundation conditions and BRE wall properties (Continued).

Item	E_{ref} (kPa)	T (m)	n	L (m)	H (m)	S_v(m)	Remark
Case 39	1,875	2.0	2,3	6.3	9.0	0.75	
Case 40	1,875	2.0	2,3	7.2	9.0	0.75	Parameters for backfill, medium and very dense sand are constant
Case 41	1,875	2.0	2,3	8.1	9.0	0.75	
Case 42	1,875	2.0	2,3	9.0	9.0	0.75	
Case 43	1,875	2.0	2,3	4.2	6.0	0.50	
Case 44	1,875	2.0	2,3	4.2	6.0	1.0	

5.3 Parametric study on performance of BRE wall

5.3.1 Settlement

The simulated settlements of the BRE wall for different properties of foundation and BRE wall are illustrated in Figure 5.1. The effects of the thickness of weathered crust, T , modulus of elasticity of weathered crust, E and wall height, H are illustrated by comparisons of the simulation results of cases 1 to 5, and 31, 35 and 39. These three factors significantly affect the settlement of BRE wall. It is of interest to note that the settlement is relatively uniform; i.e. the differential settlements at front and rear of the wall are small, even with different modulus and thickness of weathered crust. The uniform settlement is contributed from the high stiffness of the bearing reinforcements. The number of transverse members, n, reinforcement length, L, and vertical spacing, S_v, insignificantly affect the settlement as seen by the simulated results of cases 28 to 34, and 31, 43 and 44.

Figure 5.2 shows the combined effect of *E*, *T* and *H* on the maximum settlement, which occurs at the front of the wall. The data points were obtained from the simulation results of cases 1 to 27. It is found that the effects from *T* and *H* are remarkably observed when the stiffness of the weathered crust decreases. For example, for the weathered crust thickness of 2.5 meter, the $\delta v_{max}/H$ = 1.53 and 2.07 for *E* = 2,175 and 1,575 kPa. In other words, the settlement is sensitive to the *E* values.
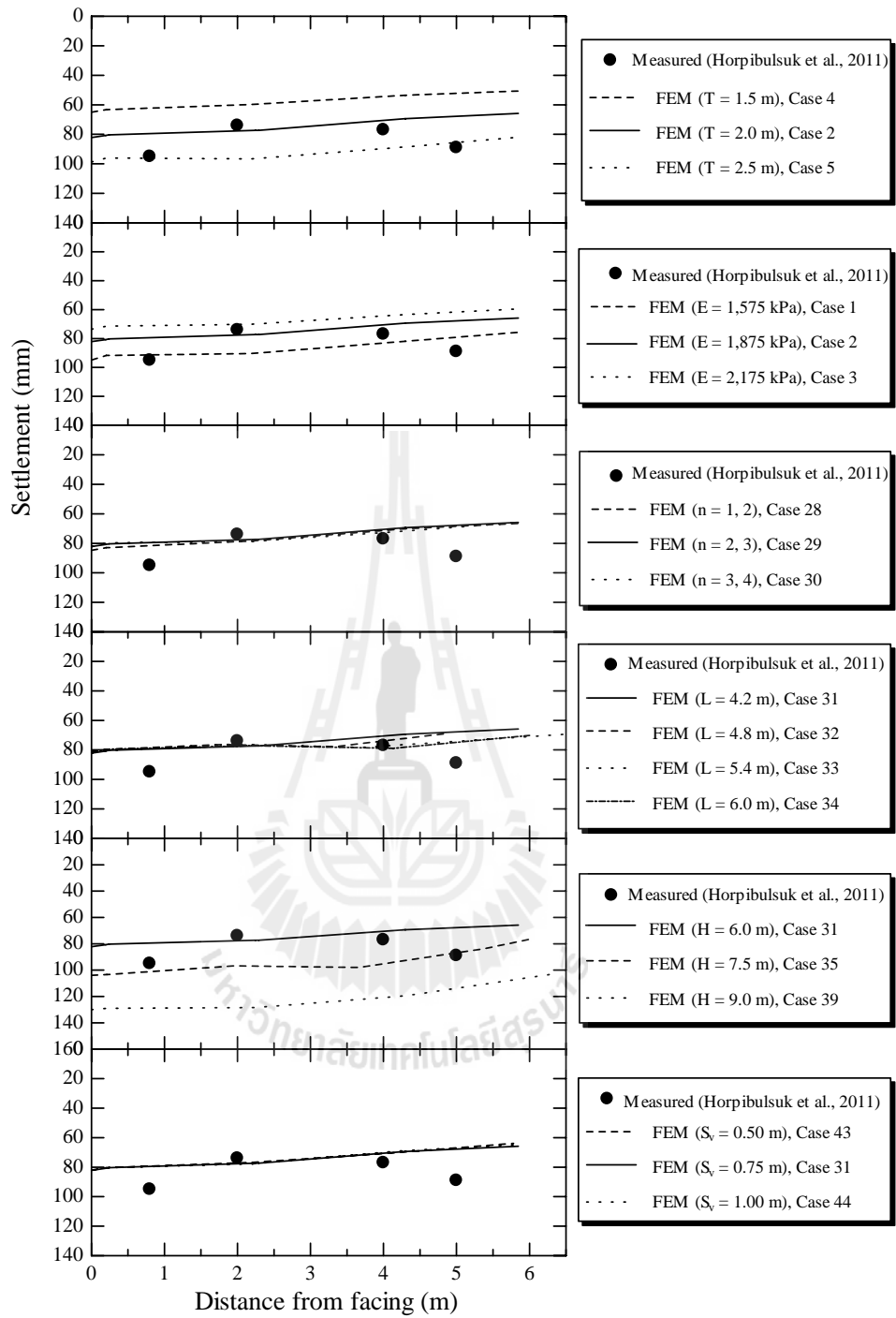
Figure 5.1 The parametric studieson the simulated settlements tothe T , E , n, L, S_v, and H values
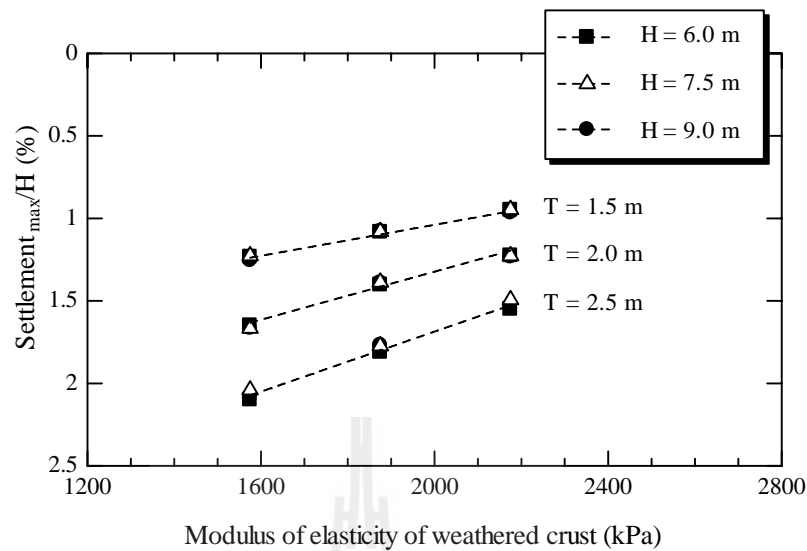
Figure 5.2 The relationship between the modulus of elasticity of the weathered crust,

E and the normalized maximum settlement, δv_{max} and wall height, H for

different thickness of weathered crust,

5.3.2 Bearing stress

The simulated distribution of bearing stresses at the end of construction from the front to back for different weathered crust and BRE wall properties is shown in Figure 5.3. For all simulation cases, the stress distribution is uniform, which is in agreement with the settlement pattern. For the same H of 6 m, the stress distribution is the same for different weathered crust properties (cases 4, 2, and 5 and cases 1 to 3), number of transverse members (cases 28 to 30) and vertical spacing of the bearing reinforcement (cases 43, 31 and 44). The bearing stress distribution is controlled by eccentric from the center of the wall base. With the same H of 6 m, the increase in reinforcement length increases the resistant moment while the overturning moment is the same; hence the reduction in the eccentric. This low eccentric is associated with

more uniform bearing stress distribution as illustrated by a comparison of the simulated results of the cases 31 to 34 for reinforcement lengths of 4.2 to 6.0 m. The effect of wall height on the bearing stress distribution is observed by a comparison of the cases 31 35 and 39 for the heights of 6.0, 7.5 and 9.0 m. In the analysis, the reinforcement length is increased with the increase in wall height for the external stability. The maximum bearing stress at the wall front increases significantly as the wall height increases. Because this increase in the wall height is associated with the reduction in eccentric, the stress distribution is more uniform as the wall height increases. To conclude, for linear elastic analysis, the bearing stress distribution is strongly dependent upon the eccentric and regardless of T, E, R and S_v. The finding is disagreement with the recommendation by AASHTO (2002), that the soil parameters are not considered in the calculation of the bearing stress. The uniform settlement and bearing stress are found for the BRE wall on the hard stratum.
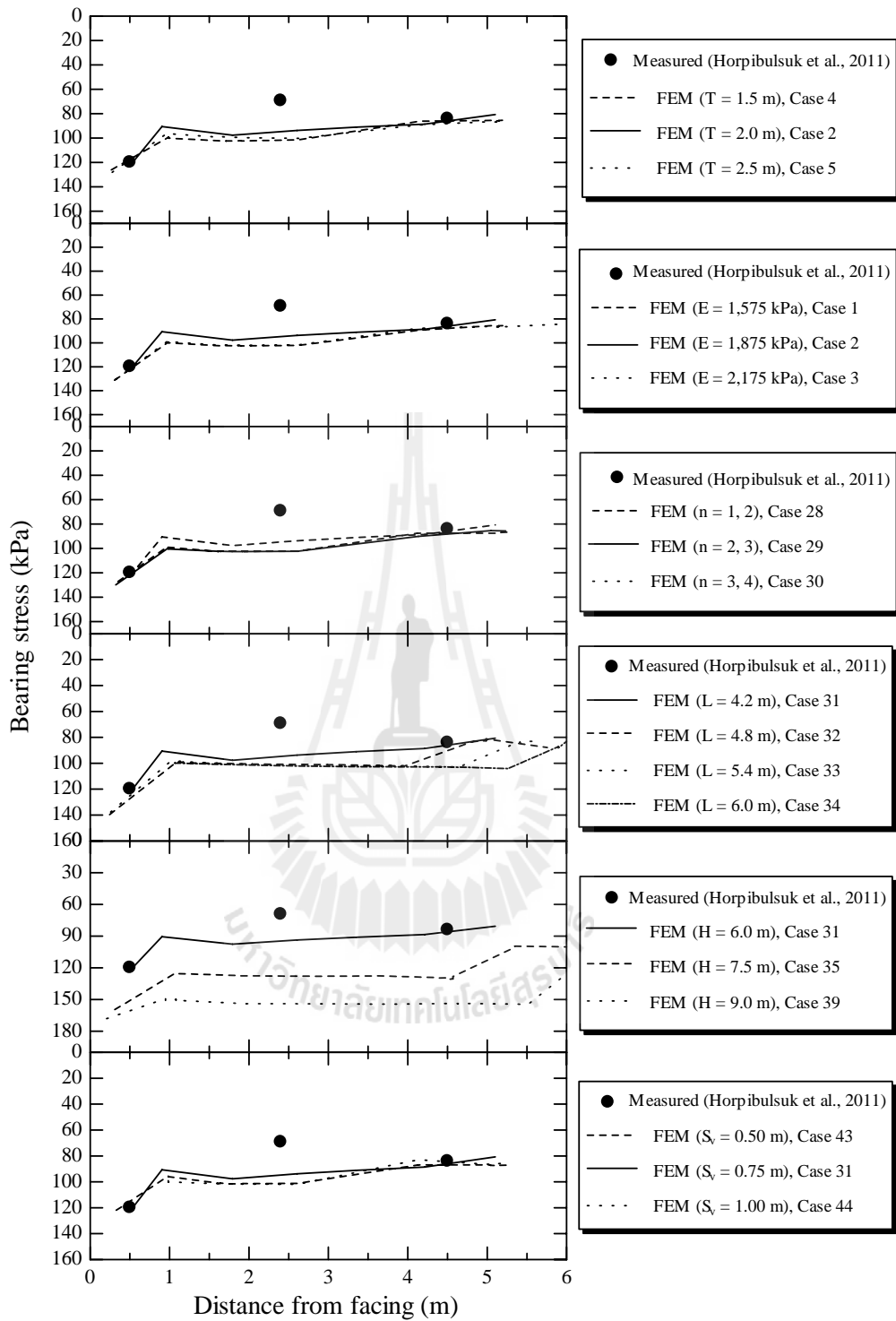
Figure 5.3 The parametric studieson bearing stresses of the BRE wall to T, E, n, L,

S_v, and H

5.3.3 Lateral movement

The simulated lateral movements are compared and shown in Figure 5.4-5.7 for different properties of weathered crust and BRE wall. The lateral movement was the sum of the lateral movements during construction and after end construction. The parametric study on the lateral movement to the thickness of weathered crust is illustrated by a comparison of simulated results of cases 2, 4 and 5 (*vide* Figure 5.4). For the three cases, the maximum lateral movement is found at about mid of the wall height. The maximum lateral movement is slight change with the difference in thickness of weathered crust. Whereas the lateral movement at wall base increases as the weathered crust thickness increases because of the increase in lateral movement of the foundation. The maximum lateral movement about the mid of the wall is clearly observed for the thick weathered crust of 2.5 m. The parametric study on the lateral movement to the modulus of elasticity of the weathered crust is illustrated by a comparison of simulated results of cases 1 to 3 in Figure 5.5. For the same thickness of weathered crust and the wall height, the lateral movement in the foundation for each E value is essentially the same. However, the lateral movement of BRE wall is significantly dependent upon E. The lower the E value, the higher the lateral movement. The maximum lateral movement is found at the top of the BRE wall. This characteristic implies that the BRE wall tends to overturn around the toe. This tendency is also confirmed by the differential settlement; i.e., the difference between maximum settlement at the front and minimum settlement at the rear is 10 mm for case 1 (lowest E value), 7 mm for case 2, and 6 mm for case 3 (highest E value). The E value significantly affects the pattern of lateral movement. The maximum lateral movement occurs at the top of the wall for soft weathered crust. This finding is also

found for the test data of the MSE wall on soft Bangkok clay reported by Bergado et al. (1995).
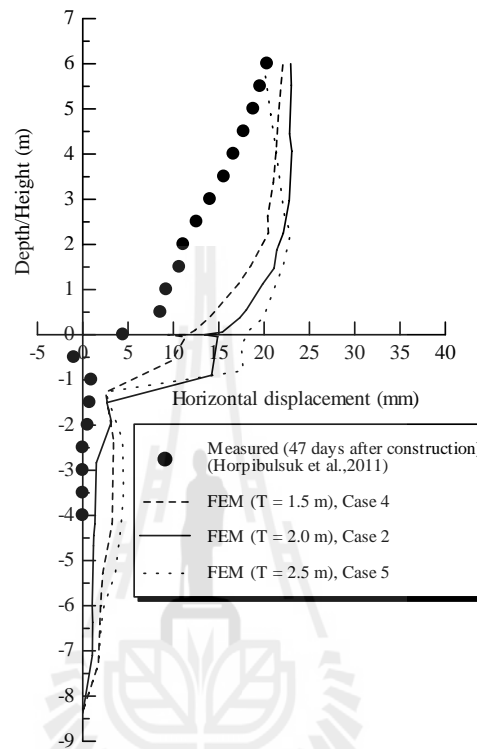
Figure 5.4 The parametric studyon lateral wall movements of the BRE wall to the weathered crust thickness, *T*.
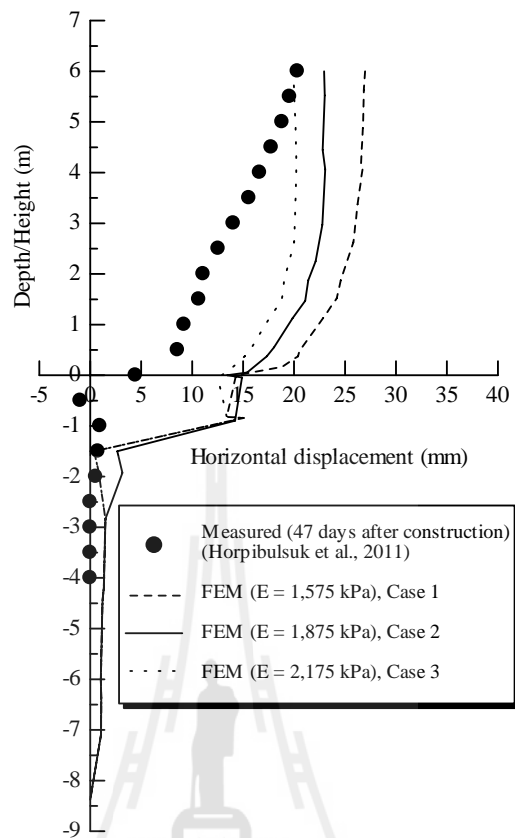
Figure 5.5 The parametric studyon the lateral wall movement of the BRE wall

tomodulus of elasticity of the weathered crust, *E*.

The parametric studyon the lateral movement to the number of transverse members (interaction coefficient, *R*) is shown in Figure5.6. The analysis is in three cases for the same wall height of 6 m and reinforcement length of 4.2 m. Case 28 is for *R* values of 0.55 (*n* = 1) and 0.65 (*n* = 2) for 1st to 3rd and 4th to 8th reinforcement layers, respectively. Case 29 is for *R* values of 0.65 (*n* = 2) and 0.75 (*n* = 3) for 1st to 3rd and 4th to 8th reinforcement layers, respectively. Case 30 is for *R* values of 0.75 (*n* = 3) and 0.85 (*n* = 4) for 1st to 3rd and 4th to 8th reinforcement layers, respectively. The change in the lateral movement at the wall base is insignificant even with the change in number of transverse members due to very high overburden

pressure. This high overburden pressure increases the pullout resistance. The effect of number of transverse members is noticed at the top of the wall where the pullout resistance is lower. As such, the increase in number of transverse members not only increases the factors of safety against pullout failure but also reduces remarkably the lateral movement.
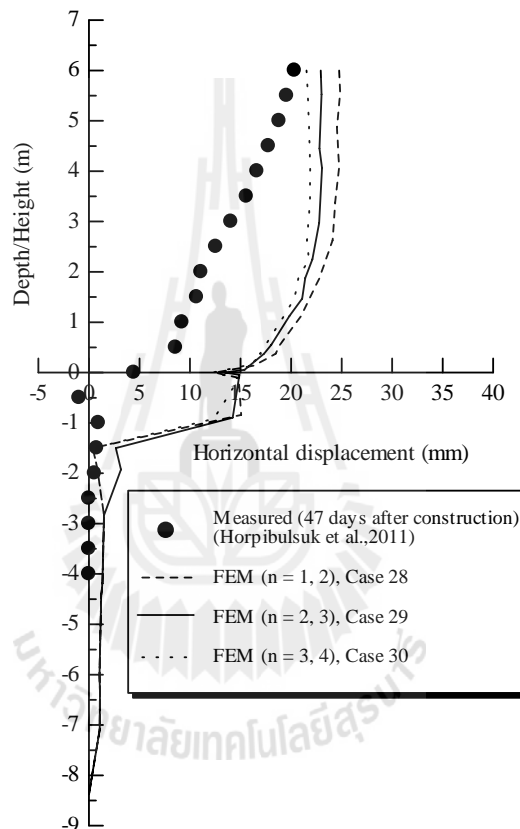
Figure 5.6 The parametric studieson the lateral wall movement of the BRE wall to

the number of transverse members, *n*.

Figure 5.7 shows the parametric study on the lateral movement to the reinforcement length, L by a comparison of simulated results of cases 31 to 34. The ratios of the length of reinforcement, L to the wall height, $H\left(L/H\right)$ were 0.7, 0.8, 0.9 and 1.0 for the parametric study. The *L/H* ratio of 1.0 gives maximum horizontal

displacement lower than the *L/H* ratio of 0.7 by about 10%. The reduction in lateral

movement is because the increase in the pullout resistance (increase in the embedded

length in the passive zone).
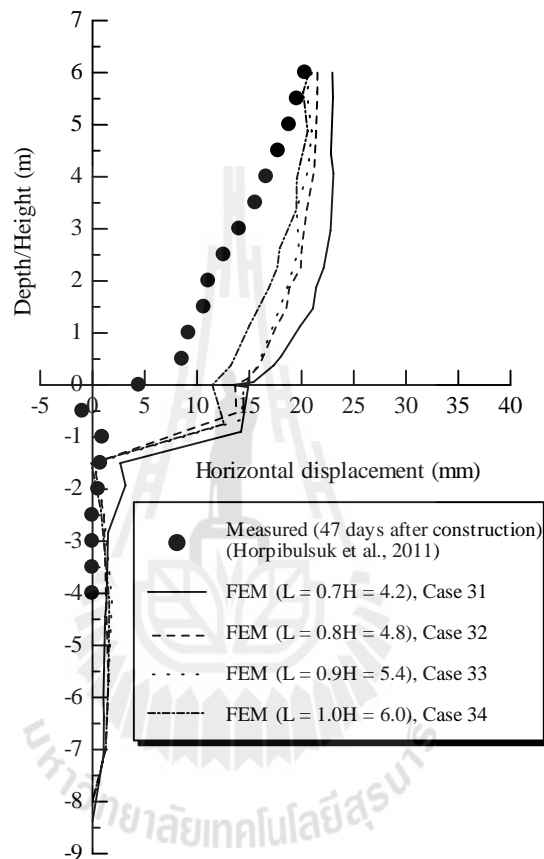
Figure 5.7 Effect of *L/H* ratioon lateral wall movement.

The numerical simulation of maximum lateral movement during

construction for MSE wall was performed by Christopher et al. (1990). The maximum

lateral movement for $S_v = 0.75$ m was presented in the form:

$$\delta_R = \frac{250\delta d_{max}}{H} \tag{5.1}$$

where δ_R is the relative displacement, depending upon the reinforcement length to wall height ratio, L/H and H is the wall height and δd_{max} is maximum lateral movement. Figure 5.8 shows the relationship between the L/H ratio and the relative displacement, δ_R for vertical spacing of the reinforcement, $S_v = 0.75$, $H = 6.0$, 7.5 and 9.0 m, $L = 4.2$ to 9.0 m, $T = 2.0$ m, and $E = 1,875$ kPa (cases 31 to 42) compared with the proposed relationship by Christopher et al. (1990) and Rowe and Ho(1997). The line by Rowe and Ho (1997) are for the hard stratum, hence it is represented as an upper boundary. As the L/H ratio increases, the δ_R value decreases up to a transitional ratio. Beyond this ratio, the δ_R value tends to approach a constant value of about 0.915. The transitional L/H ratio is 0.8. Consequently, the reinforcement larger than $0.8H$ is disadvantage in terms of lateral movement.
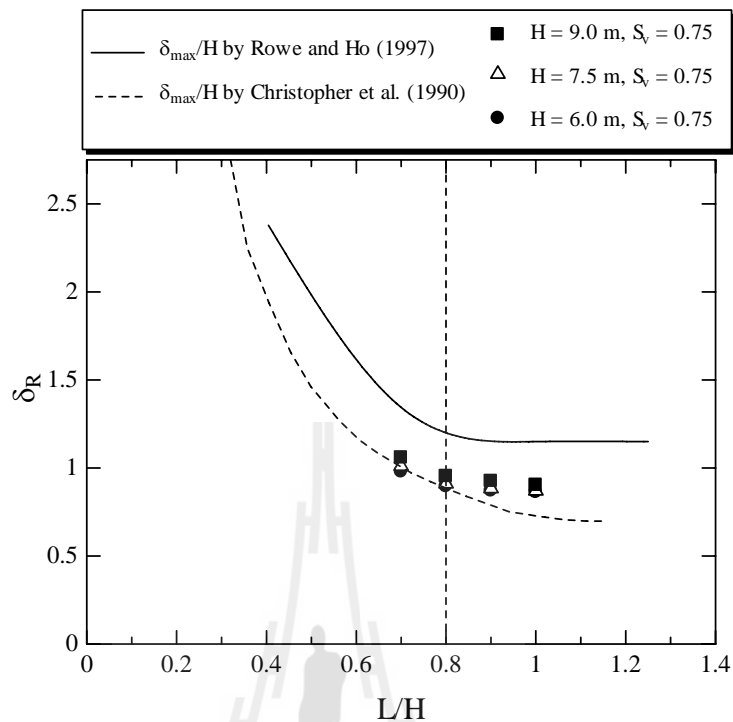
Figure 5.8 Relationship betweenthe L/H ratio and the relative displacement, δ_R

compared with that proposed by Christopher et al. (1990) and Rowe and

Ho (1997).

5.3.4 Tensions in the bearing reinforcement

Figures 5.9-5.13 show the comparison between the parametric studies

and the measured tension forces in the bearing reinforcements at 14 days after the

completion of construction. The simulated tension forces in the bearing

reinforcements are not much sensitive to the values of *T*, *E* and *n* (*vide* Figures 5.9 to

5.11 for cases 1 to 5 and 28 to 30). The parametric study on tension forces in the

bearing reinforcement to the reinforcement length is shown in Figure 5.12. It is found

that the pattern of tension forces is similar. The parametric study on the tension forces

in the bearing reinforcements to the wall height, *H* is shown in Figure 5.13. It is found

that the tension force increases as the wall height increases. It is because the increased vertical stress affects increased horizontal stress. The pattern of tension force along reinforcement is similar for all height. The possible failure plane recommended by AASHTO (2002) for inextensible reinforcements is also shown in the Figures 5.9-5.14 by a dash line. The location of the maximum tension forces can be separated into two zones: above H/2 and below H/2. The maximum tension forces are at the front of the wall for the reinforcement layer above H/2. This is due to the relatively large settlement at the wall facing and the relatively large lateral movement at the top of the wall. In the below H/2 zone, the location of the maximum tension forces is dependent upon the settlement pattern. To illustrate the effect of settlement pattern, the numerical analysis of the BRE wall with two different sets of foundation parameters is performed. The set of parameters for the SUT campus is shown in Table 2 and the set of the parameters for the thick soft soil layer underneath stiff weathered crust is shown in Table 5.2. The top layer (weathered crust) is stiffer than the second layer (soft soil layer). This soil condition is similar to Bangkok clay profile. In case of the SUT campus, the maximum tension forces are at the back and mid of the wall base for the first and second reinforcement layers, respectively because of small and uniform settlement. The same is true for the thick soft clay underneath the weathered crust. The larger settlement is found with the maximum value at about mid of the wall base (*vide* Figure 5.15). The result is similar to that reported by Bergado et al. (1995). The locations of the maximum tension forces for each reinforcement layer are close to the possible failure plane recommended by AASHTO (2002). However, it is worthwhile to note that the settlement pattern insignificantly affects the location of the maximum

tension forces for the reinforcements above the H/2. All the maximum tension forces locate at the front of the BRE wall.
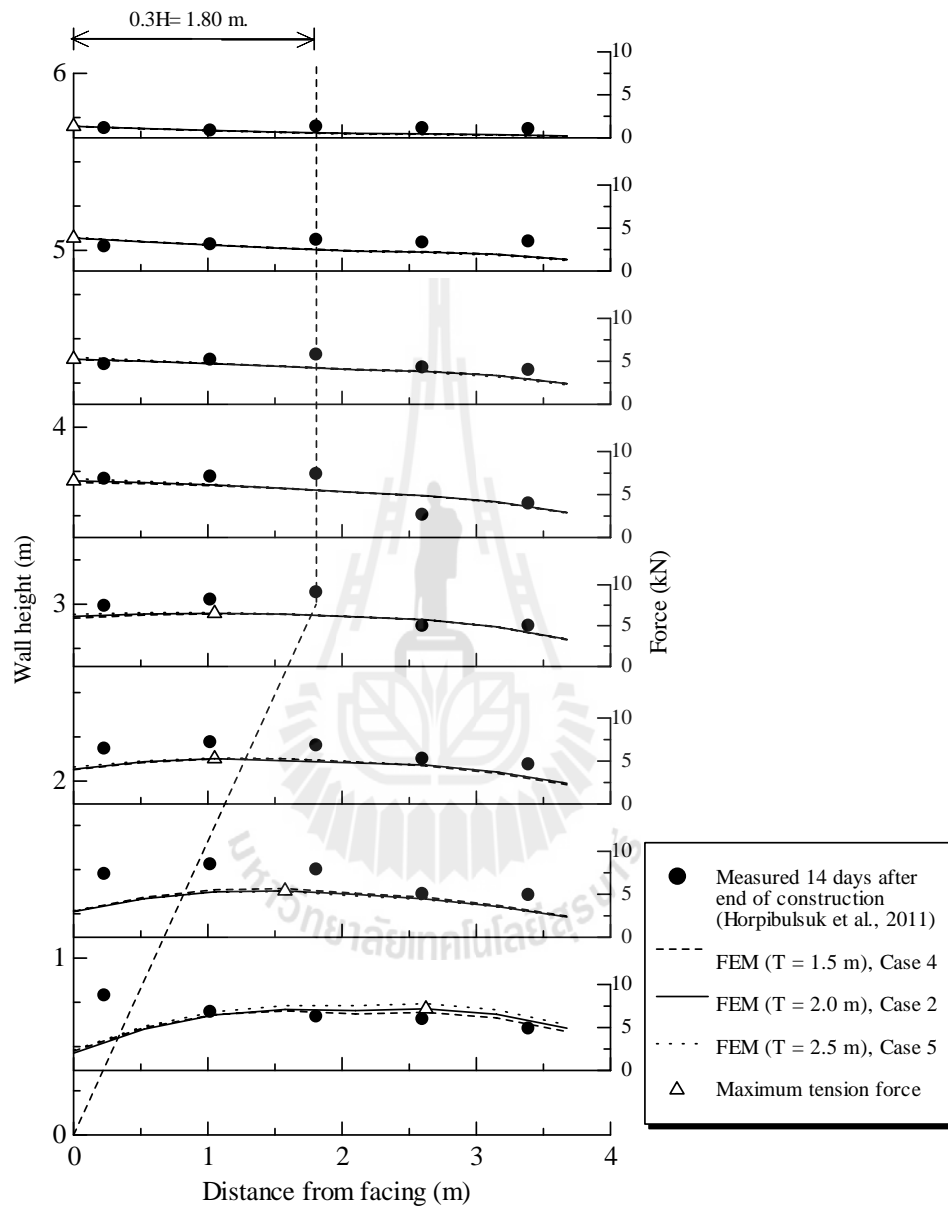
Figure 5.9 The parametric study on tension forces in the bearing reinforcements to the weathered crust thickness, *T*.
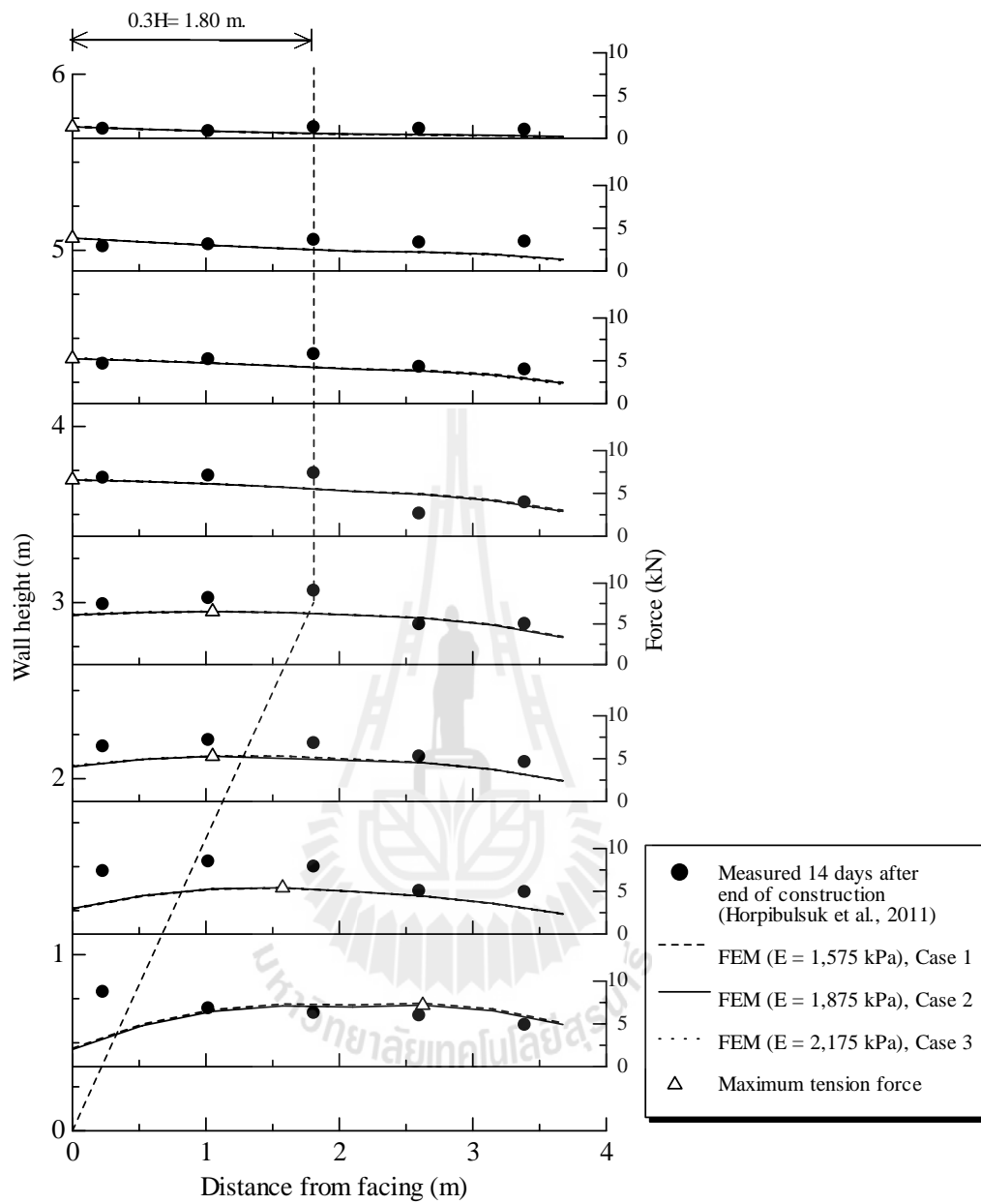
Figure 5.10 The parametric study on tension forces in the bearing reinforcements to

the modulus of elasticity of weathered crust, *E*.
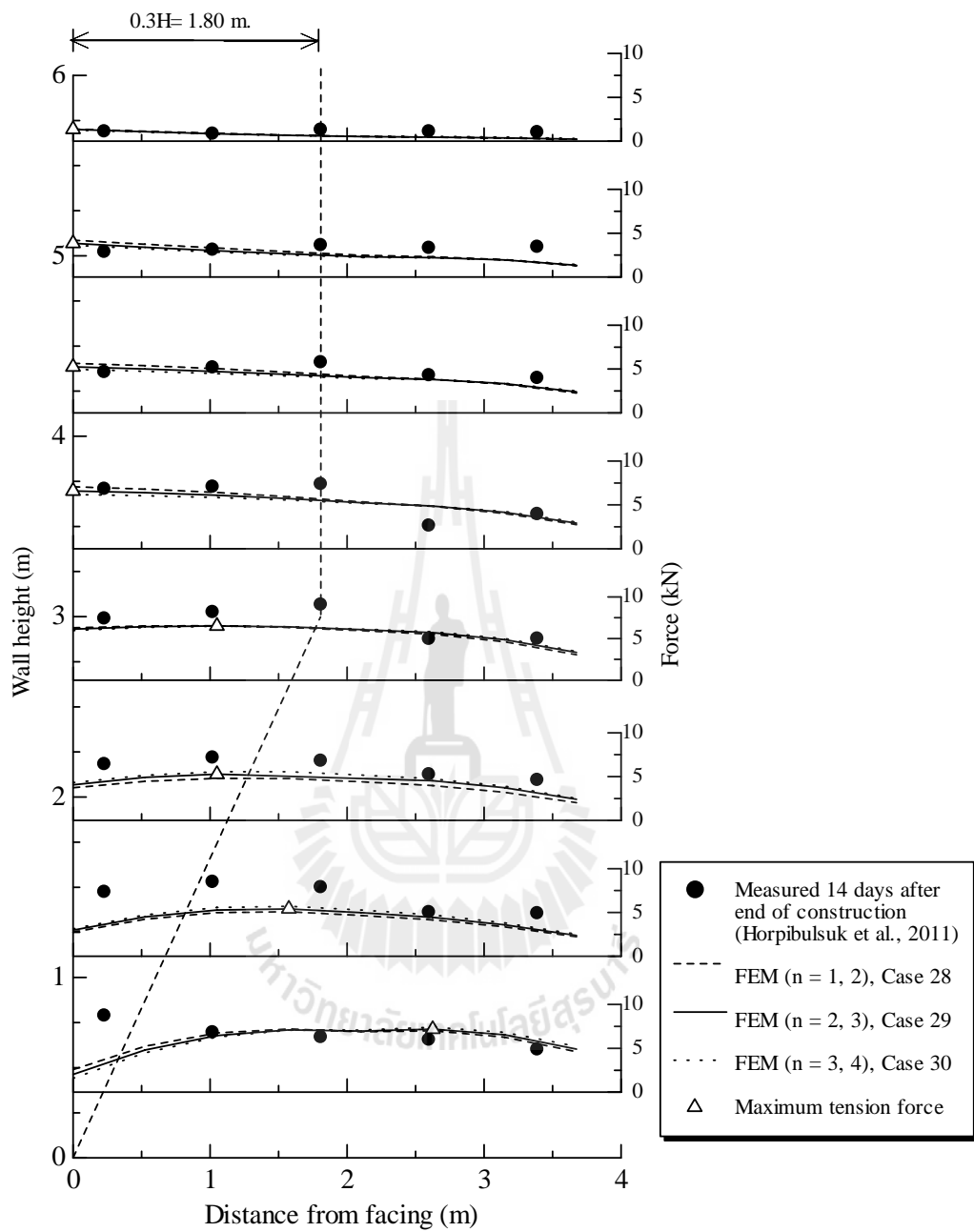
Figure 5.11 The parametric study on tension forces in the bearing reinforcements to

the number of transverse members, n.
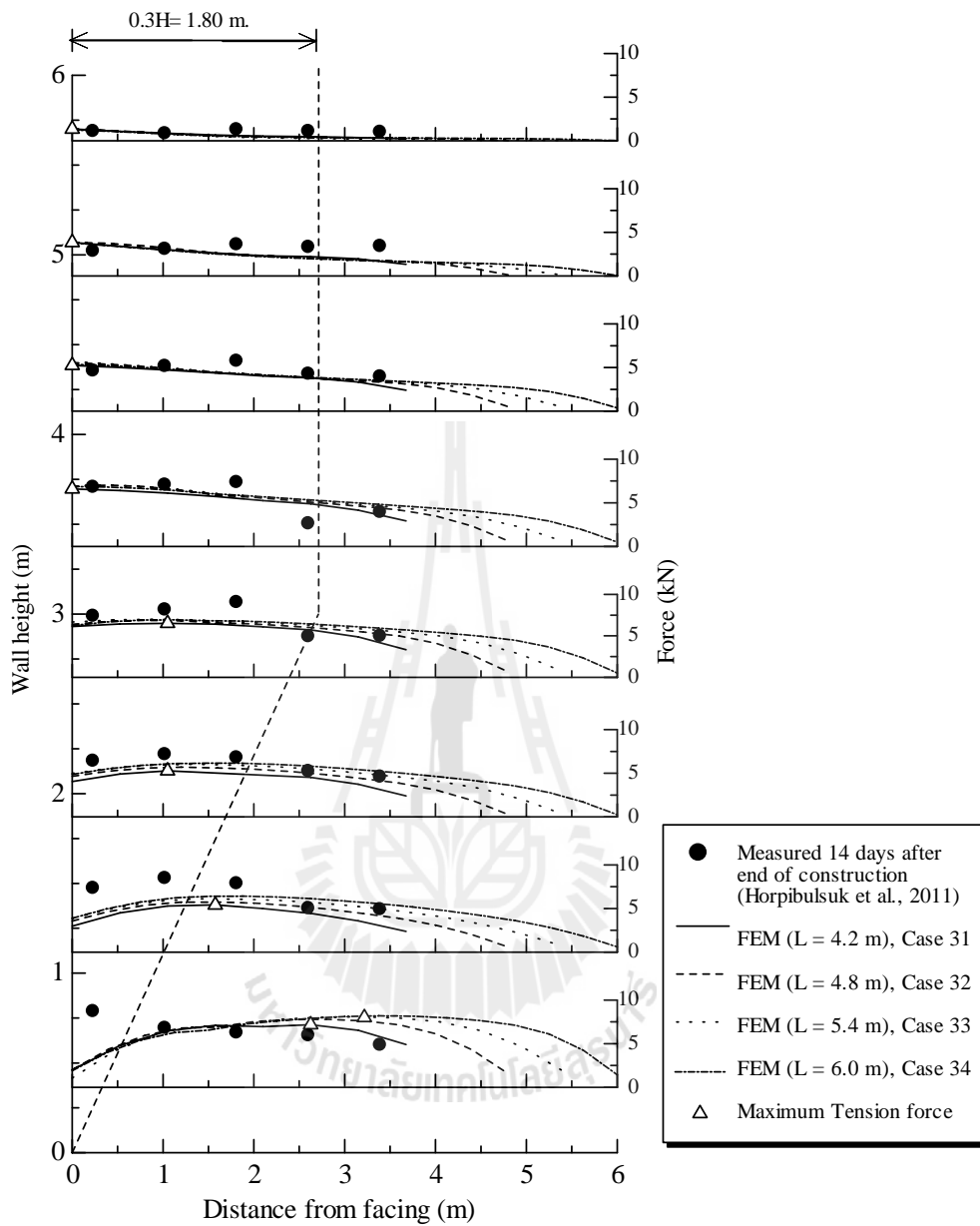
Figure 5.12 The parametric study on tension forces in the bearing reinforcements to

the reinforcement length, L.
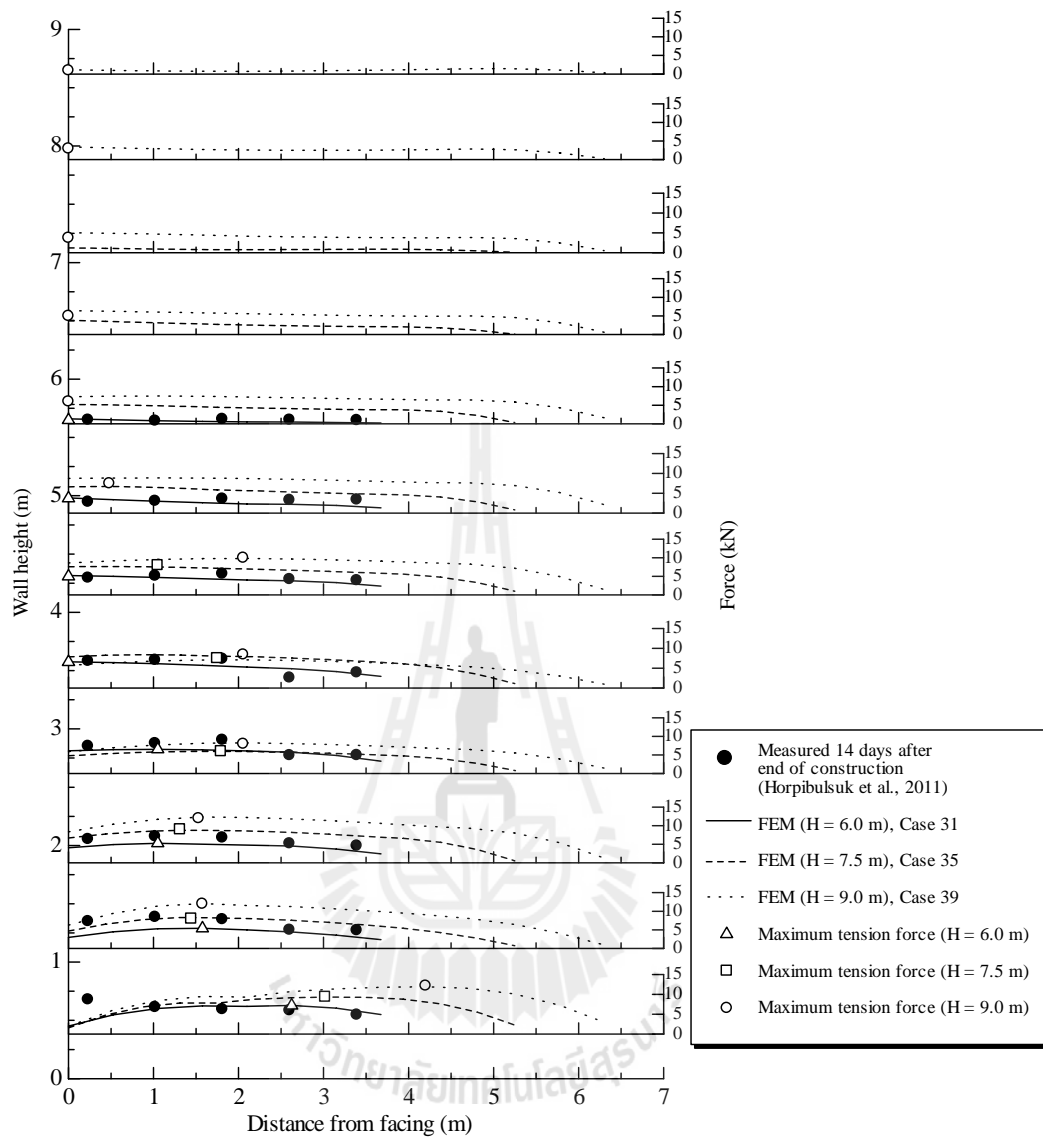
Figure 5.13 The parametric study on tension forces in the bearing reinforcements to

the wall height, H.
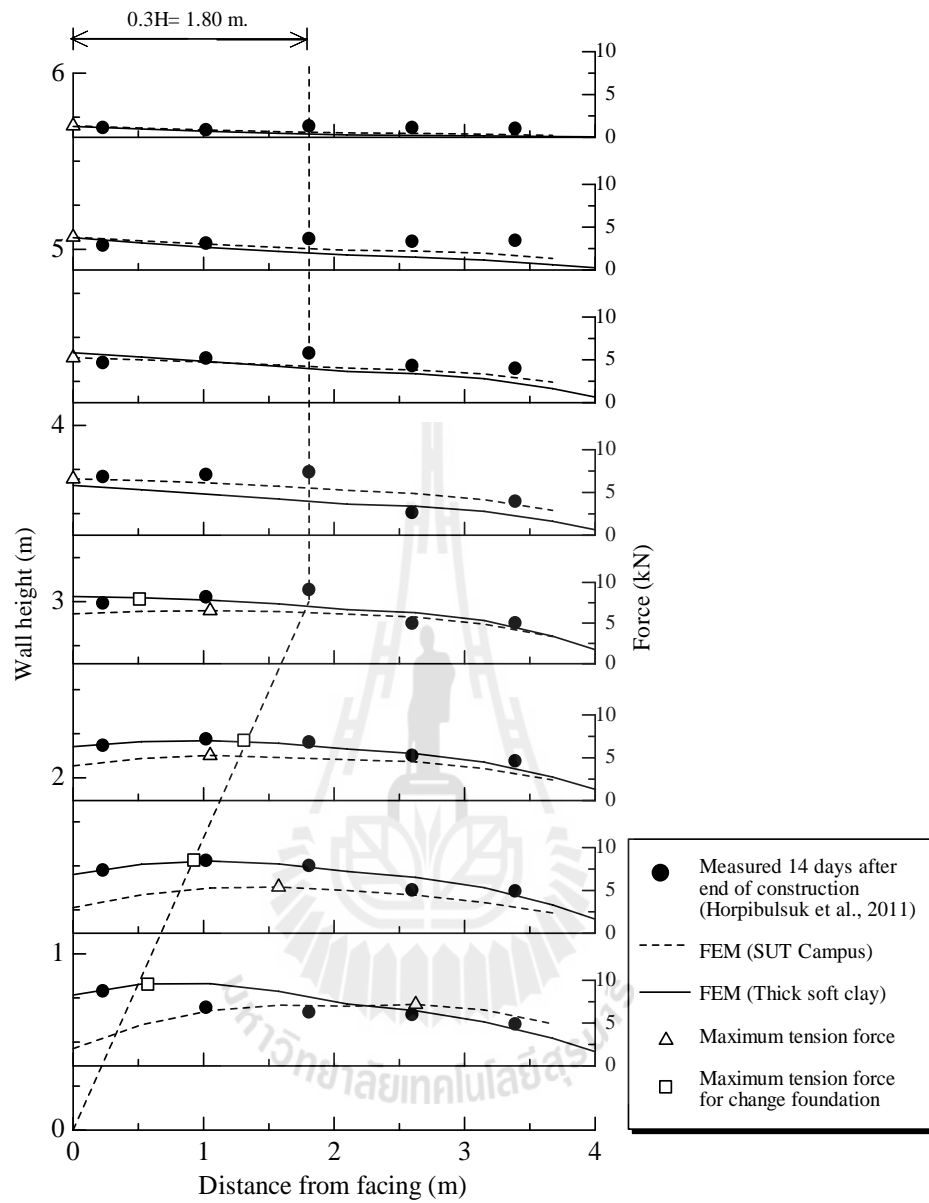
Figure 5.14 The simulated tension forces in the bearing reinforcements to the

changed foundation.

Table 5.2 Model parameters for thick soft clay underneath weathered crust

Item	Weathered crust	Thick soft clay	very dense sand
Material model	Mohr-Coulomb	Mohr-Coulomb	Mohr-Coulomb
Material type	Drained	Drained	Drained
γ_{dry}	17.15 kN/m^3	17 kN/m^3	18 kN/m^3
γ_{wet}	18.15 kN/m^3	18 kN/m^3	19 kN/m^3
k_x	1 m/day	1 m/day	1 m/day
k_y	1 m/day	1 m/day	1 m/day
E_{ref}	40000 kN/m^2	1875 kN/m^2	50000 kN/m^2
ν	0.25	0.30	0.30
c'	1 kPa	20 kPa	1 kPa
ϕ'	35°	26°	38°
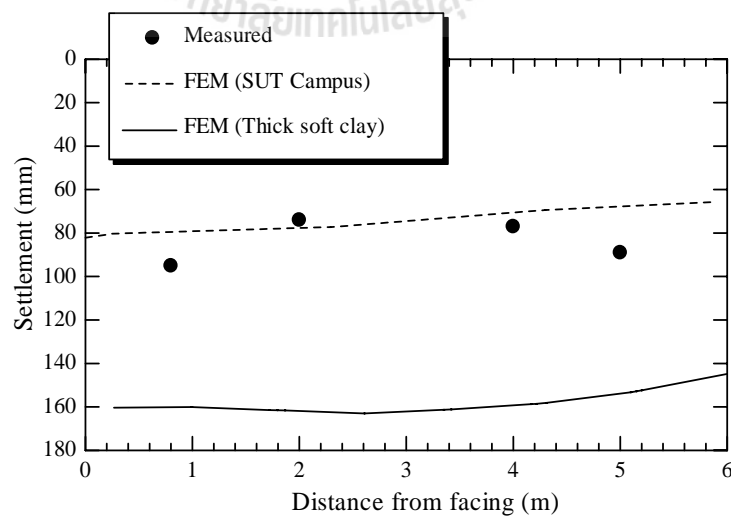
Figure 5.15 The simulated settlements to the changed foundation.

5.4 Conclusions

This chapter presents a numerical and parametric studies on the bearing reinforcement earth (BRE) wall constructed on the hard stratum by PLAXIS 2D. The parametric studies on BRE wall were performed by varying the foundation conditions (thickness and modulus of elasticity of the weathered crust) and the BRE wall properties (number of transverse members, reinforcement length, wall height and reinforcement vertical spacing). The simulated settlement of the BRE wall is dependent on the weathered crust thickness, the modulus of elasticity of the weathered crust and wall height. The settlement is relatively uniform due to the contribution from the stiffness of bearing reinforcement. Consequently, the bearing stress distribution is almost uniform for different foundation conditions and BRE wall properties. The lateral movement at wall base increases as the weathered crust thickness increases because of the increase in lateral movement of the foundation. The maximum lateral movement occurs at about the mid of the wall height for medium weathered crust and at the top of the wall height for weak weathered crust. For the weak weathered crust where the maximum lateral movement is found at the top of the BRE wall, the BRE wall tends to overturn around the toe. For medium to hard weathered crust, the change in the lateral movement at the wall base is insignificant even with the change in number of transverse members due to very high overburden pressure. The effect of number of transverse members is noticed at the top of the wall where the pullout resistance is lower. The BRE wall with the *L/H* ratio of greater than 0.8 is not recommended in practice because the lateral movement is essentially the same for different *L/H* ratios. The maximum tension plane is close to the failure plane recommended by AASHTO (2002) only for the reinforcement layers below *H/*2,

especially for the case of thick clay deposit, while the maximum tension forces are at the front of the wall for the layers above $H/2$. This implies that the maximum tension plane and failure plane do not coincide for the BRE wall in service state.

5.5 References

AASHTO (1996). Standard specifications for highway and bridge, 1th edition. Washington D.C., **American Association of State Highway and Transportation Officials**.

AASHTO (2002). Standard specifications for highway and bridge, 7th edition. Washington D.C., **American Association of State Highway and Transportation Officials**.

Alforo, M.C., Hayashi, S., Miura, N., Bergado, D.T. (1997), "Deformation of reinforced soil-embankment system on soft clay foundation, **Soils and Foundations**, Vol.37, No.4, pp.33-46.

Al Hattamleh, O., Muhunthan, B. (2006), "Numerical procedures for deformation calculations in the reinforced soil walls", **Geotextitles and Geomembranes**, Vol.24, No.1, pp.52-57.

Bathurst, R.J. (1993), "Investigation of footing resistant on stability of large-scale reinforced soil wall tests", **Proceedings of 46th Canadian Geotechnical Conference**.

Bergado, D.T., Chai, J.C., Miura, N., 1995. "FE analysis of grid reinforced embankment system on soft Bangkok clay." **Computers and Geotechnics**, Vol.17, pp.447–471.

Bergado, D.T., Chai, J.C., and Miura, N. (1996), "Prediction of pullout resistance and pullout force-displacement relationship for inextensible grid reinforcements", **Soils and Foundations**, Vol.36, No.4, pp.11-22.

Bergado, D.T., Teerawattanasuk, C., 2007. "2D and 3D numerical simulations of reinforced embankments on soft ground." **Geotextiles and Geomembranes**, Vol.26, No.1, pp.39–55.

Bergado, D.T., Teerawattanasuk, C., Youwai, S., Voottipruex, P., 2000. "FE modeling of hexagonal wire reinforced embankment on soft clay." **Canadian Geotechnical Journal**, Vol.37, No.6, pp.1–18.

Bergado, D.T., Youwai, S., Teerawattanasuk, C., Visudmedanukul, P., 2003. "The interaction mechanism and behavior of hexagonal wire mesh reinforced embankment with silty sand backfill on soft clay." **Computers and Geotechnics**, Vol.30, pp.517–534.

Chai, J. C. (1992). Interaction between grid reinforcement and cohesive-frictional soil and performance of reinforced wall/embankment on soft ground, **D.Eng. Dissertation**, Asian Institute of Technology, Bangkok, Thailand.

Hatami, K., Bathurust, R.J. (2005), "Development and verification of numerical model for the analysis of geosynthetic-reinforcement soil segmental wall under working stress condition", **Canadian Geotechnical Journal**, Vol.42, pp.1066-1085.

Hatami, K., Bathurust, R.J. (2006), "Numerical model for the analysis of geosynthetic-reinforced soil segmental wall under surcharge loading", *Journal of* **Geotechnical and Geoenvironmental Engineering**, Vol.136, No.6, pp.673-684.

Horpibulsuk, S., and Niramitkornburee, A. (2010), "Pullout resistance of bearing reinforcement embedded in sand", **Soils and Foundations**, Vol.50, No.2, pp.215-226.

Horpibulsuk, S., Kumpala, A., and Katkan, W. (2008), "A case history on underpinning for a distressed building on hard residual soil underneath non-uniform loose sand", **Soils and Foundations**, Vol.48, No.2, pp.267-286.

Horpibulsuk, S., Suksiripattanapong, C., and Niramitkornburee, A. (2010). "A method of examining internal stability of the bearing reinforcement earth (BRE) wall." **Suranaree Journal of Science and Technology**. Vol.17, No.1, pp.1-11.

Horpibulsuk, S., Suksiripattanapong, C., Niramitkornburee, A., Chinkulkijniwat, A., and Tangsuttinon, T. (2011), "Performance of earth wall stabilized with bearing reinforcements", **Geotextiles and Geomembranes**, Vol.29, No.5, pp.514-524.

Khedkar, M.S., Mandal, J.N., (2007), "Pullout response study for cellular reinforcement." In: **Proceedings of Fifth International Symposium on Earth Reinforcement, IS Kyushu '07, November 14–16, 2007**, Fukuoka, Japan, pp. 293–298.

Khedkar, M.S., Mandal, J.N., (2009), "Pullout behavior of cellular reinforcements." **Geotextiles and Geomembranes**, Vol.27, No.4, pp.262-271.

Park, T., and Tan, S. A. (2005). "Enhanced performance of reinforced soil walls by the inclusion of short fiber." **Geotextiles and Geomembranes**, Vol.23, No.4, pp.348-361.

Pinto, M. I. M. and Cousens, T.W. (1996). "Geotextile reinforced brick faced retaining walls." **Geotextiles and Geomembranes**, Vol.14, No.9, pp.449-464.

Pinto, M. I. M. and Cousens, T.W. (2000). "Effect of the foundation quality on a geotextile-reinforced brick-faced soil retaining wall." **Geosynthetics International**, Vol.7, No.3, pp.217-242.

Rowe, R.K. and Ho, S.K. (1997), "Continuous panel reinforced soil walls on rigid foundations", **Journal of Geotechnical and Geoenvironmental Engineering**, Vol.123, No.10, pp.912-920.

Skinner, G. D., and Rowe, R. K. (2005). "Design and behavior of a geosynthetic reinforced retaining wall and bridge abutment on a yielding foundation." **Geotextitles and Geomembranes**, Vol.23, No.4, pp.234-260.

CHAPTER VI

CONCLUSIONS AND RECOMMENDATIONS

6.1 Summary and conclusions

This thesis consists of three main objectives. The first isto understand the pullout resistance mechanism of bearing reinforcement embedded in different coarse-grained soils and to suggest a practical approach for approximating the pullout resistance. The second is to model the behavior of the bearing reinforcement earth (BRE) wall by 2D finite element analysis. The third is to perform the sensitivity analysis of the bearing reinforcement earth (BRE) wall by 2D finite element analysis. The conclusions can be drawn as follows

6.1.1 Pullout resistance mechanism of bearing reinforcement

6.1.1.1 Pullout friction resistance

The pullout friction resistance of the bearing reinforcement is mainly controlled by only the friction angle, irrespective of grain size distribution. The apparent friction between soil and longitudinal member, δ is greater than unity because the roughness of the deformed bar increases the failure friction area during pullout. The δ/ϕ ratio is about 1.47 for all tested soils.

6.1.1.2 Pullout bearing mechanism

The pullout bearing mechanism is essentially controlled by the B/D_{50} and normal stress, regardless of gradation (well-graded and poorly graded). As the bearing reinforcement is pulled out and shear displacement occurs along the

interface, the zone of soil surrounding the reinforcement tends to dilate. However, the volume change is restrained by the surrounding non-dilating soil, resulting in an increase in normal stress on the soil-reinforcement interface (interlocking). The interlocking effect is significant for the B/D_{50} values lesser than 12 and decreases as the increase in the normal stress.

By assuming that the general shear and modified punching shear mechanisms are the upper and lower boundaries, the equations of predicting N_q for $3 \le B/D_{50} \le 12$ and $30 \le \sigma_n \le 120$ are proposed and verified. Consequently, the maximum pullout bearing force of the bearing reinforcement with a single transverse member, P_{b1} can be approximated. The member interference is essentially dependent on the S/B, irrespective of grain size distribution and friction. The transverse member interference zones are classified into three zones. Zone 1 $(S/B \le 3.75)$ is block failure where all transverse members act like a rough block. Zone 2 $(3.75 < S/B < 25)$ is member interference failure. Zone 3 $(S/B > 25)$ is individual failure. Based on the understanding of the pullout mechanism of a single transverse member and transverse member interference, the equations for estimating pullout resistance of the bearing reinforcement with different transverse members are proposed and verified.

6.1.2 Finite element analysis of the BRE wall

The bearing reinforcement earth (BRE) wall constructed on the hard stratum was simulated by PLAXIS 2D. The geotextile elements, which cannot resist the bending moment, were used to model the bearing reinforcements by converting the contribution of both the friction and bearing resistances to the equivalent friction

resistance. This modeling is considered to be applicable and practical for working state (small pullout displacement). The equivalent friction resistance is represented by the interface factor, R, which was determined from the back analysis of the laboratory pullout test. The R values of 0.65 and 0.75 were obtained for the bearing reinforcements with 2 and 3 transverse members, respectively. The BRE wall was modeled under a plane strain condition and the reinforcements were modeled using geotextile elements, which cannot resist the bending moment. Overall, the behavior of the BRE wall is simulated satisfactorily and agreed well with the predictions. The changes in foundation settlements, bearing stresses, lateral earth pressures and tensions in the reinforcements during and after construction are in good agreement with the measured ones. This implies that the proposed method is applicable to predict the BRE wall performance in practice.

6.1.3 The parametric study on performance the BRE wall

The parametric study on the bearing reinforcement earth (BRE) wall constructed on the hard stratum by PLAXIS 2D. The parametric study on BRE wall were performed by varying the foundation conditions (thickness and modulus of elasticity of the weathered crust) and the BRE wall properties (number of transverse members, reinforcement length, wall height and reinforcement vertical spacing). The simulated settlement of the BRE wall is dependent on the weathered crust thickness, the modulus of elasticity of the weathered crust and wall height. The settlement is relatively uniform due to the contribution from the stiffness of bearing reinforcement. Consequently, the bearing stress distribution is almost uniform for different foundation conditions and BRE wall properties. The lateral movement at wall base increases as the weathered crust thickness increases because of the increase in lateral

movement of the foundation. The maximum lateral movement occurs at about the mid of the wall height for medium weathered crust and at the top of the wall height for weak weathered crust. For the weak weathered crust where the maximum lateral movement is found at the top of the BRE wall, the BRE wall tends to overturn around the toe. For medium to hard weathered crust, the change in the lateral movement at the wall base is insignificant even with the change in number of transverse members due to very high overburden pressure. The effect of number of transverse members is noticed at the top of the wall where the pullout resistance is lower. The BRE wall with the L/H ratio of greater than 0.8 is not recommended in practice because the lateral movement is essentially the same for different L/H ratios. The maximum tension plane is close to the failure plane recommended by AASHTO (2002) only for the reinforcement layers below $H/2$, especially for the case of thick clay deposit, while the maximum tension forces are at the front of the wall for the layers above $H/2$. This implies that the maximum tension plane and failure plane do not coincide for the BRE wall in service state.

6.2 Recommendations for future work

- The equations for estimating the pullout resistance of bearing reinforcement are proposed and verified for coarse-grained soils. The mode of failure and the transverse member interference of the bearing reinforcement embedded in fine-grained soils should be further studied.

- The finite element analysis of the BRE wall in this study was performed in 2-D plain strain condition. However, the horizontal spacing and shape of bearing reinforcement (3-D direction) affect the performance of the

BRE wall. Consequently, the 3-D finite element analysis of the BRE wall should be performed and compare with the 2-D one.
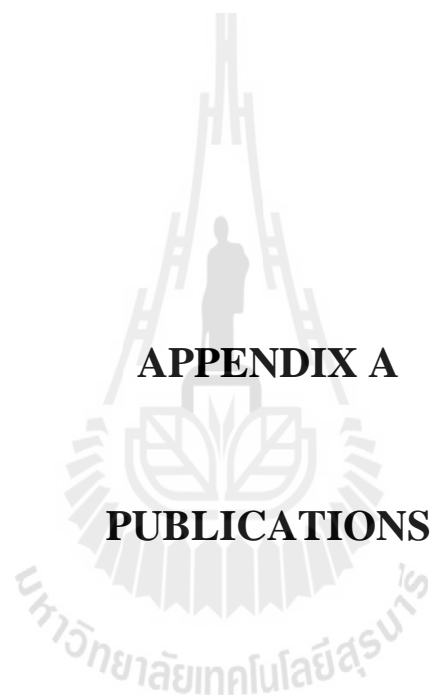
APPENDIX A

PUBLICATIONS

List of Publications

Horpibulsuk, S., Suksiripattanapong, C., Niramitkornburee, A., Chinkulkijniwat, A., and Tangsuttinon, T. (2011). **Performance of earth wall stabilized with bearing reinforcements.** Geotextiles and Geomembranes. 29 (5), 514-524.

Suksiripattanapong, C., Chinkulkijniwat, A., Horpibulsuk, S., Rujikiatkamjorn, C. and Tangsuttinon, T. (2012). **Numerical analysis of bearing reinforcement earth (BRE) wall.** Geotextiles and Geomembranes. 32, 28-37.

Suksiripattanapong, C., Horpibulsuk, S. Chinkulkijniwat, A., and Chai, J.C. (2013). **Pullout resistance of bearing reinforcement embedded in coarse-grained soils.** Geotextiles and Geomembranes. 36, 44-54.

Horpibulsuk, S., Suksiripattanapong, C., and Chinkulkijniwat, A. (2013). **Design method for bearing reinforcement earth wall.** Geotechnical Engineering Journal of the SEAGS & AGSSEA. 43. (4)

Horpibulsuk, S., Suksiripattanapong, C., Niramitkornburee, A. (2010). **A method of examining internal stability of the bearing reinforcement earth (BRE) wall.** Suranaree Journal of Science and Technology. 17 (1), 1-11.

Horpibulsuk, S., Niramitkornburee, A., Suksiripattanapong, C., Chinkulkijniwat, A., and Tangsutthinon, T., (2012). **Bearing reinforcement - a new type of earth reinforcement.** Proceedings of International Symposium on Lowland Technology. Saga, Japan, September 16-18, 2010.

Horpibulsuk, S., Suksiripattanapong, C., Niramitkornburee, A., Chinkulkijniwat, A., Tangsutthinon, T., and Bunyakait, W. (2011). **Performance of a bearing**

reinforcement earth (BRE) wall. Proceedings of 14th Asian Regional Conference on Soil Mechanics and Geotechnical Engineering, Hong Kong, China, May 23-27, 2011.

Horpibulsuk, S., Suksiripattanapong, C., Chinkulkijniwat, A., Tangsutthinon, T., and Bunyakait, W. (2011). **Performance of a bearing reinforcement earth (BRE) wall and its numerical simulation.** Proceedings of 2nd International Conference on Transportation Geotechnics, Hokkaido, Japan, September 10-12, 2012.

Suksiripattanapong, S. and Horpibulsuk, S. (2012). **Effect of particle size on the pullout mechanism of bearing reinforcement.** Proceedings of International Conference on Ground Improvement and Ground Control. University of Wollongong, Australia, 30 October – 2 November, 2012.

Suksiripattanapong, S., Horpibulsuk, S., and Chinkulkijniwat, A. (2012). **Effect of spacing of transverse member on the pullout resistance of bearing reinforcement.** Proceedings of 5th Asian Regional Conference on Geosynthetics. Bangkok, Thailand, 13-16 December, 2012.

Horpibulsuk, S., and Suksiripattanapong, C. (2012). **A novel mechanically stabilized earth wall in Thailand – Bearing reinforcement earth (BRE) wall.** Proceedings of 5th Asian Regional Conference on Geosynthetics. Bangkok, Thailand, 13-16 December, 2012.

เชิดศักดิ์ สุขศิริพัฒนพงศ์ สุขสันติ์ หอพิบูลสุข อเนก เนรมิตครบุรี อวิรุทธิ์ ชินกุลกิจนิวัฒน์ รุ้งลาวัลย์ ราชัน ธีรศักดิ์ ตั้งสุทธินนธ์ และวัฒนชัย บุณยเกียรติ (2553) **พฤติกรรมของกำแพง กันดินที่เสริมกำลังด้วยเหล็กเสริมแบกทาน.** การประชุมวิชาการวิศวกรรมโยธาแห่งชาติ ครั้ง ที่ 15. จังหวัดอุบลราชธานี.

เชิดศักดิ์ สุขศิริพัฒนพงศ์ ดิเรก บุญศรี และ สุขสันติ์ หอพิบูลสุข (2556) **อิทธิพลของขนาดเม็ดดินต่อกำลังต้านทานแรงฉุดแบกทานของเหล็กเสริมกำลังแบกทาน.** การประชุมวิชาการวิศวกรรมโยธาแห่งชาติ ครั้งที่ 18. มหาวิทยาลัยเชียงใหม่. วันที่ 8-10 พฤษภาคม 2556

Pullout resistance of bearing reinforcement embedded in coarse-grained soils

Cherdsak Suksiripattanapong [a,1], Suksun Horpibulsuk [a,*], Avirut Chinkulkijniwat [a,2], Jin Chun Chai [b,3]

[a] School of Civil Engineering, Suranaree University of Technology, 111 University Avenue, Muang District, Nakhon Ratchasima 30000, Thailand
[b] Department of Civil Engineering and Architecture, Faculty of Science and Engineering, Saga University, 1 Honjo, Saga 840-8502, Japan

ARTICLE INFO

ABSTRACT

The bearing reinforcement was developed as a cost-effective earth reinforcement. It is composed of a longitudinal member and transverse members. The longitudinal member is made of a steel deformed bar and the transverse members are a set of equal angles. The present article studies the influence of soil properties (friction angle, grain size and gradation) and dimension and spacing of the transverse members on the pullout mechanism of the bearing reinforcement. The total pullout resistance is the sum of the pullout friction and the pullout bearing resistance. The $\tan \delta / \tan \phi$ ratio, where δ is the friction angle between soils and the longitudinal member and ϕ is the internal friction angle of soil, is greater than unity because of the roughness and rigidity of the steel deformed bar. The bearing failure mechanism of a single transverse member is dependent upon the B/D_{50} value, where B is the leg length of the transverse member and D_{50} is the average grain size of the soil. The transverse member interference is dependent upon the ratio of spacing between transverse members and the leg length of transverse members, S/B. Based on a critical analysis of the test results, the pullout resistance equations of the bearing reinforcement with different dimensions and spacing between transverse members embedded in different coarse-grained soils are introduced and verified. These equations were developed based on a limit equilibrium analysis, which is a simple rational method for analyzing the internal stability of bearing reinforcement earth walls.

1. Introduction

Soil reinforcing materials, such as strips and grids have been developed in the past two decades to increase the functional abilities for reinforced structures. In Thailand, a widely used strip reinforcement is the ribbed steel reinforcing strip (it is 50 mm in width and 4.2 mm in thickness with a yield strength of 520 MPa). This reinforcement is conveniently transported to a factory for galvanization and to a construction site as well as simple and fast to install due to its strip shape. Construction costs with strips are relative high because they are imported into Thailand from Africa and are subject to high import charges. By contrast, steel grid reinforcements can be locally manufactured. The pullout resistance mechanisms of steel grid reinforcement have been extensively

studied by many researchers (Peterson and Anderson, 1980; Jewell et al., 1984; Palmeira and Milligan, 1989; Palmeira, 2009; Bergado et al., 1988, 1996; Shivashankar, 1991; Chai, 1992; Tin et al., 2011). The advantage of grid reinforcement is that the pullout bearing resistance in the resistant zone is high. However, the total volume (weight) of steel grid required is still high because of unnecessary transverse (bearing) bars in the active (unstable) zone. The transportation and installation of grid reinforcements are less convenient than those of strip reinforcements.

Horpibulsuk and Niramitkornburee (2010) have introduced a new cost-effective earth reinforcement designated as "Bearing reinforcement". It is simple to install, convenient to transport and possesses high pullout and rupture resistances with less steel volume. Fig. 1 shows the typical configuration of the bearing reinforcement, which is composed of a longitudinal member and transverse (bearing) members. The longitudinal member is a steel deformed bar and the transverse members are a set of steel equal angles. This reinforcement has been introduced into practice in Thailand since 2008 by the Geoform Co., Ltd. Several earth walls stabilized with the bearing reinforcements have been constructed in various parts of Thailand. The bearing reinforcement is connected to the facing panel at the tie point (2 U shape steel pieces) by

* Corresponding author. Tel.: +66 44 22 4322/89 767 5759; fax: +66 44 22 4607.
E-mail addresses: cherdsak_2526@hotmail.com (C. Suksiripattanapong), suksun@g.sut.ac.th, suksun@yahoo.com (S. Horpibulsuk), avirut@sut.ac.th (A. Chinkulkijniwat), chai@cc.saga-u.ac.jp (J.C. Chai).
[1] Tel.: +66 81 760 7722; fax: +66 44 22 4607.
[2] Tel.: +66 44 22 4353; fax: +66 44 22 4607.
[3] Tel.: +81 95 2 332681.
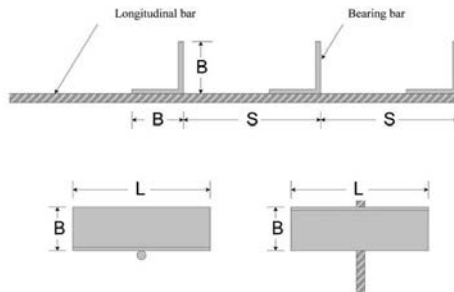
Fig. 1. Configuration of the bearing reinforcement (Horpibulsuk and Niramitkornburee, 2010).

a locking bar (a deformed bar) (Fig. 2). This mechanically stabilized earth (MSE) wall is designated as "Bearing Reinforcement Earth (BRE) wall" (Horpibulsuk et al., 2011).

The performance of a test BRE wall on hard ground was investigated on the campus of Suranaree University of Technology (SUT) (Horpibulsuk et al., 2010, 2011). The PLAXIS program was successfully used to simulate the performance of the BRE wall (Suksiripattanapong et al., 2012). In addition to the numerical analysis, the limit equilibrium design is generally considered for the BRE wall design due to its simplicity and conservation. The internal stability of the BRE wall deals with the rupture and pullout mechanisms. The pullout resistance is the sum of the pullout

friction and bearing resistance. Based on the available research on the pullout bearing mechanisms of different types of reinforcement (Alfaro et al., 1995; Hayashi et al., 1999; Alfaro and Pathak, 2005; AASHTO, 2002; Bergado et al., 1988, 1996; Shivashankar, 1991; Chai, 1992; Khedkar and Mandal, 2009; Abdi and Arjomand, 2011), three existing pullout bearing failure mechanisms for the plane strain condition are proposed: general shear failure (Peterson and Anderson, 1980), punching shear failure (Jewell et al., 1984), and modified punching shear failure (Chai, 1992; Bergado et al., 1996; Horpibulsuk and Niramitkornburee, 2010). The maximum bearing stress of a single isolated transverse member, σ_{bmax}, in coarse-grained soil is presented in the form:

$$\sigma_{bmax} = N_q \sigma_n \qquad (1)$$

where N_q is the bearing capacity factor, depending upon the mode of failure and σ_n is the normal stress. N_q for the three failure mechanisms is presented in terms of the soil friction angle, ϕ, as follows:

$$N_{q(general)} = \exp[\pi \tan \phi] \tan^2 \left(\frac{\pi}{4} + \frac{\phi}{2} \right) \quad \text{for general shear failure} \qquad (2)$$

$$N_{q(punching)} = \exp \left[\left(\frac{\pi}{2} + \phi \right) \tan \phi \right] \tan \left(\frac{\pi}{4} + \frac{\phi}{2} \right) \quad \text{for punching shear failure} \qquad (3)$$

$$N_{q(modified)} = \frac{1}{\cos \phi} \exp[\pi \tan \phi] \tan \left(\frac{\pi}{4} + \frac{\phi}{2} \right) \quad \text{for modified punching shear failure} \qquad (4)$$
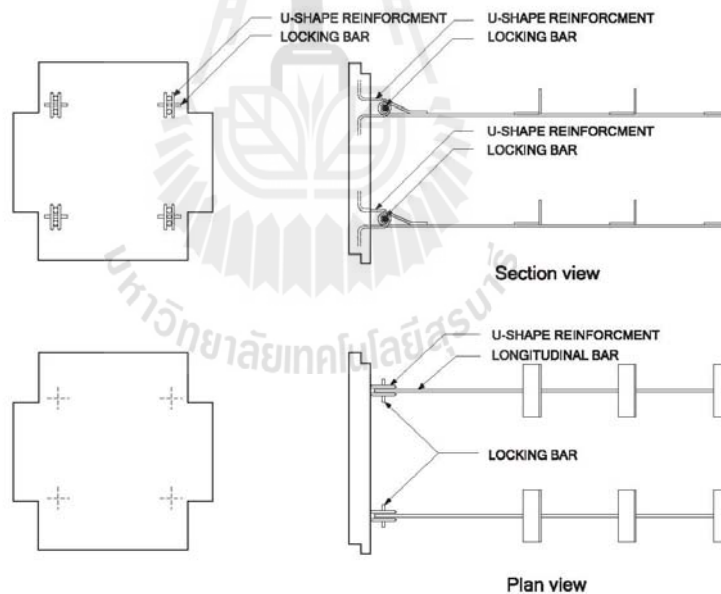
Fig. 2. Connection of the bearing reinforcement to wall facing (Horpibulsuk and Niramitkornburee, 2010).

Horpibulsuk and Niramitkornburee (2010) showed that the maximum bearing stress, σ_{bmax}, of a single transverse member for the bearing reinforcement embedded in a poorly graded sand is predicted satisfactorily based on the modified punching shear mechanism. The proposed equation was applicable to a particular compacted sand with small particles. The applicability of the proposed equation for different coarse-grained soils, which are commonly used as backfill materials, thus required examination. It was revealed that the soil particle size controls the pullout bearing mechanisms. The failure bearing mechanism of the grid reinforcement is dependent upon the average grain size, D_{50}, until the ratio of the diameter of the transverse member to the average grain size is greater than 12 (Palmeira and Milligan, 1989; Palmeira, 2009).

This article aims to study the pullout resistance mechanism of the bearing reinforcement embedded in different coarse-grained soils with different dimensions of transverse member, gradations, average grain sizes, D_{50}, and friction angles. The tested soils were well-graded gravel, well-graded sand and crushed rock. Both the well-graded sand and the well-graded gravel are consistent with the specifications of the Department of Highways, Thailand. The results for poorly graded sand from Horpibulsuk and Niramitkornburee (2010) were included in the analysis in this work. The tested soils contained less than 12% fine particles and covered all coarse-grained types as classified by the Unified Soil Classification System (USCS). The knowledge gained from this study is useful for the internal stability analysis of the BRE wall based on the limit equilibrium analysis.

2. Laboratory investigation

2.1. Soil samples

The tested soils consisted of 3 soil types with different grain size distributions and friction angles. The soils were collected from different locations in Nakhon Ratchasima, Thailand. They were well-graded gravel (GW), well-graded sand (SW) and crushed rock (GP) according to the Unified Soil Classification System (USCS). The average grain sizes, D_{50} were 5.7, 1.0 and 7.0 mm for GW, SW and GP, respectively. The compaction characteristics based on standard Proctor energy are optimum water content, OWC = 3.9 and 6.3% and maximum dry unit weight, γ_{dmax} = 20.15 and 18.15 kN/m^3 for GW and SW, respectively. The crushed rock (GP) is not compacted to obtain a friction angle lower than that of the GW and SW. The tested water content was 0.31% and the tested dry unit weight was 16.64 kN/m^3. Strength parameters of all tested soils were obtained from a large direct shear apparatus with a diameter of 35 cm. The friction angles were 45, 42 and 40°, for GW, SW and GP, respectively. The high friction angles (greater than 36°) are acceptable for MSE wall construction in Thailand. In addition to these three soils, the test results of the poorly graded sand (SP) obtained from Horpibulsuk and Niramitkornburee (2010) were also used for this study. The average grain size, D_{50} of SP was 0.31 mm. The optimum water content, OWC was 6.3%; the maximum dry unit weight, γ_{dmax} was 16.80 kN/m^3; and the friction angle, ϕ, was 40°. The crushed rock (GP) and the poorly graded sand (SP) have the same friction angle but different grain size distributions and average grain sizes,

D_{50}. These two soils were used to study the effect of D_{50} on the pullout bearing mechanism. The index properties of all the tested soils are summarized in Table 1. The pullout test results in these soils clearly show the effects of gradation, average grain size and friction angle on the pullout mechanism and the failure pullout resistance. The grain size distribution curves of the studied soils compared with the specification of the Department of Highways, Thailand are presented in Fig. 3.

2.2. Methodology

The pullout test apparatus used in this investigation is made of rolled steel plates, angles, channels, and H-sections welded or bolted together to give an inside dimension of 2.6 m in length by 0.6 m in width by 0.8 m in height as shown in Fig. 4. The front wall contains upper and lower parts with a slot in between for the reinforcement specimen. Friction between the tested soils and the side walls of the apparatus was minimized by the use of a lubricated rubber member as done by Horpibulsuk and Niramitkornburee (2010). During the pullout of the reinforcement, due to an arching effect of the front wall, the normal stress on the reinforcement near the front wall may increase (dilate) or decrease (contract). To reduce this effect, a sleeve was installed inside the slot opening, which was 150 mm in horizontal width and 100 mm in height to isolate the bearing reinforcement near the front wall. The compacted sand thickness of 300 mm was maintained above and below the reinforcement.

For any model test, the boundary effect cannot be completely avoided. One of the boundary effects for the pullout test is the effect of front wall of the pullout test apparatus. For investigating the pullout force of a single transverse member, the effect of front wall was avoided by placing the transverse member far away from the front wall. However, for investigating the influence of the spacing between the transverse members, the effect of front wall could not be completely avoided. When the spacing between the first transverse member and the front wall is equal to or smaller than the spacing between the transverse members, S, the effect of the front wall may increase or decrease (in case the slot on the wall for a tested reinforcement to pass through is too large) the pullout bearing resistance of the first transverse member. If the spacing between the front wall and the first transverse member is larger than the S value, the pullout bearing resistance of the first transverse member may be higher than other members (less interaction effect). As for the effect of the side walls and the upper and the bottom boundaries, considering the size of the tested reinforcements, it is believed that the pullout test apparatus is large enough to avoid considerable boundary effects.

Normal stress was applied with a pressurized air bag positioned between the compacted soil and the top cover of the apparatus. Before installing the air bag, a 30 mm thick layer of soil was placed on the top of the compacted soil and covered by a 4 mm thick steel plate. The purpose of this procedure was to try to produce a uniformly distributed normal stress on the top of the backfill soil (Fig. 4). The pullout force was applied by a 200 kN capacity electro-hydraulic controlled jack. The pullout displacement at the front of the pullout apparatus was monitored by a linear variation differential transformer (LVDT). The maximum applied pullout

Table 1
Index properties of soils.

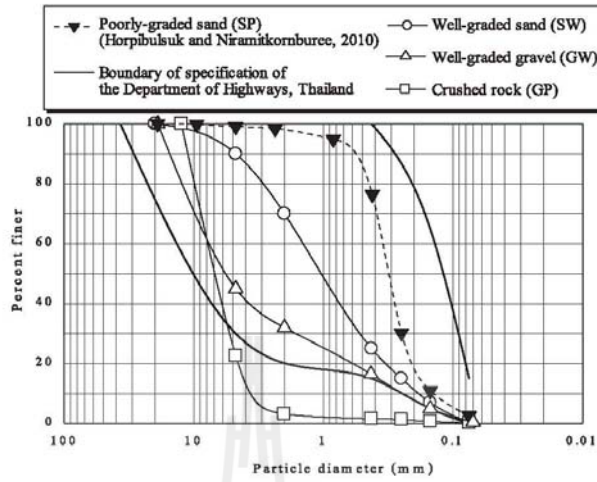| Type	Average grain size, D_{50} (mm)	Specific gravity, G_s	Tested water content, OWC (%)	Tested dry unit weight, γ_{dmax} (kN/m^3)	Friction angle, ϕ (°)
Well-graded gravel (GW)	5.7	2.73	3.9	20.15	45
Well-graded sand (SW)	1	2.69	6.3	18.15	42
Poorly graded sand (SP)	0.31	2.77	6.3	16.8	40
Crushed rock (GP)	7	–	0.31	16.64	40

Fig. 3. Grain size distribution of the tested soils.
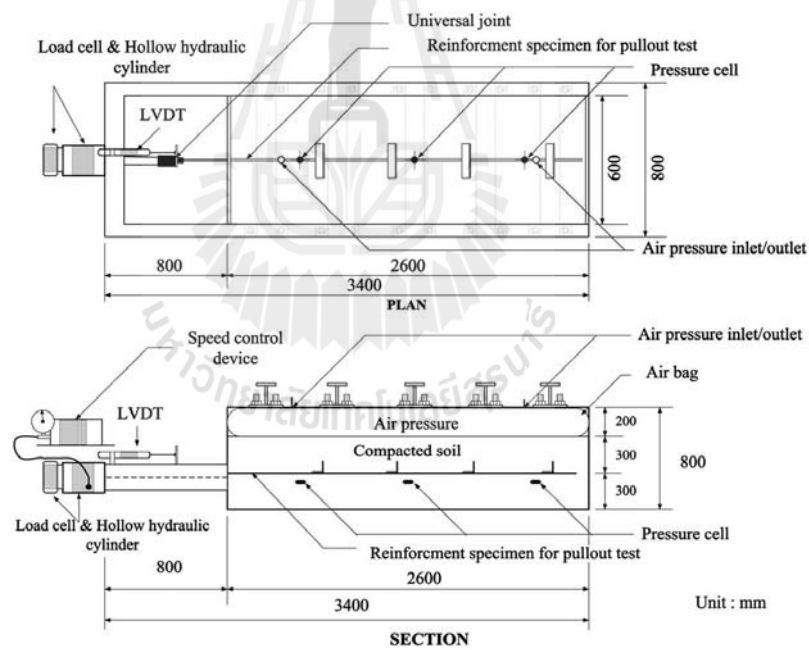
Fig. 4. Schematic diagram of pullout test apparatus (Horpibulsuk and Niramitkornburee, 2010).

C. Suksiripattanapong et al. / Geotextiles and Geomembranes 36 (2013) 44–54

displacement (end of test) is 40 mm, which is approximately 10% of the leg length (B) of the transverse member. The applied normal stress was 30, 50 and 90 kPa. These different applied normal stresses were considered to simulate total vertical stress (due to dead and live loads) on the bearing reinforcement at different depths. The pullout rate of 1 mm/min was adopted throughout the tests.

2.3. Bearing reinforcement

To understand the role of the influential factors (dimension, spacing, number of transverse members, normal stress and average grain size) on the pullout mechanism, the pullout tests on the bearing reinforcements with different dimensions, number, and spacing of transverse members embedded in the tested soils (different grain size) were conducted under different applied normal stresses. The leg length, B, and the length, L, of the tested transverse members (steel equal angles) were 25, 40 and 50 mm and 100, 150 and 200 mm, respectively; all are generally used for MSE walls. The B/L values for the tested transverse members are between 0.13 and 0.5. Although during pullout of the bearing reinforcement, the deformation around the bearing member is three-dimensional, Horpibulsuk and Niramitkornburee (2010) reported that within this B/L range the bearing capacity of the single transverse member embedded in poorly graded sand can be predicted by the modified plane strain punching shear failure model successfully, i.e. the three-dimensional effect has been inexplicitly considered by the proposed plane strain failure model. The spacing between transverse members, S, varies from 150 to 1500 mm, depending upon the number of transverse members. In this study, the number of transverse members, n, ranged from 1 to 4, which is generally the case in practice. The pullout friction resistance of a longitudinal member is investigated from the pullout test on a single longitudinal member with a diameter of 16.0 mm and length of 2.6 m.

3. Test results and discussion

3.1. Pullout friction resistance

Fig. 5 shows the pullout friction force and displacement relationship of a longitudinal member with a diameter of 16 mm and length of 2.6 m for well-graded gravel (GW), well-graded sand (SW), poorly graded sand (SP) and crushed rock (GP). For a particular soil, the maximum pullout friction force, P_{ffmax} increases with the increase in normal stresses, σ_{n}. The displacement at peak failure is insignificantly affected by the normal stress; it is approximately 3–5 mm for all the applied normal stresses and tested soils. The well-graded gravel (GW) gives the highest pullout friction force because it has the highest friction angle. The crushed rock (GP) and the poorly graded sand (SP) give the same the friction pullout force, P_{f}, for the same normal stress, σ_{n} even with different grain size distributions and D_{50} values, possibly because they have the same friction angle. Fig. 6 shows the failure envelope of all tested soils where δ is the apparent interface friction angle between soils and the steel longitudinal member. The shear stress, τ was determined from $P_{\text{ffmax}}/\pi DL$ where D and L are the diameter and length of the longitudinal member, respectively. The tan δ values are very high and are larger than the tan ϕ values for all tested soils because the roughness of the steel deformed bar increases the failure friction plane during pullout (i.e., the failure friction diameter is greater than the measured diameter of the longitudinal member) (Horpibulsuk et al., 2011). The higher tan δ value is also due to the arching effect caused by the stress concentration on the steel bar as a consequence of the higher stiffness of the steel bar compared to that of the surrounding soil. Even with the differences in tan δ and tan $\delta/\tan \phi$ values for the different soils, their δ/ϕ values are essentially the same, approximately 1.47. To conclude, the maximum friction pullout force, P_{ffmax}, and δ are mainly controlled by the friction angle and are independent upon grain size.
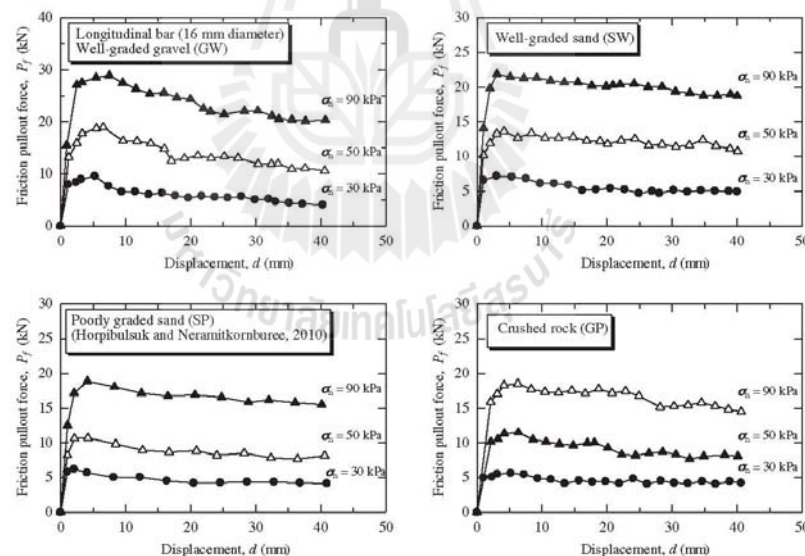

Fig. 5. Pullout test results of a longitudinal member under different normal stresses.
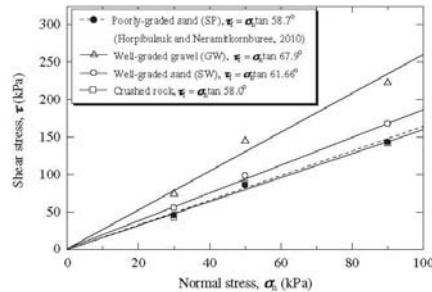
183

C. Suksiripattanapong et al. / Geotextiles and Geomembranes 36 (2013) 44–54   49

Fig. 6. Failure envelope of all tested soils.

3.2. Pullout bearing mechanism of a single isolated transverse member (n = 1)

The pullout bearing force at any displacement is the difference between the total pullout force and the pullout friction force. Fig. 7 shows the total pullout force and displacement relationship of the bearing reinforcement with a 1.0 m longitudinal member and a 40 × 150 ($B \times L$) mm transverse member for all tested soils. It is notable that initially, the pullout resistance sharply increases with displacement and then gradually increases until failure at a large displacement of approximately 40 mm, which is the end of the test. The initial sharp increase is caused by the pullout friction resistance, which fully mobilizes at small displacement while the soil-bearing capacity fully mobilizes at large displacement. The total pullout force, P_t, increases with the increase in the normal stresses, σ_n, for all tested soils. It increases as the friction angle increases for a particular normal stress. Although the crushed rock (GP) and poorly graded sand (SP) give the same the pullout friction force, P_f, for the same normal stresses, σ_n, the total pullout force, P_t, of the crushed rock (GP) is higher than that of poorly graded sand (SP). In other words, the pullout bearing force of the crushed rock is larger. This higher pullout bearing force is caused by the larger grain size.

The influence of grain size on the pullout bearing resistance is expressed by the ratio of the leg length of the transverse member, B, to the average grain size, $D_{50}(B/D_{50})$. Fig. 8 shows the bearing stress, σ_b and displacement, d, relationship of the transverse member with different B values for all tested soils. The measured bearing stress is obtained from the assumption that the soil in the angle leg acts as a rigid block (Horpibulsuk and Niramitkornburee, 2010). The bearing stress is thus determined from the ratio of the pullout force to the area of transverse member, $B \times L$. It is found that the failure bearing stresses, σ_{bmax}, for large D_{50} soils (the well-graded gravel and the crushed rock) increase as the B/D_{50} value decreases. The σ_b versus d relationships for both the SW and SP soils are independent of the B/D_{50} value because the grain sizes of both soils (SW and SP) are much smaller than B ($B/D_{50} > 25$). The well-graded sand (SW) exhibits slightly higher failure bearing stresses than the poorly graded sand (SP) because of a higher friction angle, ϕ. Thus, the pullout bearing resistance is dependent upon the average grain size, D_{50}, the leg length, B, and the friction angle, ϕ, irrespective of gradation (well-graded and poorly graded).

The maximum pullout bearing resistance can be determined from the plasticity solutions. Using the proposed equations (Eqs. (1)–(4)), the comparison between the measured and predicted maximum bearing stresses is shown in Fig. 9. For the well-graded gravel (GW) and the crushed rock (GP), with large average grain size, D_{50}, the maximum bearing stress, σ_{bmax}, at low normal stress

of approximately 30 kPa was close to that predicted by the general shear mechanism. However, the measured maximum bearing stress, σ_{bmax}, at high normal stress of 90 kPa was very close to that predicted by the modified punching shear mechanism. The same is not true for the small D_{50} soils (SP and SW). The measured pullout bearing stress is predicted satisfactorily based on the modified punching shear mechanism for the different tested normal stresses. As the bearing reinforcement is pulled out and shear displacement occurs along the interface, the zone of soil surrounding the reinforcement tends to dilate. However, the volume change is restrained by the surrounding non-dilating soil, resulting in an increase in normal stress on the soil–reinforcement interface (interlocking effect). The interlocking effect is significant for the large particle soils and can be ignored for the small particle soils. Hence, the pullout mechanism of the bearing reinforcement
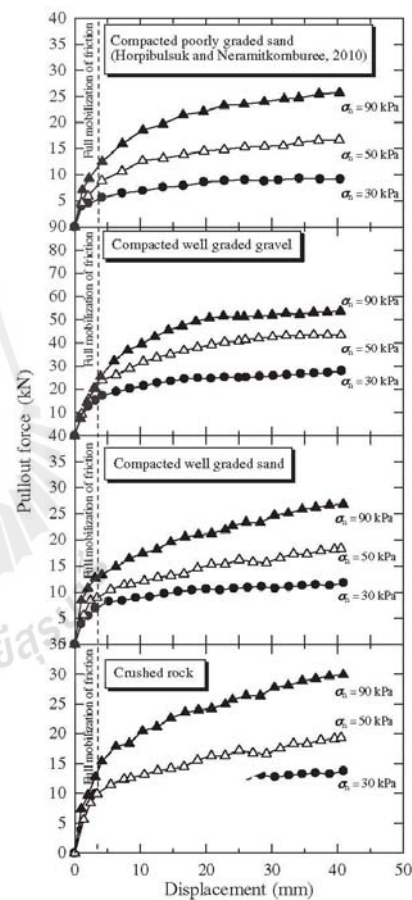

Fig. 7. Typical pullout test result of the bearing reinforcement in tested soils.
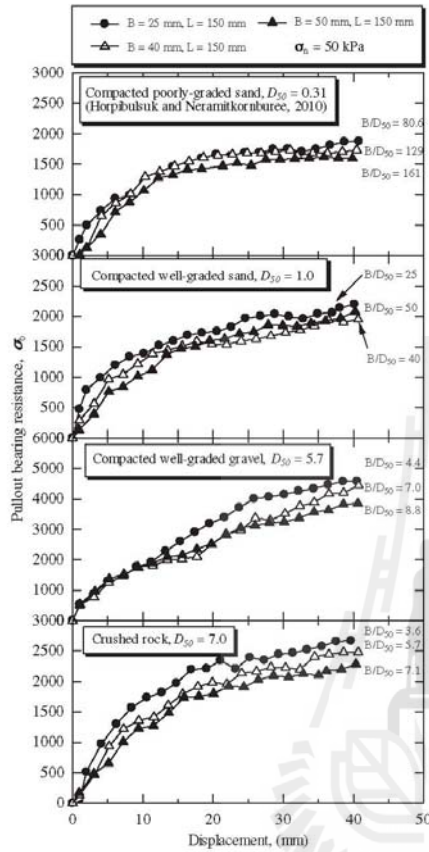
Fig. 8. Bearing stress and displacement relationship of the bearing reinforcement with a 2.6 m longitudinal member and different leg lengths, B for all tested soils.

Fig. 9. Maximum pullout bearing resistance of a single isolated transverse member for all tested soils.

embedded in the gravelly soils (both well-graded and poorly graded) under low normal stress approaches the general shear failure. This effect decreases as the normal stress increases.

To understand the development in the bearing capacity with the friction angle, which is used as an engineering parameter in practice, the measured bearing capacity factor, N_q, and friction angle, ϕ, relationship for all tested soils is plotted and shown in Fig. 10, where N_q is the measured σ_{bmax}/σ_n. The measured N_q values were compared with the values predicted by the three mechanisms. It is found from Figs. 9 and 10 that the modified punching shear mechanism can be used to predict the pullout bearing stress of different transverse member dimensions for the small particle soils (SP and SW), regardless of the gradation (either well-graded or poorly graded), and that the general shear N_q is the upper boundary for the two large particle soils (GP and GW).

The effect of B/D_{50} on the pullout bearing mechanism for large D_{50} soils is illustrated in Fig. 11, which is the relationship between $N_q/N_{q(modified)}$ and B/D_{50} of single isolated transverse member for all
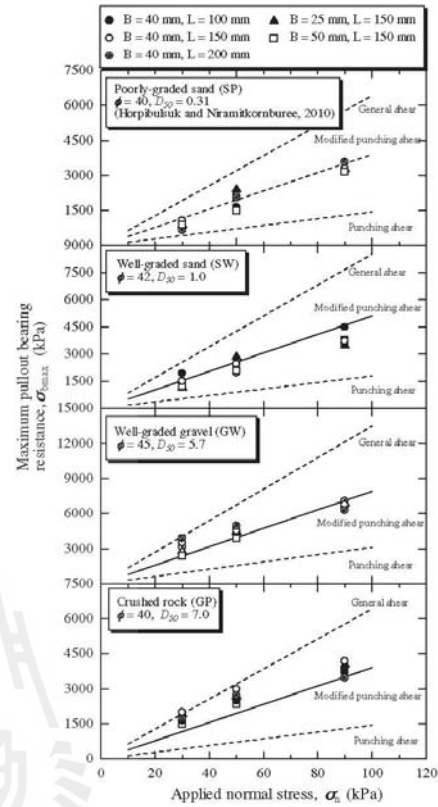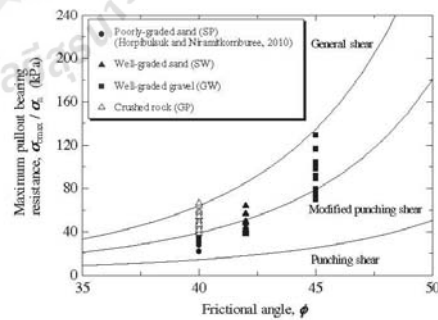

Fig. 10. Measured and predicted bearing capacity factor, N_q for all tested soil.

tested soils. For the small particle soils (SW and SP), $N_q/N_{q(modified)}$ is close to unity (the N_q value can be approximated from Eq. (4)). However, for the large particle soils (both well-graded and poorly graded), $N_q/N_{q(modified)}$ decreases as the B/D_{50} value increases and tends to approach unity when the B/D_{50} value is close to 12, which agrees well with the pullout results of the grid reinforcement reported by Palmeira (2009). The failure mechanism of bearing reinforcement is classified into two zones, which is dependent upon the B/D_{50} value, regardless of gradation (well-graded or poorly graded). Zone 1, where $B/D_{50} \leq 12$, is the interlocking induced failure while Zone 2, where $B/D_{50} \geq 12$, is the modified punching shear failure.

In Zone 1, the interlocking effect decreases with the increase in the normal stress and B/D_{50} value. The clear picture of the influence of normal stress on the N_q value for different B/D_{50} values is depicted in Figs. 12 and 13. Assuming that general shear and modified punching shear solutions are the upper and lower boundaries, the N_q values for all tested soils (different friction angles) at $B/D_{50} = 12$ under different normal stresses are approximated from Eq. (4). At a B/D_{50} of 3, the N_q value at $\sigma_n < 30$ kPa can be approximated by Eq. (2); additionally, the N_q value decreases with increasing normal stress and is determined by Eq. (4) when $\sigma_n > 120$. This premise yields the following equations for predicting the N_q value for different normal stresses and B/D_{50} values:

$$N_{q1}/N_{q(modified)} = a + b \ln\left(\frac{B}{D_{50}}\right) \quad \text{for } 3 \leq B/D_{50} \leq 12 \qquad (5)$$

$$N_{q2}/N_{q(modified)} = c + d \ln(\sigma_n) \quad \text{for } 30 \text{ kPa} \leq \sigma_n \leq 120 \text{ kPa} \qquad (6)$$

where N_{q1} is the N_q value at $\sigma_n = 30$ kPa for $3 \leq B/D_{50} \leq 12$ and N_{q2} is the N_q value at the required B/D_{50} value and normal stress. The a, b, c and d are constants, depending upon the normal stress, σ_n; B/D_{50}; and the friction angle, ϕ. The constants a and b in Eq. (5) can be obtained with the two physical conditions at $\sigma_n = 30$ kPa: 1) when B/D_{50} equals 3, $N_{q1} = N_{q(general)}$ and 2) when B/D_{50} equals 12, $N_{q2} = N_{q(modified)}$ equals 1. The constants a and b are thus determined by the following equations:

$$b = 0.722 \left(1 - \frac{N_{q(general)}}{N_{q(modified)}}\right) \qquad (7)$$

$$a = 1 - 2.485b \qquad (8)$$

Once the N_{q1} value for a required B/D_{50} at $\sigma_n = 30$ kPa is known, the N_{q2} value at target normal stress (30 kPa $\leq \sigma_n \leq$ 120 kPa) can be

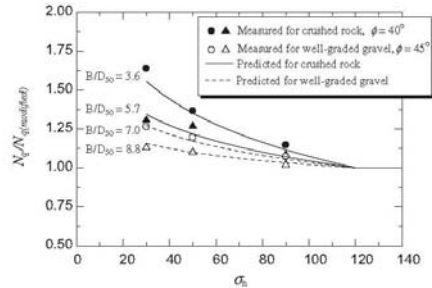determined by Eq. (6). The two physical conditions to determine the constants c and d are: 1) when σ_n equals 30 kPa, $N_{q2} = N_{q1}$ and 2) when σ_n equals 120 kPa, $N_{q2} = N_{q(modified)}$ equal 1. The constants c and d are determined from:

$$d = 0.722 \left(1 - \frac{N_{q1}}{N_{q(modified)}}\right) \qquad (9)$$

$$c = 1 - 4.787d \qquad (10)$$

The predicted N_q values at a different normal stresses and B/D_{50} values for crushed rock and well-graded sand are shown in Figs. 12 and 13. The predicted and measured values are in very good agreement.

3.3. Pullout resistance of the bearing reinforcement (n > 1)

The bearing reinforcement consists of several transverse members placed at regular intervals. The pullout resistance of the bearing reinforcement can be increased by increasing either the length of the longitudinal member or the number of transverse members. The former is a more expensive solution because the contribution of pullout bearing resistance is relatively higher than that of the pullout friction resistance. It was revealed that for a steel grid, the transverse member interference, which controls the development in the pullout resistance, is dependent upon the spacing of transverse members and the diameter of transverse members (Palmeira and Milligan, 1989; Palmeira, 2009; Bergado

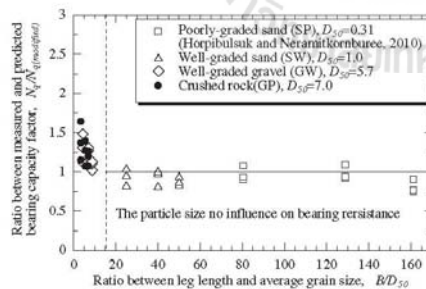Fig. 12. Measured and predicted $N_q/N_{q(modified)}$ and σ_n relationship.

Fig. 11. $N_q/N_{q(modified)}$ and B/D_{50} relationship for all tested soil.

Fig. 13. Measured and predicted $N_q/N_{q(modified)}$ and B/D_{50} relationship.

C. Suksiripattanapong et al. / Geotextiles and Geomembranes 36 (2013) 44–54
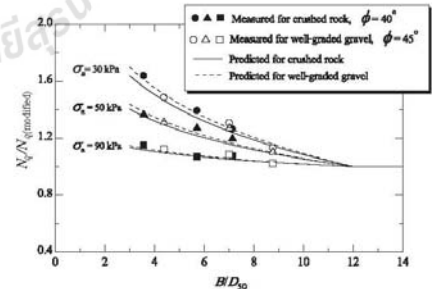
and Chai, 1994; Bergado et al., 1996). Similarly, Horpibulsuk and Niramitkornburee (2010) demonstrated that the transverse member interference for the bearing reinforcement is controlled by the spacing of transverse members and the leg length of transverse member, B, regardless of the length of the transverse member, L. During the pullout of the bearing reinforcement, the transverse members interfere with each other. A dimensionless parameter, the transverse member spacing ratio, S/B, was introduced to investigate the influence of spacing, S, and the dimension (B and L) of transverse members on the pullout bearing characteristics. Generally, the larger the S/B is, the higher the pullout bearing resistance up to a certain maximum value, due to less interference among transverse members.

Fig. 14 shows the typical relationship between the maximum pullout bearing force, P_{bn}, and transverse member spacing ratio, S/B, for 40×150 mm transverse members ($n = 2$–4) under different applied normal stresses compared with maximum pullout bearing force of a single isolated transverse member ($n = 1$), P_{b1}, for all tested soils. The result is in agreement with that reported by Horpibulsuk and Niramitkornburee (2010), indicating that the failure mechanism of the bearing reinforcement is classified into three zones, depending on the S/B value. Zone 1 is referred to as block failure when the $S/B \leq 3.75$. Zone 2 is regarded as member interference failure when $3.75 < S/B < 25$. Zone 3 ($S/B > 25$) is individual failure where soil in front of each transverse member fails individually. The interference factor, F was proposed as follows (Horpibulsuk and Niramitkornburee, 2010):

$$F = \frac{P_{bn}}{nP_{b1}} = e + f \ln\left(\frac{S}{B}\right) \qquad (11)$$

where e and f are constants, depending on n. These two constants can be obtained from two physical conditions: 1) when S/B equals 3.75, the interference factor equals $1/n$ because P_{bn} and P_{b1} are the same, and 2) when S/B equals 25, the interference factor equals unity. These two conditions establish the lower and upper values of F at corresponding values of $S/B = 3.75$ and 25, respectively. From these two conditions, the constants e and f can be determined by the following equations:

$$f = 0.527\left[1 - \frac{1}{n}\right] \qquad (12)$$

$$e = 1 - 3.219f \qquad (13)$$

It is found that the interference factor, F, predicted by Eqs. (12) and (13) can fit the experimental data. Based on the previous (Horpibulsuk and Niramitkornburee, 2010) and present studies, it is concluded that the member interference is dependent on only S/B, irrespective of grain size distribution and friction angle for the soils investigated. These two factors play a great role in determining P_{b1}. As such, even with the same S/B (same F), the P_{bn} values would be different for different grain size distributions and friction angles.

4. Suggested procedure of estimating internal stability

The full-scale test and numerical results (Horpibulsuk et al., 2010, 2011; Suksiripattanapong et al., 2012) showed that the possible failure plane (maximum tension plane) and the maximum tension forces in the reinforcement can be approximated from the coherent gravity structure hypothesis. The lateral earth pressure, σ_h, at each reinforcement level is calculated using $K = K_0$ at the top of the wall and decreases linearly to $K = K_a$ at a 6 m depth. Below a 6 m depth, $K = K_a$ is used.

The suggested method for the examination of the internal stability of the BRE wall is being presented. It has been successfully used for designing several BRE walls under the supervision of the Department of Highways, Thailand. BRE wall projects in Thailand include the Northern Saraburi Interchange; the Highway Bridge, Highway No. 418; and the Highway Route No.4 Phathalung-Trang, etc. It is considered that the pullout resistance mobilized is only due to axial pullout and the contribution of transverse deformation of the reinforcement is ignored. This consideration is conservative because in reality, the reinforcements are subjected to transverse displacement and oblique pull due to the deformation of the backfill (Shewbridge and Sitar, 1989; Leschinsky and Reinschmidt, 1985; Athanasapoulos, 1993; Bergado et al., 2000; Madhav and Umashankar, 2003; Kumar and Madhav, 2009). Consequently, the field pullout resistance is higher than the laboratory one. A suggested procedure for examining the internal stability against pullout failure of a BRE wall for B/D_{50} values greater than 3.0 is proposed as follows:

Determine the maximum pullout force in the bearing reinforcement

1. Based on the coherent gravity structure hypothesis, approximate the maximum tension (possible failure) plane for the designed BRE wall and hence the embedded length, L_e, for each reinforcement level.
2. Determine the maximum pullout forces in the bearing reinforcements by multiplying the vertical stress by the coefficient of lateral earth pressure, K, and the vertical and horizontal spacing (S_v and S_h) of the bearing reinforcements.

Determine the pullout friction resistance of the bearing reinforcement

3. Perform sieve and direct shear tests on the backfill material to determine D_{50} and shear strength parameters.
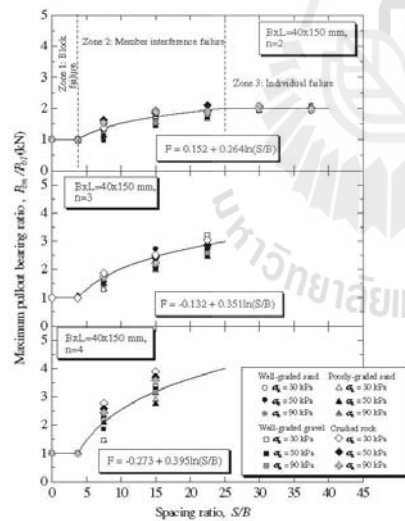

Fig. 14. Measured and predicted P_{bn}/P_{b1} and S/B relationship for 40×150 mm transverse members.

Table 2
Measured and predicted pullout bearing force of bearing reinforcement embedded in crushed rock with 40 × 150 mm transverse members for $n = 3$.

S (mm)	S/B	σ_n (kPa)	N_q	P_{b1} (kN)	F	Measured P_{bn} (kN)	Predicted P_{bn} (kN)
300	7.5	30	52.39	9.43	0.575	18.41	16.27
300	7.5	50	47.45	14.24	0.575	27.90	24.56
300	7.5	90	41.78	22.56	0.575	39.28	39.92
600	15	30	52.39	9.43	0.819	24.60	23.17
600	15	50	47.45	14.24	0.819	36.34	34.99
600	15	90	41.78	22.56	0.819	50.51	55.43
900	22.5	30	52.39	9.43	0.961	29.87	27.19
900	22.5	50	47.45	14.24	0.961	42.57	41.05
900	22.5	90	41.78	22.56	0.961	65.12	65.04

4. Determine apparent δ for the friction pullout resistance, which can be directly obtained from a pullout test on a longitudinal member or approximated from $\delta/\phi = 1.47$.
5. Determine the maximum pullout friction force of longitudinal member at the required normal stress level from $P_f = \pi D L_e \sigma_n \tan \delta$.

Determine the pullout bearing resistance of the bearing reinforcement

6. Determine N_q using the plasticity solutions based on the general shear and modified punching shear failure mechanisms (Eqs. (2) and (4)).
7. From the selected B, determine constants a, b, c and d from Eqs. (7)–(10).
8. Determine the N_q value for the required normal stress level.
   8.1 For $\sigma_n > 120$ kPa, $N_q = N_{q(punching)}$.
   8.2 For 30 kPa $\leq \sigma_n \leq 120$ kPa, N_q is approximated from Eq. (6).
   8.3 For $\sigma_n < 30$ kPa, N_q is the value approximated from Eq. (6) at $\sigma_n = 30$ kPa.
9. Determine P_{b1} from $P_{b1} = N_q \sigma_n BL$.
10. Determine the interference factor, F, of the required transverse members (required n, S, B, and L) using Eqs. (11)–(13).
11. Determine the maximum pullout bearing force with n transverse members, P_{bn} from $P_{bn} = nFP_{b1}$. Table 2 shows an example of the predicted pullout bearing force of bearing reinforcement embedded in crushed rock with 40 × 150 mm transverse members for $n = 3$. The prediction error is acceptable for engineering practice.

Examination of internal stability against pullout failure

12. Determine the maximum total pullout force, P_t, which is the sum of the maximum pullout friction and bearing forces ($P_t = P_f + P_{bn}$).
13. Determine the factor of safety against pullout failure. This factor of safety must be greater than 1.5.

5. Conclusions

This article presents a study on the pullout mechanism of the bearing reinforcement embedded in coarse-grained soils having various friction angles, average grains and gradations. Finally, the procedure for examining the internal stability against pullout failure of the BRE wall is suggested. The conclusions can be drawn as follows:

1. The pullout friction resistance of the bearing reinforcement is mainly controlled by only the friction angle, irrespective of grain size distribution. The apparent friction between soil and the longitudinal member, δ, is greater than the soil friction angle because of the roughness and the rigidity of the steel deformed bar. The δ/ϕ ratio is approximately 1.47 for all tested soils.
2. The pullout bearing mechanism is essentially controlled by B/D_{50} and normal stress, regardless of gradation (well-graded and poorly graded). As the bearing reinforcement is pulled out and shear displacement occurs along the interface, the zone of soil surrounding the reinforcement tends to dilate. However, the volume change is restrained by the surrounding non-dilating soil, resulting in an increase in normal stress on the soil–reinforcement interface (interlocking). The interlocking effect is significant for B/D_{50} values less than 12 and decreases as the normal stress increases.
3. By assuming that the general shear and modified punching shear mechanisms are the upper and lower boundaries, the equations of predicting N_q for $3 \leq B/D_{50} \leq 12$ and 30 kPa $\leq \sigma_n \leq 120$ kPa are proposed and verified. Consequently, the maximum pullout bearing force of the bearing reinforcement with a single transverse member, P_{b1}, can be approximated.
4. The member interference is essentially dependent on S/B, irrespective of grain size distribution and friction. The transverse member interference zones are classified into three zones. Zone 1 ($S/B \leq 3.75$) is block failure where all transverse members act like a rough block. Zone 2 ($3.75 < S/B < 25$) is member interference failure. Zone 3 ($S/B > 25$) is individual failure. Because the friction angle and B/D_{50} play a great role in determining P_{b1}, even with the same S/B (same F), the P_{bn} values would be different for different grain size distributions and friction angles.

References

AASHTO, 2002. Standard Specifications for Highway and Bridge, seventh ed. American Association of State Highway and Transportation Officials, Washington, DC.
Abdi, M.R., Arjomand, M.A., 2011. Pullout tests conducted on clay reinforced with geogrid encapsulated in thin layers of sand. Geotextiles and Geomembranes 29, 588–595.
Alfaro, M.C., Pathak, Y.P., 2005. Dilatant stresses at the interface of granular fills and geogrid strip reinforcement. Geosynthetics International 12 (5), 239–252.
Alfaro, M.C., Hayashi, S., Miura, N., Watanabe, K., 1995. Pullout interaction mechanism of geogrid strip reinforcement. Geosynthetics International 2 (4), 679–698.
Athanasopoulos, G.A., 1993. Effect of particle size on the mechanical behavior of sand–geotextile composites. Geotextiles and Geomembranes 12, 252–273.
Bergado, D.T., Chai, J.C., 1994. Prediction of pullout load–displacement relationship for extensible reinforcement. Geotextiles and Geomembranes 30 (5), 295–316.
Bergado, D.T., Sampaco, C.L., Alfaro, M.C., Balasubramaniam, A., 1988. Welded-wire reinforced earth (mechanically stabilized embankments) with cohesive backfill on soft clay. 2nd Progress Report Submitted to USAID Bangkok Agency.
Bergado, D.T., Chai, J.C., Miura, N., 1996. Prediction of pullout resistance and pullout force–displacement relationship for inextensible grid reinforcements. Soils and Foundations 36 (4), 11–22.
Bergado, D.T., Teerawattanasuk, C., Long, P.V., 2000. Localized mobilization of reinforcement force and its direction at the vicinity of failure surface. Geotextiles and Geomembranes 18, 311–331.
Chai, J.C., 1992. Interaction between grid reinforcement and cohesive-frictional soil and performance of reinforced wall/embankment on soft ground. D.Eng. dissertation, Asian Institute of Technology, Bangkok, Thailand.
Hayashi, S., Shaha, J.T., Watanabe, K., 1999. Change in interface stress during pullout test on grid strip reinforcement. Geotechnical Testing Journal, ASTM 22, 32–38.
Horpibulsuk, S., Niramitkornburee, A., 2010. Pullout resistance of bearing reinforcement embedded in sand. Soils and Foundations 50 (2), 215–226.

Horpibulsuk, S., Suksiripattanapong, C., Niramitkornburee, A., 2010. A method of examining internal stability of the bearing reinforcement earth (BRE) wall. Suranaree Journal of Science and Technology 17 (1), 1–11.

Horpibulsuk, S., Suksiripattanapong, C., Niramitkornburee, A., Chinkulkijniwat, A., Tangsuttinon, T., 2011. Performance of earth wall stabilized with bearing reinforcements. Geotextiles and Geomembranes 29 (5), 514–524.

Jewell, R.A., Milligan, G.W.E., Sarsby, R.W., Dubois, D., 1984. Interaction between soil and geogrids. In: Proceedings of the Symposium on Polymer Grid Reinforcement in Civil Engineering, Thomas Telford Limited, London, UK, pp. 11–17.

Khedkar, M.S., Mandal, J.N., 2009. Pullout behavior of cellular reinforcements. Geotextiles and Geomembranes 27 (4), 262–271.

Kumar, P.V.S.N.P., Madhav, M.R., 2009. Analysis of reinforced soil wall considering oblique pull: bilinear failure mechanism – linear subgrade response. Lowland Technology International 11 (1), 1–11.

Leschinsky, D., Reinschmidt, A.J., 1985. Stability of membrane reinforced slopes. Journal of Geotechnical Engineering, ASCE 115, 1285–1300.

Madhav, M.R., Umashankar, B., 2003. Analysis of inextensible sheet reinforcement subjected to transverse displacement/force: linear subgrade response. Geotextiles and Geomembranes 21, 69–84.

Palmeira, E.M., 2009. Soil–geosynthetic interaction: modelling and analysis. Geotextiles and Geomembranes 27, 368–390.

Palmeira, E.M., Milligan, G.W.E., 1989. Scale and other factors affecting the results of pull-out tests of grids buried in sand. Geotechnique 39 (3), 511–524.

Peterson, L.M., Anderson, L.R., 1980. Pullout resistance of welded wire mats embedded in soil. Research Report Submitted to Hilfiker Co, from the Civil and Environmental Engineering Department, Utah State University, USA.

Shewbridge, S.E., Sitar, N., 1989. Deformation characteristics of reinforced sand in direct shear. Journal of Geotechnical Engineering, ASCE 115, 1134–1147.

Shivashankar, R., 1991. Behaviour of mechanically stabilized earth (MSE) embankment with poor quality backfills on soft clay deposits, including a study of the pullout resistance. D.Eng. dissertation, Asian Institute of Technology, Bangkok, Thailand.

Suksiripattanapong, C., Chinkulkijniwat, A., Horpibulsuk, S., Rujikiatkamjorn, C., Tangsuttinon, T., 2012. Numerical analysis of bearing reinforcement earth (BRE) wall. Geotextiles and Geomembranes 32, 28–37.

Tin, N., Bergado, D.T., Anderson, L.R., Voottipruex, P., 2011. Factors affecting kinked steel grid reinforcement in MSE structures. Geotextiles and Geomembranes 29, 172–180.

BIOGRAPHY

I, Cherdsak Suksiripattanapong, was born on October 7, 1983 in Nakhon Ratchasima, Thailand. In 2007, I obtained a Bachelor's degree in Civil Engineering from the Faculty of Engineering and Architecture, Rajamangala University of Technology Isan. In 2010, I obtained a Master's degree in Civil Engineering from the School of Civil Engineering, Suranaree University of Technology. Then I continued to study for a Philosophical Doctor degree at the same university. During my Ph.D. study, I have also worked as a teaching assistant in the School. I was awarded a Royal Golden Jubilee (RGJ) Ph.D. Program Scholarship from the Thailand Research Fund (TRF) in 2010. I visited the Faculty of Engineering, University of Wollongong, Australia for research under the supervision of Dr. Cholachat Rujikiatkamjorn from October, 2012 to April, 2013. I have so far published five papers in international and national journals, and 8 papers in international and national conferences.